FRACTURE CHARACTERIZATION FROM ATTENUATION AND GENERATION OF TUBE WAVES

by

Ernest L. Hardin, III

B.S., University of Utah
(1978)

SUBMITTED TO THE DEPARTMENT OF EARTH, ATMOSPHERIC, AND
PLANETARY SCIENCES IN PARTIAL FULFILLMENT OF THE
REQUIREMENTS FOR THE DEGREE OF

MASTER OF SCIENCE

in

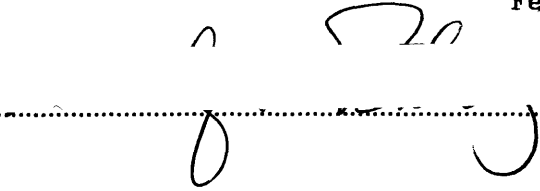Earth and Planetary Science

at the

MASSACHUSETTS INSTITUTE OF TECHNOLOGY

February, 1986

Signature of Author
Department of Earth, Atmospheric, and Planetary Sciences
February 7, 1986

Certified by
M. Nafi Toksoz
Thesis Advisor

Accepted by
Chairman
Departmental Committee on Graduate Students

FRACTURE CHARACTERIZATION FROM
ATTENUATION AND GENERATION OF TUBE WAVES

by

Ernest L. Hardin

Submitted to the Department of Earth, Atmospheric, and Planetary
Sciences on February 7, 1986 in partial fulfillment of the requirements
for the Degree of Master of Science in Earth and Planetary Science.

ABSTRACT

Tube waves are commonly observed in Vertical Seismic Profiling (VSP)
experiments conducted in crystalline rock. They are low-frequency Stoneley
waves whose attributes are readily calculated from linear elasticity. Often these
events originate where major fracture systems intersect the borehole. If a gen-
erating fracture is considered as an open, parallel-plate system with arbitrary
orientation, the generation process may be modelled (Beydoun, et al., 1985).
Useful estimates of fracture characteristics (orientation and hydraulic
transmissivity) may be obtained from the model parameterization.

The Stoneley phase observed in Full Waveform Acoustic Logs (FWAL) is
about two orders of magnitude higher in frequency than the VSP tube waves.
Compared to other phases present in FWAL seismograms, relatively more of the
strain energy of this phase is trapped in the borehole fluid, and its behavior is
useful for examining fluid-fracture interaction. The Stoneley phase is typically
attenuated when a significant fracture intervenes between the source and
receiver of the FWAL tool. If an attenuating fracture is considered as an open,
parallel-plate reservoir saturated with compressible fluid, the attenuation pro-
cess may be modelled (Mathieu, 1984). Fractures may then be discriminated on
the basis of parallel-plate aperture, which is directly related to hydraulic
transmissivity.

Field testing has been conducted in cooperation with the U.S. Geological
Survey and Weston Geophysical to evaluate these models in northeastern New
England. Conventional temperature, caliper, resistivity and televiewer logs
show the presence of fractures and their orientation, and provide indirect evi-
dence of associated flow. Tube waves are generated in hydrophone VSP surveys,
and substantial attenuation of the FWAL Stoneley wave is observed in these
wells. Transmissivity values predicted from VSP and FWAL analyses compare
favorably with flow tests and direct observation of flow effects in the borehole.
Orientation information from VSP analysis is in agreement with televiewer logs.

Transmissivity estimates from VSP interpretation using the open, parallel-
plate model are much smaller than from FWAL attenuation or pump tests. The
discrepancy is important even for such a widely ranging parameter as transmis-
sivity. Hydraulically significant fractures must in reality be propped open by
asperity contact at the fracture walls, and fracture closure is partly resisted by
asperity deformation. This resistance is modelled as a proportionality between
incident stress and closure. A new model for predicting transmissivity from
observed tube wave amplitude is formulated using the stiffness concept. Intrin-
sic stiffness factor can be calculated given independent determination of
transmissivity. Stiffness magnitudes are obtained which are comparable to the
stiffness of an undrained water layer with thickness equivalent to the flow

aperture. Transmissivity predictions using the water-layer stiffness approximation are in agreement with FWAL interpretation and pump test results.

Thesis Supervisor: M.N. Toksoz

Title: Professor of Geophysics

ACKNOWLEDGEMENTS

TABLE OF CONTENTS

Fracture Characterization

1. INTRODUCTION

Increasing importance of natural and artificial fractures in resource recovery and site characterization has created a need for methods to identify significant fractures and quantify their properties. In this study fracture parameters are deduced from seismic observations using two published models for different fracture responses, and an original model based on published work.

It has long been known that sonic logs and Full Waveform Acoustic Logs (FWAL) exhibit effects of fractures (Paillet, 1983 & 1980; Mathieu, 1984) Fractures are associated with apparent slowness anomalies in the sonic log, and with amplitude attenutation of FWAL waveforms. In recent Vertical Seismic Profiling (VSP) studies in crystalline rock, major open fractures have been shown to generate a characteristic response. Huang and Hunter (1981) observed tube waves originating at distinct depths, when conducting checkshot VSP using a hydrophone streamer. They attributed tube wave generation to the presence of open fractures intersecting the borehole. In similar surveys at Hamilton, Massachusetts and Mirror Lake, New Hampshire, tube wave generation and FWAL attenuation were also observed at major fractures.

Mechanistic models for these fracture responses are published, so this study begins by applying the tube wave generation model of Beydoun, et al. (1985), and the FWAL Stoneley attenuation model of Mathieu (1984) to the same fractures. Data sets from two separate New England water wells are used, consisting of standard wireline logs, FWAL and hydrophone VSP. Seismic interpretation is compared to independent estimates of fracture parameters from hydrologic pump test results and borehole televiewer images. The objective of the comparison is to calibrate the seismic techniques to more conventional flow test results, so that they may be incorporated into site characterization metho-

dology. In this study fluid transport is considered to take place only along structural features such as joints or shear zones which can be identified in televiewer logs. The parallel plate analogy is used throughout as a basis for considering the mechanical and flow behavior of fractures. Fractures are assumed to be planar and to extend uniformly away from the hydraulic or mechanical influence of the borehole.

1.1 Tube Wave Description

Tube waves are low frequency Stoneley waves, a fundamental normal mode which can propagate along the cylindrical borewall interface of a fluid filled hole. In a rigid formation where the formation shear velocity is significantly greater than the borehole fluid velocity, tube wave velocity and dispersion are minimally dependent on formation properties (Cheng and Toksöz, 1983; White, 1983). Phase velocity of the guided tube wave is always lower than that of the borehole fluid. Particle motion is prograde elliptical at the borewall, grading to linear along the borehole axis (Biot, 1952; Cheng and Toksöz, 1981). Displacement amplitude in the solid decays approximately exponentially away from the borehole.

For a homogeneous formation, linear elasticity predicts some dispersion with the phase velocity asymptotic to the fluid velocity at high frequency (Cheng and Toksöz, 1981). The dispersion relationship for a given application is dependent on the fluid and formation properties and the hole diameter. Within the VSP band (10 to 1000 Hz.) and the typical FWAL band (2-20 kHz.), phase velocity is nearly constant and principally dependent on formation properties. At higher frequencies such as are encountered in FWAL, phase velocity may become increasingly dependent on borehole radius.

A guided wave effect may not exist if the formation shear velocity is much less than the borehole fluid velocity. This limit is determined exactly by

the formation and fluid properties (Schoenberg, et al., 1981). In crystalline rock as in many other rock types the shear velocity exceeds this limit and tube waves can propagate without geometric attenuation. At exploration seismic frequencies most of the strain energy of the tube wave is trapped in the fluid. With increasing frequency, more of the total energy of the wave is involved with the motion of the borewall.

1.2 Hydrophone VSP (Vertical Seismic Profiling) Experiments

This section describes the physical geometry and apparatus used to acquire hydrophone VSP data in the field. Hydrophones in the borehole register both the direct wave from a remote source (which must couple to the borehole), and tube waves which may be excited. Since most of the energy associated with a tube wave propagates in the fluid, pressure response (hydrophones) is more easily measured than borewall displacement (eg. wall-locking geophones) for the study of tube wave phenomena. Tube wave pressure amplitude varies only a few percent over the cross section of the borehole at VSP frequencies (Biot, 1952), so centralization of the hydrophones is unnecessary.

The Hamilton, Massachusetts test well (Britton #2) is a deep water well drilled to app. 570m. in Cape Ann gabbro and granodiorite near Hamilton, Massachusetts. The hole was drilled percussively with a final gauge of 0.30m., and is uncased except for a surface layer of glacial debris. From gyroscopic deviation surveys it is evident that from about 200m. to 300m. the well deviates increasingly up to 11 degrees from vertical and continues at this orientation to total depth.

Two VSP surveys were conducted at Hamilton; the first using surface explosive and weight drop sources, and a single available shothole. Signal strength from weight drop and surface explosive sources was adequate for generation of identifiable tube waves, but not for capture of the direct compressional wavelet

necessary for interpretation. Multiple shot trace stacking was not used.

The second survey was conducted eight months later using three shotholes exclusively. The three shotholes penetrate well below the surface layer, as depicted in Figure 1. Multiple offsets are used to exploit the geometrical dependence of the tube wave generation model. All of the Hamilton boreholes are naturally water filled up to the bottom of the surface layer. Source strength for the Hamilton VSP sections varies up to 0.45 kg. charges of ammonium-nitrate based explosive.

In the equipment used at Hamilton, borehole fluid pressure is recorded digitally from the output of a six-channel hydrophone streamer with receiver spacing of 3m. Hydrophone frequency response is uniform to better than 3db amplitude over the seismic source band. Each hydrophone (Benthos, Inc. AQD-1) contains an integral preamplifier, and analog signals are transmitted to the surface on a seven-conductor wireline. Traces were acquired using a 12-bit digitizer with fixed gain, sampling rate 4 kHz., and total time window of 500 msec.

The phases are well separated in the three record sections (Figures 2, 3 and 4), with tube wave events generated at depths of 146m., 210m. and 290m. in apparent coincidence with the direct compressional arrival. Receiver spacing is much smaller than the separation of generating horizons, giving multi-sensor coverage of tube wave events close to their depth of generation. No direct shear arrival or reflected body wave of any type is identifiable in the section. Numerous tube wave reflections and events possibly originating deeper in the well extend late into the acquisition window.

At the Mirror Lake site, the observation well (EBR-4) was percussively drilled to a depth of 225m. The hole is one of a 10m. square pattern of similar holes (Figures 5, 36) which penetrate a metamorphic sequence of schist and gneiss, intruded by thick, irregular veins of quartz monzonite (Winters, 1984).

All four of the holes are uncased except for a 15m surface layer of sand, gravel and glacial till. The total depth of EBR-4 is approximately twice that of the other three holes.

Four shotholes were drilled into the surface layer to a depth of 9m. Thickness of the surface layer varies, so that some of the shotpoints lie just a few meters above the bedrock contact. Shothole A penetrates bedrock at about 6m depth, and shothole C bottoms in the surface layer very close to the contact. Cuttings indicate that a till layer of a few meters thickness lies directly on bedrock, and is overlain by unconsolidated sand and gravel. The level of standing water in each shothole corresponds approximately to published water table depth data (Winters, 1984). Each shothole is completely cased with 9cm diameter Schedule-40 steel pipe. Standing water was maintained at the level of the water table during the experiment. The horizontal distance from the observation well to each shot point is of the same order as the total depth of the well (Figure 5).

A single VSP survey was conducted over three days at the Mirror Lake site. Explosive charges varying up to 0.12kg dynamite were detonated electrically, and a near-source geophone was used to monitor detonation timing and source signature. Analog triggering and geophone signals were transmitted to the observation well over a 300m multi-pair cable. A total of four sections were acquired, which is one more than the minimum needed to obtain distinct fracture parameters from inversion of the tube wave generation models of equations (19) and (A2). In each section the dominant events are tube waves which originate at about 44m and propagate both upward and downward. In addition, smaller amplitude tube waves originating at 220m, 135m and 103m are observed, and the direct compressional arrival is evident.

The recording equipment used at Mirror Lake is functionally equivalent to that used in the Hamilton VSP experiment. A 3-channel streamer with one AQD-1 hydrophone per channel is deployed on a 4-conductor wireline. The record sections were sampled at 8 kHz., with 12-bit accuracy, and without stacking.

The principle difference between the two surveys described is the depth of the shotholes. At the Hamilton site the shotpoints are located far into the unweathered bedrock, so the wave reflected off the surface layer is diminished by geometrical attenuation. Further, the direct compressional arrival is unaffected by any filtering effects of propagation through the surface layer. A majority of the shots in the Mirror Lake survey were detonated in the surface layer, and the source signature changed gradually with successive shots due to casing degradation. From monitor phone records (Figures 6 and 7) it is clear that section D is most affected, and that sections A and C are very slightly affected in this way.

1.3 Stoneley Waves in Full Waveform Acoustic Logging (FWAL)

At acoustic logging frequencies (typically 2-20 kHz.) several guided waves may be observed in a borehole excited by a dilatational source in the fluid. For crystalline rock the shear velocity is greater than the acoustic velocity of the borehole fluid. In this case compressional and shear head waves, "leaky" compressional modes, and guided shear (psuedo-Rayleigh) modes are typically present in addition to the Stoneley phase.

As borehole diameter increases, the presence of the logging tool is less important and pseudo-Rayleigh phase and group velocities are reduced. Dispersion curves for the first and higher pseudo-Rayleigh modes are shifted to lower frequencies with increasing radius (Cheng & Toksöz, 1981). Typically this shift increases the efficiency of excitation of these modes by the source, and they

become more prominent with respect to the Stoneley phase. If a minimum in group velocity vs. frequency for the first pseudo-Rayleigh mode is substantially within the source band, the associated Airy phase may be strongly expressed in the received waveforms. This is the case for the Hamilton FWAL data set, from Britton well #2 (Figures 8 and 9). The phase arriving at app. 1.1 msec is probably the Airy phase, and the Stonely arrival at app. 1.5 msec is indistinguishable.

In smaller boreholes such as Mirror Lake EBR-4 (diameter 0.15m.) the affect of the rigid FWAL tool is comparable to further reducing the effective borehole diameter. A significant upward shift of pseudo-Rayleigh dispersion curves toward higher frequencies results, with a reduction in excitation of these modes. Excitation of the relatively nondispersive Stoneley phase increases in smaller boreholes since source dilatation is effectively distributed over a smaller borehole cross section, and so the Stoneley phase becomes an identifiable feature of the waveform.

The efficiency of source energy conversion to Stoneley waves is inversely related to frequency (Cheng & Toksöz, 1981). Below the cutoff frequency for the first pseudo-Rayleigh mode, the waveform is completely dominated by the Stoneley packet. This behavior is shown in Figures 10,11 and 12, which are FWAL data sections for the same interval of EBR-4, acquired with FWAL tools operating in different bands. At a nominal center frequency of 34 kHz. the pseudo-Rayleigh arrival is impulsive. With a similar type of source (magnetostrictive) and 15kHz. center frequency the arrival is more emergent and smaller in amplitude relative to the Stoneley phase. With a sparker source operating at about 5 kHz. the head waves are diminished and the pseudo-Rayleigh phases are not present, leaving the Stoneley phase.

1.4 Conventional Logs

This section is a description and comparison of various wireline logs ac-
quired for the two study wells. The logs clearly show the existence of fractures,
with electrical responses that suggest the presence of flow or clay minerals, and
(for Britton well #2) temperature profiles indicative of flow. Mineral alteration
is naturally associated with discontinuities, gouge formation, and the chemical
activity of groundwater. A useful correlation between mineralization (electrical
response) and hydraulic significance does not follow, however (Paillet, 1985). To
summarize the evaluation of conventional logs, fracture responses are clearly
evident, but it is difficult to distinguish the (VSP) tube wave generating hor-
izons. Further, in the wells studied it is impossible to predict from the wireline
logs the depth of features which are important in simple pump tests. These
failures are probably related since in both wells studied (well EBR-4 in particu-
lar) inflow horizons are well correlated to (VSP) tube wave generation.

A suite of conventional logs was acquired at the Hamilton well including
caliper, natural gamma, sonic (noncentralized), initial entry temperature log
(downgoing recording on first entry into borehole after thermal equilibration),
borehole acoustic televiewer, self potential and resistivity. There are clear indi-
cations of the (VSP) tube wave generating horizons, except for the electrical
logs, as shown in the comparison plots (Figures 13 and 14). The caliper opened
fully at each horizon, indicating natural cavities or displacement of material
from the borewall during drilling. Natural gamma anomalies at each horizon in-
dicate constitutive differentiation. Apparent interval transit time increases un-
iformly from 180 to >300 μsec/meter. at fractured horizons. The borehole tem-
perature log (Figure 14) has been reduced by the subtraction of a linear geoth-
ermal gradient of 3.0 C°/100m. Temperature anomalies (app. 0.5 C° above back-
ground) indicate where warmer formation fluid flows into the well through open
fractures. Images acquired with the borehole televiewer (Figure 15) unambigu-

ously show tabular features intersecting the hole obliquely at each tube wave generating horizon. The large apparent aperture of these features is due to flushing of material from a thin zone during drilling. Whether the zone is fractured or filled with chemically altered material is unclear from these images.

At the four Mirror Lake site, the four EBR wells were logged using caliper, single-point resistivity, natural gamma, borehole televiewer and uncompensated sonic tools (Paillet, 1985). In addition the three shallow wells EBR-1,2 and 3 were logged for self-potential (SP), focused resistivity, short and long normal resistivity, and neutron porosity tools (Winters, 1984). Televiewer images show an abundance of subhorizontal fractures from the surface down to about 100m, whereupon fracture traces become more sparse (Figure 17). Fracture indications tend to be grouped at particular depths, and orientation is relatively consistent within such assemblages. Dip angles range up to about 40°. The majority of fractures in EBR-4 dip to the east, although some dip south and a few dip toward the west (Paillet, 1985).

For adjacent wells it is interesting to note the correlation of SP, focused resisitivity and single-point resistivity with fractures detected by the televiewer and VSP response (Figures 16 thru 17). SP response is generally flat in the fractured zones, which indicates that ionic concentration is relatively uniform within the borehole and the connecting fracture network. Significant electro-chemical activity, and steady fluid exchange (flow) with the borehole are therefore absent in these zones (Serra, 1984, p.79). The single-point resistance is affected by mineralization which may be associated with fractures. Clay minerals can provide cations for current conduction in resistive formations even when connate waters are fresh. Significant anomalies are seen at the larger fractures, indicating the presence of altered minerals. Extent of alteration does not necessarily correlate to fracture transmissivity (Paillet, 1985).

Resistivity decreases sharply to 500 ohm-m. or less at negative peaks which are well correlated to fractures. The peaks at 38m., 44m. and 54m. are of possible importance in the investigation of VSP tube wave generation processes. Sharpness of resistivity anomalies at fractures increases with the resolution of the log, giving further indication that the peaks are fracture-related. Such peaks occur only at select fractures among many which are evident in the televiewer images.

Natural gamma response is dominated by quartz monzonite intrusion, with slight activity which could possibly be associated with fractures. Variability of this response in the monzonite zones is such that fracture responses are indiscernible, and suggests more heterogeneous facies than are represented in the cuttings log. Realigning the gamma logs from the four EBR wells it is possible to produce good correlation for lithology changes, but without elucidating fracture trends.

The maximum velocity from the sonic log is about 5.5 km/sec. Most measurements lie in the range 4.5 to 5.25 km/sec. Variability of the sonic velocity vs. depth is related to fractures. Fractures in the interval 38m. to 54m. generate off-scale slowness response. Lesser responses are prevalent throughout the section, and may be correlated to fractures. The caliper log provides scant indication of fracture location or attributes in the EBR wells. fracture parameters, are lacking for the wireline logs.

1.5 Fracture Flow Units

In one spatial dimension Darcy's law states that flow velocity is proportional to pressure gradient:

$$v_{avg} = \frac{L_0^2}{12\mu} \frac{\partial H}{\partial s} = \frac{\rho g L_0^2}{12\mu} \frac{\partial h}{\partial s} \tag{1}$$

where $\frac{\partial h}{\partial s}$ is the dimensionless head gradient (Ziegler, 1976). The constant of

Fracture Characterization

proportionality $\frac{\rho g L_0^2}{12\mu}$ is the hydraulic conductivity, and is a property of the

fracture independent of fluid properties. The factor $\frac{L_0^2}{12}$ is called intrinsic per-

meability and pertains to the flow behavior of a fracture which carries some

particular fluid. Fracture transmissivity is defined as the integrated discharge

over the fracture aperture, or

$$T = v_{avg}\frac{L_0}{\partial h/\partial s} = \frac{\rho g L_0^3}{12\mu} \tag{2}$$

For realistic hydrogeology problems it is useful to consider effective fracture

conductivity (denoted by superscripted K_c^*) by summing transmissivity values

for various fractures in an interval, and dividing by the interval length D:

$$K_c^* = \frac{\sum T_i}{D} = \frac{\sum (v_{avg}L_0)_i}{\frac{\partial h}{\partial s}D} = \frac{\rho g \sum (L_0^3)_i}{12\mu D} \tag{3}$$

Effective intrinsic permeability (also superscripted) is given by

$$K^* = \frac{K_c^* \mu}{\rho g} = \frac{\sum (L_0^3)_i}{12D}. \tag{4}$$

For a single fracture the hydraulic conductivity is not defined until a value is

chosen for D. If the fracture is considered as a single porous layer then $D = L_0$,

and the effective conductivity becomes

$$K_c^* = \frac{K^* \rho g}{\mu} = \frac{\rho g L_0^2}{12\mu} \tag{5}$$

This study is dedicated to estimation of transmissivity T for single fractures,

from seismic observations. This is equivalent to estimation of equivalent

parallel-plate aperture L_0, or single-fracture conductivity K_c^* with $D = L_0$. Note

that aperture, conductivity and transmissivity as defined are proportional to

the first, second and third powers of flow aperture. The usage of these terms is

consistent with the parallel-plate fracture analogy.

2. INTERPRETIVE MODELS

Mechanistic models for understanding seismic responses are based on the parallel plate fracture analogy. The (VSP) tube wave generation models involve dynamic closure of the parallel plate system, which expels fluid into the borehole creating a tube wave. The FWAL Stoneley attenuation model also involves fluid transfer between a single fracture and the borehole, but with the parallel plate separation fixed and fluid storage in the fracture due to compressibility. This section gives a recapitulation of the published models, with underlying assumptions. In addition, original methods for applying the models to field data are presented, and fracture parameters are calculated for certain horizons in Britton well #2 and well EBR-4.

2.1 Tube Wave Generation in VSP Surveys

White (1983) showed that a tube wave may be generated when an incident plane compressional wave interacts with the borehole at a contact between formations. Tube wave amplitude is predicted for the case of perpendicular borehole-interface geometry, using a long-wavelength assumption and approximate displacement continuity conditions at the contact. In the data presented here, and in the surveys of Huang and Hunter (1981) and others, tube waves are typically generated at horizons which are distinguished only by fracture traces in an otherwise homogeneous formation. For body wave energy to be converted to tube waves at these thin features, requires interaction in the form of fluid transfer between the formation and the borehole.

2.1.1 Tube Wave Generation (VSP) Model, Displacement Formulation

In the derivation of Beydoun, et al. (1985), fractures are idealized as fluid-saturated, parallel-plate which are embedded in an isotropic elastic medium (Figure 18). The fracture-borehole system is initially at hydrostatic equilibrium. A plane wave with wavenumber unit vector **p** impinges on a fracture with

unit normal **n.** Fracture width is assumed to oscillate around the static aperture L_0 at the same frequency and displacement amplitude as the incident P-wave, or

$$L(t) = L_0 - \zeta_0 \cos(\omega t) \tag{6}$$

where ζ_0 is the amplitude of fracture closure. This condition applies everywhere on the model fracture; the model is refered to in this study as the displacement formulation. To simplify calculation of fluid injection into the borehole the following assumptions are made:

1. $L_0 >> \zeta_0$
2. Laminar fluid flow in the fracture.
3. Fluid compressibility small.
4. Fluid injected into the fracture does not significantly change the borehole fluid pressure, ie., the borehole pressure H takes on a constant value $H = H_0$ when fracture wall velocity is zero.
5. Low frequency approximation with frequency dependence (P-wavelength much larger than borehole radius or fracture width).
6. Fracture intrinsic permeability is invariant with time.
7. Maximum fracture normal displacement ζ_0 is related to the incident P-wave displacement amplitude u in the formation by:

$$\zeta_0(t) = u(t)\cos\varphi , \qquad \cos\varphi = \frac{\mathbf{n \cdot p}}{|\mathbf{n}||\mathbf{p}|} . \tag{7}$$

For the two-dimensional case of linear, laminar incompressible flow (use laminar flow and geometric assumptions) in response to fracture closure, Darcy's Law is formulated

$$q(s,t) = -\frac{KL(t)}{\mu} \frac{\partial H(s,t)}{\partial s} \tag{8}$$

The fluid flow rate in the presence of a pressure gradient $\partial H(s,t)/\partial s$ is related to the fracture aperture $L(t)$. An additional elevation gradient term $\rho_f(g\,\partial Z/\partial s)$ is neglected. Since the idealized fracture system is symmetric with respect to the borehole axis at the point of intersection, errors due to elevation gradient effects are small for mildly dipping (<60°) fractures (Bower, 1983). The volume of fluid ejected into the 2-D fracture during one half-cycle (π/ω) of periodic fracture movement is

$$V_{2D}(L_0) = \zeta_0 \left[\frac{K}{\pi \gamma \mu} \right]^{\frac{1}{2}} F(\omega, \zeta_0 / L_0) \tag{9}$$

with

$$F(\omega, \zeta_0 / L_0) \approx 2\omega \int_0^{\frac{\pi}{\omega}} \left[\frac{T}{2} - t \right]^{\frac{1}{2}} sin(\omega t) \, dt \qquad (\zeta_0 \ll L_0). \tag{9a}$$

As is common in reservoir problems (Ziegler, 1976) calculation of 2-D flow is simplified with the assumption of an effective distancsdfkl;jjasdjklf; e from the "borehole" boundary at which fracture flow is nil. Effective 2-D length is used as a limit of integration in the determination of total flow. It is convenient to define this length as

$$d(L_0) = \left[\frac{2\pi K}{\mu \gamma \omega} \right]^{\frac{1}{2}} = L_0 \sqrt{\frac{\pi}{3\mu \gamma \omega}} \tag{10}$$

which yields the distance from the bolehole axis at which the pressure gradient is diminished to about a tenth of its maximum during fracture movement.

The two-dimensional result is adapted to the axisymmetric three-dimensional problem by comparing the 2-D and 3-D expressions for steady state flow in response to constant presure at effective length d:

$$q_{3D} = 2\pi R \chi q_{2D} \tag{11}$$

where

$$\chi(L_0) = \frac{d(L_0)}{R \ln\left[\frac{R + d(L_0)}{R} \right]} \tag{11a}$$

The factor χ is purely geometrical, so that

$$V_{3D} = 2\pi R \chi V_{2D}$$

relating fluid volumes V_{2D}, V_{3D} ejected in one half-cycle of fracture movement.

Most of the strain energy of a propagating tube wave is trapped in the fluid, so the amplitude of a tube wave excited by a periodic dilatant source in the fluid may be approximated by equating the source strength to the dilatancy as-

sociated with the coherent tube wave. Neglecting phase response, body waves radiated into the solid, and associated energy of the normal mode in the solid, Beydoun, et al. (1985) developed a relationship between fluid flow and tube wave pressure amplitude. Upgoing and downgoing tube waves of equal amplitude are predicted.

The tube wave dilatation in the fluid (Δ_f^T) determines the amplitude of the tube wave generated by ejected fluid. The transfer of energy from the compressional body wave to the normal mode is taken as real-valued and linear with respect to frequency. The integral of volume strain Δ_f^T over one half-cycle is equated to the fluid volume ejected from the fracture in the same time period. The volumetric strain and amplitude of tube wave are determined using the displacement potential for tube waves. If the tube wave displacement potential in the fluid is taken to be (ignoring sinusoidal time dependence)

$$\Phi_f^T(r,z,t) = CI_0(nr) \sin(\omega t - kz) \tag{13}$$

then tube wave dilatation in the fluid is

$$\Delta_f^T = \nabla^2 \Phi_f^T \tag{14}$$

The expression is integrated twice to yield

$$-V(L_0) = 4\pi RC(L_0)(2 - c^2/\alpha_f^2)I_1(nR)k/n \tag{15}$$

Substituting the expression derived above for ejected fluid volume and rearranging,

$$C(L_0) = \zeta_0 \chi(L_0) L_0 \left[\frac{1}{12\pi\gamma\mu} \right]^{\frac{1}{2}} F(\omega, \zeta_0/L_0) \frac{(1 - c^2/\alpha_f^2)}{2(2 - c^2/\alpha_f^2)I_1(nR)} \tag{16}$$

Parameter $C(L_0)$ is dependent on fracture properties and couples fracture movement to tube wave pressure amplitude, since pressure amplitude in the fluid is given by

$$p^t = \rho_f \omega^2 C(L_0) I_0(nr) \tag{17}$$

To determine in situ permeability the observed tube wave amplitude is normalized by the pressure amplitude of the direct compressional phase at the same sensor. The P-wave pressure response is written in terms of the displacement in the formation (White, 1983) using the low frequency approximation:

$$p^a = \zeta_0 \frac{\omega \rho_f c^2 \alpha [1 - 2(\beta \cos(\vartheta)/\alpha)^2]\cos(\vartheta)}{\beta^2[(1 - (c \cos(\vartheta)/\alpha)^2]\cos(\varphi)} , \qquad \cos(\vartheta) = \frac{\mathbf{b} \cdot \mathbf{p}}{|\mathbf{b}||\mathbf{p}|} \quad (18)$$

where $\mathbf{b}$ is the borehole axis unit direction vector. The normalized tube wave pressure amplitude is the ratio:

$$\frac{p^t}{p^a} = C(L_0) \frac{\omega \beta^2 \cos(\varphi)[1-(c \cos(\vartheta)/\alpha)^2]I_0(nR)}{\zeta_0 \cos(\vartheta)c^2 \alpha [1-2(\beta \cos(\vartheta)/\alpha)^2]} \quad (19)$$

The amplitude of P-wave displacement in the formation is thus eliminated by cancellation. The ratio of tube wave to compressional wave amplitude can be determined from a single trace if necessary and does not require hydrophone calibration. The two phases must be represented by recognizable wavelets and be correctable for interference from extraneous phases, in order for the spectral ratio comparison to be meaningful.

2.1.2 Linear Inversion of (VSP) Generation Model, for Fracure Orientation

For fixed frequency and fixed survey geometry, the tube wave vs. P-wave spectral amplitude ratio in terms of fracture parameters is:

$$\frac{p_t}{p_a} = B(L_0) \cos(\varphi) \quad (20)$$

Where $B(L_0)$ is a nonlinear function of equivalent flow aperture, borehole radius, formation properties, and fluid properites. Function $B(L_0)$ is the tube:P amplitude ratio for zero-offset, normal incidence geometry. For fixed survey geometry, φ is a function of fracture strike and dip, which are designated ψ and σ.

Borehole pressure is discretely sampled in the time domain, windowed to isolate the direct P-wave and tube wave events, and transformed using the

discrete Fourier transform (FFT), so that the spectral ratio at discrete frequencies is available for comparison to theory. Multiple VSP offsets are needed to utilize the geometrical dependence of spectral amplitude ratio, for fracture orientation estimation.

For three or more offsets, at a fixed frequency, linear least squares inversion may be used to obtain fracture-normal vector direction cosines, leaving an undetermined transmissivity-dependent factor common to all offsets. The problem is represented as

$$
\begin{bmatrix} (p_t/p_a)_1 \\ (p_t/p_a)_2 \\ \cdot \\ \cdot \\ \cdot \end{bmatrix} = \begin{bmatrix} p_{1,x} & p_{1,y} & p_{1,z} \\ p_{2,x} & p_{2,y} & p_{2,z} \\ \cdot & \cdot & \cdot \\ \cdot & \cdot & \cdot \\ \cdot & \cdot & \cdot \end{bmatrix} \begin{bmatrix} n_x \\ n_y \\ n_z \end{bmatrix} B(L_0) \tag{21}
$$

where

$$
B(L_0) \;=\; C(L_0) \, \frac{\omega\beta^2[1-(c\,\cos(\vartheta)/\alpha)^2]I_0(nR)}{\zeta_0\cos(\vartheta)c^2\alpha[1-2(\beta\cos(\vartheta)/\alpha)^2]} \tag{21a}
$$

and $C(L_0)$ is given by (17). Parameters $p_{i,x}, p_{i,y}, p_{i,z}$ are components of the wavenumber vector **p** corresponding to the *ith* shot point. Similarly, $n_{i,x}, n_{i,y}, n_{i,z}$ are the components of unit fracture normal **n.**

2.1.3 Nonlinear Inversion of (VSP) Generation Model

Where source frequency content and data quality permit acquisition of spectral ratios over a frequency band, a different inversion approach is potentially useful. The inversion consists of finding a solution vector $\mathbf{x} = (L_0, \psi, \sigma)$ which results in the best possible fit of the model to the processed data, over the source band. For a single offset the scheme is as follows:

$$
\lambda(\psi, \sigma) \begin{bmatrix} \cdot \\ \cdot \\ \mathbf{A}(L_0, \omega_i) \\ \cdot \\ \cdot \end{bmatrix} \mathbf{x} \;=\; \mathbf{Gx} \;=\; \mathbf{d} \tag{22}
$$

where

$$\mathbf{A}(L_0, \omega_i) = \frac{A_1(\omega_i) \cdot L_0^2}{\ln\{A_2(\omega_i) + A_3(\omega_i) L_0\}} \ , \tag{22a}$$

and **d** is a vector of spectral ratios determined for all offsets and frequencies from the data. Nonlinear least squares inversion is used to minimize the residual quantity

$$SSQ = |\mathbf{f}|^2 = |\mathbf{W}[\mathbf{Gx} - \mathbf{d}]|^2 \tag{23}$$

where **W** is a diagonal matrix of weight factors by which additional frequency dependence is incorporated. The norm SSQ is taken with respect to all offsets and applicable frequencies. Each diagonal element is the ratio of the normalized source amplitude to the standard deviation of the tube wave vs. P-wave amplitude ratio determined from many traces, at a particular frequency.

The parameter φ cannot independently specify the orientation of a plane in space. The required additional information is derived from the frequency dependence of the aperture L_0, and to a larger extent by multiple VSP offsets. Multiple offsets can be explicitly represented in the inversion scheme:

$$SSQ = |\mathbf{f}|^2 = \left| \begin{bmatrix} \mathbf{W}^{(1)} & & & \\ & \mathbf{W}^{(2)} & & \\ & & \cdot & \\ & & & \cdot \end{bmatrix} \cdot \left\{ \begin{bmatrix} \mathbf{G}^{(1)} \\ \mathbf{G}^{(2)} \\ \cdot \\ \cdot \end{bmatrix} \mathbf{x} - \begin{bmatrix} \mathbf{d}^{(1)} \\ \mathbf{d}^{(2)} \\ \cdot \\ \cdot \end{bmatrix} \right\} \right|^2 \tag{24}$$

where the superscripted parenthetical indices refer to the different offsets.

The scheme used to find the minimizing **x** is Levenberg-Marquardt inversion (Marquardt, 1963), a damped least squares procedure. Modifications by Brown (1972) improve convergence by adjusting the scalar damping parameter at each iteration. The problem is linearized by considering the local behavior of the residual norm about an a priori parameter vector. A sequence of approximations to the minimizing solution is generated by

$$\mathbf{x}_{n+1} = \mathbf{x}_n - [\alpha_n D_n + J_n^T J_n]^{-1} J_n^T \mathbf{f} \tag{25}$$

where J_n is the numerical Jacobian describing the behavior of the components

of vector $f(x, \omega)$ with respect to the components of x in the vicinity of x_n. Vector D_n is a diagonal matrix consisting of the diagonal of $J_n^T J_n$, and α_n is damping parameter. The Jacobian is estimated using the second-order central difference approximation to partial derivatives:

$$\frac{\partial}{\partial x_j} f(x_n, \omega_i) \approx \frac{1}{2h_j} [\; f(x_n + h_j s_j, \omega_i) - f(x_n - h_j s_j, \omega_i) \;] \qquad (26)$$

where

$$h_j = \max |x_j|, 0.1 \cdot \varepsilon^{\frac{1}{2}}, \qquad (26a)$$

s_j is a unit vector in the direction of the solution component x_j, h_j is the step size along this direction used to estimate the partial derivative, and ε is the precision of the floating point machine number unity. The many evaluations of $f(x, \omega)$ required are made to the next higher precision.

2.1.4 Analysis of Britton Well #2, Hamilton, Massachusetts

This setting for field application of the VSP model is optimal since homogeneity of the formation prevents scattering of the primary compressional wavelet. Shot points are located deep in the bedrock so the surface reflection of the source is diminished by geometrical spreading. For these reasons a single compressional wave packet interacts with tube wave generating horizons, and tube wave interpretation is simplified. Additionally the intrinsic attenuation of the formation can be presumed negligible at exploration frequencies.

Source spectra are studied by temporally windowing the arriving compressional wavelet at several receivers, and computing their spectra via the discrete Fourier transform (FFT). The spectra are normalized and combined to produce a composite amplitude spectrum for each section which is equally weighted with respect to individual traces (Figure 19). Based on evaluation of the source spectra the traces are digitally bandpass-filtered using a 3-pole Butterworth recursive filter applied twice to the data, in opposite directions to suppress phase shifts. The corner frequencies of the passband are 150 and 400 Hz. The traces

are further filtered to suppress harmonic line noise present during acquisition, utilizing the time window between shot detontation and the direct arrival. This time window is analyzed to determine the characteristics of 60 Hz. harmonics which fit the data in the least squares sense. Frequency is known to be an integral multiple of 60.0 Hz., and Marquardt inversion is used to find phase and amplitude. These components are then subtracted from the entire data trace. Errors in predicted noise amplitude or phase caused by variability of these properties of the actual noise are not observed in the resulting traces (Figures 20 thru 22). Stationarity and phase effects are thus limited to components of the noise whose amplitude is small compared to the useful components of the signal.

A tube wave event is defined as a disturbance originating at a particular depth, concurrent with the direct compressional arrival, and travelling up- and downhole from this depth. Each tube wave event is evaluated independently, using traces from the three filtered VSP sections. For each trace the arriving P-wavelet and the selected tube wave event are windowed, and the tube:compressional amplitude ratio spectrum calculated. A spreading correction is made to each P-wavelet spectrum, based on the difference between source-receiver separation for the recording hydrophone and the direct path from the source to the generating fracture. These distances are known from directional surveys. For each section composite P-amplitude and tube vs. P amplitude ratio spectra are prepared by stacking the results for all applicable traces. Since for each section several (~15) traces are used to produce the composite spectra, a pointwise standard deviation may be used as an estimator of the significance of the ratio spectrum. For each section this estimator was substantially less than the observed amplitude ratios except at the edges of the pass band (Figure 23).

Fracture Characterization

Theoretical amplitude spectral ratio curves (displacement formulation) for normal P-wave incidence and different values of transmissivity are presented in Figure 24. The inversion methods of sections 2.1.2 and 2.1.3 are then employed to find values for fracture orientation and transmissivity which best fit the observed ratios.

Linear inversion is the simpler method and yields results which compare favorably with the nonlinear method. For Britton well #2 a frequency of 250 Hz. was selected as representative of behavior over the source band. Orientation resulting from inversion of 250 Hz. ratios, as well as the ratio values used, are presented in Table 1. Approximate transmissivity is obtained by comparing the resulting value for $B(L_0)$ with the curves of Figure 24.

Marquardt inversion is used to match calculated and observed amplitude ratio curves for the three sections over the source band (150 - 400 Hz.). Each VSP section yields a set of residuals at discrete frequencies, which are weighted by the ratio of the normalized source amplitude to standard deviation of the tube-to-P amplitude ratio, for the appropriate frequency and VSP section. The resulting spectra are shown in Figure 25 for the fracture at 290m. The corresponding fracture parameters are summarized in Table 1.

When strike, dip and permeability for a tube wave generating horizon have been calculated there remains the question of uniqueness of the solution. One simple way to examine this is to vary each independent component of $\mathbf{x}$ around the minimizing solution and observe the corresponding behavior of $|\mathbf{f}|^2$. For each of the three horizons studied in Britton well #2, the log of this norm is plotted against variation of each independent variable (Figure 26). Within the closed intervals in which the strike and dip angles must range, the solution points are minimal. For the aperiodic range of permeability the solution points are also minimal, with the additional condition that at low values of K the sum

of squares is bounded by the norm of the spectral ratio values determined from the data.

2.1.5 Analysis of Well EBR-4, Mirror Lake, New Hampshire

The linear inversion method described above was applied to the tube wave generating horizons at 44m. and 225m., yeilding the results presented in Table 1. The amplitude ratio data used in the inversion correspond to a peak source-band frequency of 150 Hz. Dip angles of these fractures are small ($<10°$), and the direct paths from the shotpoints impinge on the upper fracture with shallow incidence. For these reasons the calculated strike angles vary somewhat from the results of nonlinear inversion and televiewer indications.

Nonlinear Marquardt inversion is used to match amplitude ratio curves for the four sections (Figures 27 thru 30) over the source band (100 - 300 Hz.). The upper range of the source band varies over the four VSP sections acquired. Sections A and C extend to frequencies well above 300 Hz., whereas section D contains virtually no energy above this frequency. Generally the upper range is variable, and reduced relative to the Britton experiment because the shotpoints are located in the surface layer and not in crystalline bedrock. Transmissivity values for linear and nonlinear methods are comparable.

2.2 Stoneley Wave Attenuation in Full Waveform Logs

FWAL waveforms used in this study were acquired using a two-receiver, single transmitter tool which could be configured with various source transducers. When an open fracture intervenes between receivers a significant dimunition of waveform amplitude is observed at the farther receiver. Attenuation of the Stoneley phase is best understood because the energy of this mode is largely trapped in the borehole fluid. Amplitude of this mode can be characterized by the fluid pressure amplitude anywhere in the borehole. At a fracture opening the pressure amplitude is limited by fluid flow into the formation. The amplitude

of the tube wave transmitted to the far receiver is thus related to fracture transmissivity. This effect forms the basis of predicting fracture transmissivity from attenuation response.

Head waves and pseudo-Rayleigh modes are similarly attenuated at fractures. Much of the energy of these modes is elastic, and is reflected and radiated away from the borehole. Attenuation of these modes will depend on the realism of the parallel-plate fracture analogy. Induced fluid flow in the fracture, by which transmissivity effects are manifested, will be relatively unimportant. Fracture characterization is therefore limited to study of the Stoneley phase.

2.2.1 FWAL Stoneley Wave Attenuation Model

In the attenuation model of Mathieu (1984) the borehole is a long fluid-filled cylindrical cavity in an infinite elastic solid. The fracture-borehole system is saturated, and fluid flow in the fracture obeys Darcy's law. When a tube wave travels past the fracture, a portion of the propagating strain energy is lost to fluid flow. Incident energy is also scattered as transmitted and reflected tube waves as depicted in Figure 31. Continuity of pressure at the fracture requires

$$P_I(r) + P_R(r) = P_T(r) \qquad 27$$

(borrowing the notation of Mathieu, for consistency), where P_I and P_R are pressure functions for the incident and reflected tube waves, and P_T is for the transmitted wave. Fluid pressure associated with a tube wave is given by (Cheng and Toksöz, 1981)

$$P(r,z,t) \; \alpha \; I_0(nr)e^{i(\omega t - kz)} \; . \qquad (28)$$

increasing in amplitude outward from the borehole axis. Pressure amplitude of the transmitted tube wave is taken as limited-by and equal to the pressure at the borewall which is "seen" by the fracture. This is a reasonable approximation since (28) varies by no more than 10-20% over the borehole cross section. Fracture opening pressure and transmitted tube wave pressure are thus equal at

the borewall:

$$P_T(R) = P_F(R) \tag{29}$$

By averaging flow associated with tube wave particle velocity over the cross sectional area of the borehole, and averaging fracture flow rate over the aperture of the idealized system, mass conservation may be imposed to obtain an approximate balance of flows at the fracture horizon, at any moment in time. Thus if $<v>$ represents particle velocity averaged over flow area, and S_B, S_F are the flow areas of the borehole and fracture openings, then

$$S_B<v_I> = S_B<v_R> + S_B<v_T> + S_F<v_F> \tag{30}$$

where $<v_F>$ is the radial velocity of fracture flow averaged over the aperture. Characterizing the fracture response by Darcy's law, this balance equation provides the basis for deducing equivalent parallel-plate fracture aperture from comparison of P_I and P_T. The FWAL tool can be used to obtain only relative pressure $\dfrac{P_T}{P_I}$, by comparing pressure signal amplitude with- and without an intervening fracture. None of the velocities (flow rates) in the conservation equation are measureable, and so it is necessary to invoke the concept of acoustic impedance to obtain an equivalent parallel-plate fracture aperture. Impedance is defined as

$$Z = \frac{<P>}{<v>} \tag{31}$$

where $<P>$ is fluid pressure averaged over flow area. Impedance Z_B for borehole tube wave propagation, and impedance Z_F for flow in a parallel plate fracture system can be readily calculated (Appendix B). The measurable pressure ratio can then be expressed

$$\frac{P_T}{P_I} = \frac{P_F}{P_I} = \frac{Z_F v_F}{Z_B v_I} = \frac{1}{1+X} \tag{32}$$

where

$$X = \frac{nL_0}{2} \frac{I_0(nR)}{I_1(nR)} \frac{Z_B}{Z_F} \tag{32a}$$

$$Z_B = c\rho_f \; , \quad Z_F = \left\{ \frac{L_0^2}{12\mu} \left[\frac{1}{2R} + \frac{2}{\pi} \left(\frac{\omega}{b} \right)^{\!\frac{1}{2}} \right] \right\}^{-1} \tag{32b,c}$$

This relationship is compared with observed fractional attenuation to determine an appropriate value for transmissivity $\frac{L_0^3}{12} \frac{\rho g}{\mu}$. Calculated fractional attenuation is plotted against aperture and frequency in Figures 32 and 33, using geometry and formation parameters appropriate for well EBR-4.

2.2.2 Application of FWAL Attenuation Model

Evaluation of fractional attenuation of FWAL waveforms is simplified since the recorded signal is exactly the pressure amplitude required. The effect of a significant fracture on these waveforms is such that phase changes occur within the Stoneley packet in addition to attenuation. Direct comparison of waveform feature amplitude is thus undefined, and a spectral approach is used. Spectral ratio methods for estimation of intrinsic attenuation in FWAL have been used in association with the head waves and pseudo-Rayleigh modes, with limited success (Willis, 1983). An important finding of this work is that when using waveforms from different transmitter-receiver pairs to characterize attenuation of a particular phase, stability can be improved with a constant length window shifted to the arrival of the phase at each receiver. Window length is determined so as to include as much of the phase as possible while excluding other phases.

A similar approach is useful in the investigation of Stoneley phase attenuation. For multiple receiver FWAL data, Stoneley phase amplitude is compared at the near and far receivers. Since formation properties vary only slightly exclusive of fractures in the crystalline sections considered, Stoneley velocity is stable at about 95% of the borehole fluid velocity (clean water). The beginning of the window is located at the earliest onset of the Stoneley phase for each

transmitter-receiver pair. The invariant window length is determined so as to include only the packet arriving at the fluid delay.

The ratio of far:near amplitude is determined from the respective amplitude spectra, in the form of a ratio spectrum. In the results presented here, a Hamming (1977) window is applied to the constituent time windows. To calculate a log of pressure ratio vs. depth it is desirable to reduce the ratio spectrum at each depth to a single representative value. Since the FWAL attenuation model is minimally dependent on frequency (Figure 32), it is reasonable to average the ratio spectrum over the frequency band where the incident tube wave has significant amplitude.

When signals from near and far receivers are compared for an unfractured interval in a homogeneous formation, a pressure ratio of unity should result. This is not often the case, because FWAL receiver gain is uncalibrated. To prevent receiver bias from producing a baseline transmissivity response, observed pressure ratio is corrected by a factor derived from the pressure ratio in a known unfractured interval or casing.

Structural features of the borehole and the formation adjacent to the hole produce variability in FWAL waveforms. Changes in borehole diameter can scatter tube wave energy, creating secondary tube waves and radiating body waves (Stephen, et al., 1985). Changes in the elastic properties of the formation can produce reflections (Paternoster, 1985), and reduce transmission (Bhasavanija, 1983) which may be interpreted as apparent attenuation. Also important is the stability of the spectral ratio method when a fracture intervenes between the transmitter and the near receiver. When this occurs both near and far waveforms are attenuated and the spectral ratio method may be vulnerable to noise or extraneous phases. Calculated transmissivity seems most reasonble where fracture spacing is on the order of the source-receiver separation and

not much less. Extremal points calculated for densely fracture zones, and just below highly attenuative features, are probably erroneous. Significant features in the calculated logs consist of several points over a small depth interval which is greater than the receiver spacing of the tool.

2.2.3 FWAL Analysis of Well EBR-4, Mirror Lake, New Hampshire

Three different FWAL tools were deployed in well EBR-4: resonant-source tools with characteristic frequencies of 34 and 15 kHz., and a sparker source tool which operates at about 5 kHz. A comparison of fracture transmissivity for each type is presented in Figure 34. These calculated logs have been prepared from the FWAL data of Figures 10, 11 and 12. The use of transmissivity accentuates the variability in attenuation with depth. For these calculations a single fracture is assumed to intervene between the two receivers. Transmissivity calculated from the higher frequency tools responds more impulsively at or near fractures than the transmissivity at 5 kHz. (sparker source). Since the Stoneley packet is contaminated by higher frequencies (sections 1.3 and 2.2), the responses are probably due in part to scattering of pseudo-Rayleigh energy at fractures and where fractures induced spalling of the borewall. Transmissivity calculated for sparker data is less localized but seems to corrlate with televiewer and pump test fracture indications (Figure 34).

3. DISCUSSION

Fracture parameters calculated using the published models are summarized in Table 2. A discrepancy exists between transmissivity derived from FWAL Stoneley attenuation and from VSP tube wave generation, for the Mirror Lake experiment. The Stoneley phase was not observed in FWAL data from the Britton well. FWAL Stoneley attenuation is a relatively near-field phenomenon which is sensitive to fractures which are open near the borehole. Conversely, the VSP response is evidently produced at those fractures which are in hydraulic communication and are capacious for some distance away from the borehole. Both models are approximate since simplifying assumptions must be made to avoid excess parameterization. It will be shown below that the FWAL model is in much better agreement with flow test and televiewer data than the VSP model. An explanation for the discrepancy is presented in section 3.3, in the form of a (VSP) tube wave generation model which utilizes stress equlibrium across a fracture with intrinsic stiffness.

Comparable frequency dependence of the (VSP) model (Beydoun, et al. 1985) and ratio spectra derived from field data support the low frequency approximation which is central to the model. If the approximation were violated because of turbulent flow the theoretical and observed spectral ratios would probably have deviated markedly over the source band. Ratio spectra calculated from field data by the method of section 2.1.3 are affected by the windowing process, which tends to homogenize the spectra. However, the source band for the Britton experiment spanned more than two octaves over which consistent frequency dependence was observed.

Survey instrumentation typically available for hydrophone VSP has finite dynamic range. If the hydrophone signal amplifier gain is set to just record the compressional wavelet, then the smallest amplitude ratio which can be record-

ed with precision is app. unity, leaving most of the digital range for tube wave recording without clipping. The range of measurable tube-to-P amplitude ratios is thus about 30 db, corresponding to a range of transmissivity of 66db. The presence of noise which cannot be removed from the source band tends to reduce this range. Measurable range is thus constrained by the borehole radius, formation and fluid properties, source bandwidth, dynamic range of recording equipment, and sensivity of that equipment to ambient noise.

3.1 Plane Fracture Orientation

Acoustic borehole televiewer logs of the (VSP) tube wave generating horizons show distinctly that these features are tabular and intersect the borehole obliquely (Figure 15). Reasonable agreement is obtained between the orientation of these features determined from VSP model inversion, and the orientation from televiewer images corrected for well deviation and magnetic field orientation (Table 2).

The premise that fracture parameters determined from inversion are unique, given that the low frequency approximation is valid, is supported by the agreement between predicted fracture orientations and independent observations at Britton well #2 (Table 2). The mode conversion mechanism is evidently controlled by incident angle, and thus by the direction of particle motion associated with the incident wave. The actual amplitude of closure, and whether closure is everywhere uniform on the fracture are not clarified by these results.

For well EBR-4 the agreement between inversion and televiewer orientation is not so striking. This is due partly to the survey geometry and the character of the source. The VSP survey geometry was designed to provide multi-offset coverage over the full length of the hole. Practical considerations did not permit zero-offset coverage. All of the direct paths from the shot points to the horizon at 44m. were therefore very shallow, providing offset coverage for this

depth which was inferior to the Britton well survey. The source band was lower, and the source-time function more complicated for the Mirror Lake survey because the shot points were located in the surface layer. The highest quality orientation calculations (Britton well #2) were obtained using frequency dependence (nonlinear inversion) and were associated with the most impulsive source. Simple filter theory may

In principle the nonlinear inversion frequency dependence is sufficient to obtain fracture orientation data from fewer than three VSP offsets. In practice, the applicability of the model assumptions to the real earth is such that three or more offsets are needed to geometrically resolve fracture orientation. Observed tube:P-wave amplitude ratio was lower than predicted near the edges of the source band, suggesting that the assumed conversion mechanism may be only part of the complete process of tube wave generation.

3.2 Comparison with Independent Transmissivity Determinations

3.2.1 Inflow Measurement at Britton Well #2

Britton well # 2 was drilled pneumatically, with air as circulating medium, and thus water inflow during the drilling process could be crudely determined. Drill pipe was added to the string in 6m stands and groundwater flow into the hole was observed during the circulation hiatus when each stand was installed. Before drilling resumed the hole was blown clear of water and the pressure required to do so recorded. The rate of inflow over the entire uncased length of hole can thus be estimated given the approximate time of each operation. The spatial resolution of the method is limited to the length of one stand, and inflow may at any time have be affected by hydraulic communication between fractures away from the borehole. Some drawdown behavior was observed whereby the rate of inflow decayed during a day of drilling, but inflow trends from each stand to the next were large enough to be identifiable.

The flow rate through an equipotential surface of radius r in steady, axisymmetric flow in a horizontal parallel plate fracture system is given by Darcy's law (Ziegler, 1976):

$$Q = 2\pi r T \frac{\partial h(r)}{\partial r} \; , \qquad (33)$$

To determine T from observable quantity Q it is convenient to assume that hydraulic head is zero at the borewall $(h(R) = 0)$ and is a known constant $(h(d) = h_d)$ at some radial distance d from the borehole. The first order differential equation above is then integrated for h and the boundary conditions are applied:

$$T = \frac{Q}{2\pi h_d} \ln\!\left[\frac{d}{R}\right]. \qquad (34)$$

As each tube wave generating horizon was penetrated, inflow increased by roughly 1 liter per second, which is taken as an approximate inflow estimate. If the corresponding far-field fracture pressure was of order 1 bar $(h_d = 10m.)$, then the transmissivity of the inflow horizons encountered in drilling is $T = 0.1 - 1.0 \; cm^2/sec$ (Tables 2 and 4). The borehole head $h(R)$ is increasingly positive as the hole fills above the level of the fracture, resulting in underestimation of T. In addition gravitational effects and angular borehole-fracture geometry are neglected. This estimate is rough, but it corresponds to an equivalent flow aperture which is an order of magnitude greater than predicted by (19).

3.2.2 Pump Testing at Mirror Lake Well EBR-4

A constant-discharge pump test was performed on two successive days immediately prior to the VSP experiment (Paillet, oral communication). While water was pumped from well EBR-4, the levels of wells EBR-1, 2 and 3 were monitored. In addition a sensitive flowmeter was used in EBR-1, 2 and 3 to determine the depths where outflow (and inflow) occurred. Hydraulic communication was

produced between the peripheral wells and EBR-4 by pumping, and the path of communication was defined by flow measurement. Water level changes in the peripheral wells were used during the test to establish that steady flow conditions were achieved. The levels in EBR-1, 2 and 3 fell at a fairly constant rate from the start, as 7.6 liters/minute were discharged from EBR-4 (Figure 35). Water loss from storage in all four boreholes constituted about 30% of the total discharge from pumping. Water level in the four wells fell virtually in unison throughout the test.

A wireline flowmeter operating on a heat-pulse, mass flow principle (Hess, 1982) was deployed successively in the four wells. The tool was positioned at a fixed depth in the hole and axial fluid velocity in the borehole measured repeatedly. Flow measurements at different depths were used to locate discrete inflow/outflow horizons to within one meter.

To the accuracy of the tool (about 5% of total discharge), all of the inflow to EBR-4 entered at 44 meters. This depth corresponds exactly to indications of a major fracture in the televiewer and FWAL logs, to within the accuracy of depth measurement or roughly 0.3 meters. The principal observed VSP tube wave generating horizon lies within a few meters of this depth as well.

Outflow from EBR-1, 2 and 3 was also isolated to single, discrete fractures in each well. If fracture orientation from televiewer logs is extrapolated away from each well to the other wells, it becomes apparent that the flow paths connnecting EBR-1, 2 and 3 with EBR-4 do not follow any identifiable planar fracture. Either there is communication between different sets of subparallel fractures, or the major fracture is not planar.

Inflow was observed in EBR-2, about 4 meters below the outflow horizon. The two depths correspond to similar televiewer indications of parallel fractures. During the test the level in EBR-2 was lower than that of EBR-1 and 3, so

inflow to EBR-2 is strong evidence for indirect flow paths between the four wells. Extrapolated televiewer orientation trends show possible correlation of the inflow point of EBR-4 with the outflow from EBR-2, however the apparent thickness of the fracture (zone) differs significantly. Correlation between the outflow points of EBR-1 and 3 with the features of EBR-2 and 4 is difficult, as is correlation of the outflow points of EBR-1 and EBR-3 (Figure 36).

Transmissivity between the wells was evaluated (Paillet, oral communication) using a formula for a couplet of wells connected by a single, infinite parallel-plate fracture. Considering the fracture as a thin porous layer they calculated transmissivity between pairs of wells consisting of EBR-4 and EBR-1, 2 or 3. The results vary between 0.3 cm^3/sec and 2.3 cm^2/sec and are given in Table 3. These are approximate since only well couplets are considered, and actual flow paths between the wells are probably indirect.

3.3 Intrinsic Fracture Stiffness

For the two tube wave generating horizons for which independent estimates are available, transmissivity calculated from the VSP tube wave generation response is significantly smaller than that deduced from direct flow observation. Moreover, the FWAL attenuation model predicts transmissivity values which are comparable in magnitude to the flow test data. It is reasonable then to consider how the VSP model departs from realism and what are the impacts on calculated transmissivity.

A realistic, in situ fracture transmits the static forces of overburden, Poisson-effects caused by changing load conditions and finite rigidity, and tectonic forces. A significant portion of the stress-bearing performance of a saturated fracture system may come from fluid pressure (effective stress), but equilibrium is maintained by bridging of irregularities in the fracture walls. Natural conditions may exist where fracture opening support is derived from ex-

cessive fluid pressure or large pressure gradients, but these are local effects which only change the scale length of bridging by asperities.

In the displacement formulation (21) the incident P-wave displacement amplitude is taken as the assumed amplitude of fracture closure. If the fracture stiffness (resistance to normal closure) were close to that of the formation, closure would be small since the fracture width is much less than a wavelength. Conversely, if the fracture offered little resistance to closure it would behave much like a free surface: closure would be about twice the P-wave displacement and there would be no transmitted P-wave. Examination of field data shows little dimunition of transmitted amplitude (Figure 22). The fracture closure assumption is a compromise, tending to underestimate permeability since the closure amplitude associated with observed transmissivity is smaller than the P-wave displacement.

The variability of bridging in any direction may be expressed as the characteristic scale length, or distance between points of contact. To develop an asperity contact model for comparison to the displacement formulation, it is helpful to recognize that the scale length is much smaller than a wavelength at exploration frequencies. Fracture deformability can then be simplified to a relation between perpendicular compressive stress and fracture closure. For seismic processes no detectable "set" is imparted to a fracture by the passage of a seismic wave, and elastic behavior is assumed. If linear behavior is also assumed, then fracture deformability is specified by a single parameter: intrinsic stiffness (or its inverse compliance). Such a model is equivalent to a thin layer of finite thickness, which is more deformable and permeable than the imtact mass.

Derivation of (observable) tube:compressional wave pressure ratio using intrinsic stiffness κ begins with a relationship of fracture aperture to external

stress and internal pressure:

$$L(s,t) = (P_f(s,t) - P_n(t))/\kappa. \tag{35}$$

where P_f is the transient fluid pressure in the fracture associated with the incident normal stress P_n. (For consistency of notation with section 2.1.1, $P_f(s,t) = H(s,t) - H_0$.) The incident normal stress is uniform everywhere on the fracture, and the static equilibrium imposed by (15) ensures that it is uniform across the fracture as well. By contrast, in (7) the fracture wall displacement is everywhere uniforme.

The incident stress is easily found for an incident plane wave travelling along an arbitrary axis x' with harmonic displacement. Axial and transverse normal stresses are simply

$$u(x',t) = \zeta_0 e^{i(\omega t + kx')} \tag{36a}$$

$$P_{x'x'} = i\rho\omega\zeta_0\alpha e^{i(\omega t + kx')} \tag{36b}$$

$$P_{z'z'} = P_{y'y'} = i\rho\omega\zeta_0\frac{(\alpha^2 - 2\beta^2)}{\alpha}e^{i(\omega t + kx')}. \tag{36c}$$

If the arbitrary axis x' forms an included angle of φ with the fracture normal, then the normal stress on the fracture is derived from Mohr's circle:

$$P_n = \frac{P_{x'x'} + P_{z'z'}}{2} + \frac{P_{x'x'} - P_{z'z'}}{2}\cos 2\varphi = i\omega P_\zeta e^{i\omega t} \tag{37}$$

Substitution yields the following expressions for aperture and its time derivative:

$$L(s,t) = L_0 + (P_f(s,t) - i\omega P_\zeta e^{i\omega t})/\kappa \tag{38a}$$

$$\frac{\partial L}{\partial t} = \frac{1}{\kappa}\left[\frac{\partial P_f}{\partial t} + \frac{\omega^2 P_\zeta}{\kappa}e^{i\omega t}\right] \tag{38b}$$

If the amplitude ζ_0 of transient closure is much smaller than the static aperture $(|L(s,t) - L_0| \ll L_0)$ then to a good approximation the static aperture may be used in flow calculations. A description of 1-D steady fracture flow is found in the "cubic law" (Snow, 1965)

$$q(s,t) = -\frac{L_0^3}{12\mu}\frac{\partial P_f}{\partial t} , \qquad \frac{\partial q}{\partial s} = \frac{-L_0^3}{12\mu}\frac{\partial^2 P_f}{\partial s^2} \tag{39a,b}$$

Following the displacement formulation, the continuity equation is used to relate inflow, displacement and storage of fluid in a volume element of fracture fluid:

$$-dqdt = \frac{dL}{dt}dsdt + L(s,t)\gamma\frac{dP_f}{dt}dsdt. \tag{40}$$

Rearranging and switching to partial derivatives (functions $L(s,t)$ and $P(s,t)$ are both separable in independent variable s and t) gives

$$-\frac{\partial q(s,t)}{\partial s} = \frac{\partial L(s,t)}{\partial t} + L(s,t)\gamma\frac{\partial P_f(s,t)}{\partial t} \tag{41}$$

Substituting (38a,b) and (39a,b) the following nonlinear equation is found:

$$\frac{\partial^2 P_f}{\partial s^2} = \frac{\partial P_f}{\partial_t}\left\{ D_1 + D_2\,e^{i\omega t} \right\} + D_3 P_f\,\frac{\partial P_f}{\partial t} \tag{42}$$

$$D_1 = \frac{12\mu}{L_0^3}\left[\frac{1}{\kappa} + \gamma L_0 \right] , \qquad D_2 = -i\cdot\frac{12\mu\omega\gamma P_{\zeta_0}}{L_0^3\kappa} \tag{42a,b}$$

$$D_3 = \frac{12\mu\gamma}{L_0^3\kappa} , \qquad D_4 = \frac{12\mu\omega^2 P_{\zeta_0}}{L_0^3\kappa} \tag{42c,d}$$

Whereas (42) is nonlinear, the importance of linear vs. nonlinear terms to the solution depends on the coefficients $D_1, D_2, \ldots$ By assigning realistic values to formation and fluid properties, and reasonable bounds to the pressure behavior, the coefficients for the second and third terms of the right hand side are shown to be relatively small (Appendix A). The approximate linear equation is

$$\frac{\partial^2 P_f}{\partial s^2} = D_1\frac{\partial P_f}{\partial t} + D_4\,e^{i\omega t}. \tag{43}$$

The boundary conditions applicable to the analytical solution are $P_f(0,t) = 0$, and finite pressure at arbitrarily large s. The resulting solution (Appendix A) is

$$P_f(s,t) = \frac{iD_4}{\omega D_1}\left[1 - e^{\left\{-s\sqrt{\frac{\omega D_1}{2}}(1+i)\right\}}\right]e^{i\omega t} \tag{44}$$

A linear approximation is used to relate the readily obtained 2-D solution (20) to realistic 3-D geometry. Pressure P_f is approximated by a linear function on the interval $s = [0,d]$ in order the resulting 2-D ejected volume V_{2D} may easily be converted to the necessary 3-D volume V_{3D}. The ratio of compressional:tube wave pressure ratio can then be obtained in the same manner as the displacement formulation (Appendix A). This ratio is plotted for various values of stiffness in Figure 37 using normal incidence, zero-offset geometry.

Pressure ratio is plotted against $\log_{10}$ of fracture stiffness in Figure 38. The four curves correspond to source offsets for the Mirror Lake experiment. "Observed" amplitude ratio values at 150 Hz. for offsets A thru D are indicated.

Pressure ratio increases between the water-layer and virtual-layer stiffness bounds. For stiff fractures pressure ratio is reduced because the fracture is held open by asperity contact. As stiffness decreases the effective radius $S_{10\%}$ does also, which reduces borehole pressure "amplification" by the cylindrical geometry, which in turn reduces the generated tube wave amplitude. This behavior can be seen in Figure 39, where 2-D pressure is plotted against distance s from the "borehole" boundary. For decreasing stiffness, the 2-D pressure attains larger amplitude, but closer to the borehole. For unrealistic stiffness values far below the equivalent water-layer bound (by a factor of 4 or more), pressure ratio p^t/p^a actually decreases due to this effect.

If equivalent parallel-plate flow aperture is assigned to static aperture L_0, then the appropriate stiffness may be found by matching the "observed" pressure ratios to the model (Figure 38). For the Mirror Lake EBR-4 fracture at 44m., the average flow aperture from all tests is 0.55 mm. Stiffness values appropriate for each offset at 150 Hz (source band center frequency) vary

between 2.6×10^{12} to 1.2×10^{13} (MPa/meter). The corresponding equivalent water-layer, and virtual layer stiffness values are 3.6×10^{12} and 3.5×10^{14} MPa/m., respectively. The following observations are based on Figures 37 and 38:

1. Calculated stiffness values lie toward the low end of the expected range.
2. One of the values is smaller than the equivalent water-layer value.
3. A spread of values is obtained for the fracture at 44m.
4. Frequency dependence of the pressure model is greater than that of the ratio spectra derived from data.

Intrinsic stiffness evidently contributes to the forces which resist closure, imparting roughly as much stiffness as an undrained water layer with thickness equal to the parallel-plate flow aperture. If intrinsic stiffness is to be characterized by a thin layer, the layer compressibility may actually be far less than water. This is because the mechnical aperture is several times greater than the flow aperture. It is known from in situ experiments in jointed crystalline rock that mechanical (real) aperture is typically several times larger than equivalent parallel-plate flow aperture (Voegele, et al., 1981). The difference is attributed to flow path tortuosity. In the compressible layer model, compressibility must increase with increasing thickness, to attain the same stiffness. In this context the low stiffness values deduced for EBR-4 represent the ratio of real aperture (larger than flow aperture) to equivalent layer compressibility which is significantly greater than that of water.

The disparate values for fracture stiffness are difficult to explain. Effective radius $s_{10\%}$ typically takes on values of 8 to 10 meters depending on stiffness and frequency. From flow measurements and televiewer correlation, the continuity of the fracture at 44 m. in EBR-4 is less than 10 m., or the separation of EBR boreholes (Figure 36). Thus the EBR holes probably interfere, reducing the tube wave amplitude observed in any one hole. Moreover, the nature of interference may depend on azimuth of the incident wave (stiffness values for similar azimuths B & C are nearly the same). Evidence that flow paths for com-

munication between holes (section 3.2.2) are irregular and utilize different fractures with conjugate orientation, further complicates interpretation of fracture responses in terms of laterally contiguous models.

Transmissivity of $\sim$0.5 cm^2/sec was estimated for the fracture at 290 meters in Britton well #2 (Tables 2 and 4). This corresponds to a parallel-plate flow aperture of 400 μm. Using this value in the stress model (20), and setting stiffness κ to that for an undrained water layer with thickness equal to flow aperture, results in tube:P pressure ratios of order unity or less at the peak frequency (200 Hz). To match the "observed" ratios of 2.5 - 8 using the same stiffness assumption requires a flow aperture of $\sim$700μm, or transmissivity of $\sim$3 cm^2/sec. The stiffness model could be parameterized so as to yield (VSP) amplitude ratios and flow apertures which closely match field data, by reducing the stiffness. Relatively less stress would then be transmitted across the fracture by the asperities, and more by the fluid. Increased fluid pressure gradients would drive greater dynamic fluid exchange with the borehole. The equivalent-water-layer compromise tends to underestimate dynamic flow (VSP response), and underestimate pump test response.

4. CONCLUSIONS

1. The borehole televiewer, FWAL (Stoneley wave attenuation) and hydrophone VSP (tube wave generation) responses are characteristic of different types of fractures. The televiewer records the trace of every fracture and does not distinguish weathered, open, or hydraulically important features. The FWAL tool attenuation response occurs at only a few of the fractures detected by the televiewer, and is always associated with such a fracture (when the borewall is otherwise smooth). The FWAL responds to fractures which are open only near the hole, possibly due to drilling damage, in addition to those which are major fluid conduits. In the work reported here the VSP response occurs only at hydraulically significant features, probably because greater depth of investigation and sampling area.

2. Based on this work, the following sequence is suggested for integrating the seismic methods into hydrologic site investigation. For borehole permeability testing in jointed material, the televiewer and/or FWAL should be used to establish the axial distribution fractures. Where there are few fractures, transmissivity is relatively low. The FWAL in conjuction with a caliper can discriminate significant features if the borewall is smooth and if the Stoneley phase is excited. Relative trends in the density of apparently open fractures may be associated with overburden depth or structural origin. The FWAL response may be helpful in understanding conventional density, gamma, temperature and electrical logs. Hydrophone VSP utilizing an impulsive source at a single moderate offset distance, should respond at major open fractures. Once tube wave generating horizons have been located, additional offsets may yield orientation information depending on the character of the data. Spectral ratio methods seem to work best if the generating horizon is a single fracture, and the wavetrain is not complicated by multiple fractures or reverberation. Borehole flowmeter measure-

ments of the type made at Mirror Lake EBR-4, with or without an associated pumping event, can pinpoint the sources and sinks of steady flow. This may be the only direct measurement which detects zones of flow in response to natural exception to hydrostatic conditions, connected by the open borehole. Pump testing is the end member of the sequence, and probably most costly for sampling heavily fractured formations.

3. The displacement formulation of the (VSP) tube wave generation model underestimates transmissivity by about one order of magnitude. This was observed in EBR-4 and Britton #2, with the reliability of independent transmissivity estimates considerably better for EBR-4. The underlying reason is probably the assumption for amplitude of fracture closure. The stress formulation provides transmissivity values which are in agreement with the pump test and FWAL results, but requires a priori knowledge of fracture stiffness.

4. As a first approximation, fracture stiffness is of the same order as that of the undrained fluid layer with thickness equal to the flow aperture. Additional field data sets which include pump test results are needed to generalize about stiffness, or to find other means of determining this parameter. Shear zones or seams filled with soft, relatively impermeable clay-like material may actually have stiffness which is much smaller than expected from the flow aperture. This behavior would result in overestimated transmissivity, but might be predicted from televiewer images showing very large apertures (Figure 15).

5. The basic assumptions underlying the (VSP) generation model are supported by agreement with field results. Frequency dependence in the source band is comparable to that observed. Some evidence that incident energy couples to the fracture fluid through normal displacement of the fracture wall is given by the agreement of calculated orientation with televiewer indications at Britton #2 (fractures at 210, 290 m.). Orientation calculations are more successful with a broadband source discharged well within the bedrock, reducing the surface

reflection and surface layer reverberation, and improving accuracy of recorded frequency dependence of p_t/p_a. The dynamic range of permeable features which can be investigated depends somewhat on the apparatus used, in addition to formation properties, borehole geometry, and the ambient signal noise level.

5. Wells EBR-1,2,3 and 4 provided a good opportunity to correlate structural characterization and transmissivity determinations between three adjacent boreholes. Structural expressions deduced from televiewer images could not be correlated between holes space 10 m. apart, which is only confirmation that fracture continuity cannot be estimated from single-borehole observations. Individual fractures can be observed in the thin fracture zone at 44 m in EBR-4, which exhibit orientations quite different from the zone at large. (Orientation deduced from VSP tube wave generation is more consistent with that inferred for the zone.) Transmissivity measured under steady flow conditions at the same horizon varied by a factor of 2 between different pairs of wells. Inflow observed in one of the observation wells during constant discharge from EBR-4 is strongly suggestive of channel flow. Quantitative work in such a heterogeneous medium requires close attention to the characteristic scale of measurement, and the relation of the affected region to the rock mass.

APPENDIX A

VSP Generation Model, Stress Formulation Linear Approximation

To compare magnitudes of the various terms of the right hand side of (42), known values for α, β, ρ, γ, φ, and ω are adopted, and the magnitudes of the derivatives are estimated. If the strain amplitude of the incident wave is taken as 10^{-6}, then the displacement amplitude is known to be $A = \frac{\alpha}{\omega} \cdot 10^{-6}$, and P_ζ is determined. The magnitude of the fluid pressure is limited to the incident stress magnitude $|P(s,t)| \leq \omega P_\zeta$. The time derivative of the fluid pressure is approximated by the maximum time derivative of the incident pressure:

$$\left| \frac{\partial P_f}{\partial t} \right| \approx \omega^2 P_\zeta$$

Stiffness for a fracture of specified aperture is bounded approximately by the behavior of an equivalent layer of water, and a layer of intact rock ("virtual" layer). For the undrained fluid case stiffness is $\kappa = \frac{k}{L_0}$, where k is dynamic bulk modulus. In the virtual fracture case stiffness is the ratio of stress to integrated strain or $\kappa = \rho \alpha^2 / L_0$.

Taking the magnitude of the fourth term $D_4 e^{i\omega t}$ as unity, the terms of the right hand side are compared in Table A1. The estimated magnitudes of the second and third terms are equivalent and are more than four orders of magnitude smaller than the remaining terms. This result is independent of fracture stiffness. Based on the $\times 10^4$ difference in magnitude, the second and third (nonlinear) terms of (42) are dropped from the model. Errors in magnitude estimates for the dropped terms, due to approximations used for P_f and $\frac{\partial P_f}{\partial t}$, are assumed to be much less than 10^4. The linearized model then takes the tractable form

$$\frac{\partial^2 P_f}{\partial s^2} = D_1 \frac{\partial f}{\partial t} + D_4 e^{i\omega t} \tag{A1}$$

with analytical solution

$$P_f(s,t) = A_1 e^{A_2 t + A_3 s} + \frac{A_4}{\omega} e^{i\omega t} + A_5 s + A_6. \tag{A2}$$

Substituting into (A1) yields the conditions

$$A_4 = \frac{iD_4}{D_1}, \qquad A_3 = \pm\sqrt{D_1 A_2}. \tag{A3a,b}$$

If $P(s,t)$ is to be finite at large s or t, then it is clear that $A_5 = 0$, $A_3 = -\sqrt{D_1 A_2}$, and A_2, A_3 are complex with magnitudes no greater than unity. At large s the pressure reduces to

$$P_f(s \to \infty, t) = \frac{iD_4}{\omega D_1} e^{i\omega t} + A_6 = \frac{i\omega P_\zeta}{1 + \kappa \gamma L_0} e^{i\omega t} + A_6. \tag{A4}$$

At the borewall the condition $P(0,t) = 0$ is applied as in the displacement formulation, which yields

$$P(0,t) = A_1 e^{\text{Re}\{A_2\}t \ (\cos \text{Im}\{A_2\}t \ + \ i \ \sin \text{Im}\{A_2\}t)} + \frac{iD_4}{\omega D_1} e^{i\omega t} + A_6. \qquad \text{(A5)}$$

Equating like terms yields

$$A_1 = -\frac{iD_4}{\omega D_1} , \qquad A_6 = 0. \qquad \text{(A6a,b)}$$

$$P(s,t) = \frac{iD_4}{\omega D_1} \left[1 - e^{\left\{ -s \sqrt{\frac{\omega D_1}{2}} (1+i) \right\}} \right]_{e^{i\omega t}} \qquad \text{(A7c,d)}$$

$$P_\zeta = \rho \zeta_0 (\alpha - \frac{\beta^2}{\alpha}(1 - \cos 2\varphi)) \qquad \text{(A6e)}$$

Pressure amplitude of the generated tube wave may be calculated in the same manner as the displacement formulation (Beydoun, et al. 1985), if the 2-D pressure function is first linearized. This approach while approximate, circumvents solution of the linearized but nonseparable partial differential equation in cylindrical coordinates.

The distance $s_{10\%}$ from the borehole at which the pressure gradient magnitude decays to 10% of its value at the borewall, is determined analytically:

$$\left| \frac{\partial p(s_{10\%})}{\partial s} \right| = 10\% \left| \frac{\partial p(0)}{\partial s} \right| , \qquad s_{10\%} = \ln\left\{ \frac{1}{10\%} \right\} \sqrt{\frac{2}{\omega D_1}} \qquad \text{(A7a,b)}$$

Variation of the 2-D pressure in the interval $[0, s_{10\%}]$ must be approximated as a linear function, in order to apply the 2-D result to fracture flow in 3-D. A plot of complex pressure function P_f with time dependence $e^{i\omega t}$ removed, is shown for frequency of 200 Hz. (Figure 39). The dominant imaginary component is in-phase with the normal stress field incident on the fracture. The integral of pressure magnitude on $s = [0, s_{10\%}]$ represents the dominant behavior and can be used to obtain the linear approximation:

$$P_f(s,t) \approx s P^*(t) , \qquad P^*(t) = \frac{2}{s_{10\%}} \int_0^{s_{10\%}} |P_f(s,t)| \, ds \qquad \text{(A8a,b)}$$

The volume ejected from the 2-D fracture during a half-cycle of fracture closure is corrected to 3-D radial flow, and equated to the integrated dilatation for one half-cycle of a tube wave at the same frequency. Tube wave amplitude factor C is thus determined in terms of the amplitude of particle motion for the plane wave incident on the fracture. This is an upper bound on the amplitude of the generated wave, since fluid dilatation is conserved. Ejected 2-D volume is

$$V_{2D} = \frac{L_0^3 P^*}{12\mu s_{10\%}} \int_0^{\frac{\pi}{\omega}} \sin \omega t \, dt = \frac{L_0^3 P^*}{6\mu \omega s_{10\%}}$$

The correction to radial geometry follows the displacement formulation exactly. Using (10), (11a) and (12).

$$V_{3D} = 2\pi R \chi V_{2D}$$

using the same definitions for χ and d. Tube wave amplitude factor C is then

$$C = \frac{n V_{3D}}{4\pi R k (2 - c^2/\alpha_f^2) I_1(nR)}. \qquad (A11)$$

Pressure amplitude of the direct compressional wave at the borehole sensor was determined by White (1983, p.149). Following the displacement formulation the tube:compressional wave pressure amplitude ratio takes the form

$$\frac{p^t}{p^a} = \frac{(\rho_f c^2 C I_0(nR)) \ (\beta^2(1 - \frac{c}{\alpha}\cos \vartheta)^2)}{\omega \alpha \rho_f c^2(1 - 2(\frac{\beta}{\alpha}\cos \vartheta)^2)}$$

APPENDIX B

FWAL Attenuation Model, Impedance Derivations

Borehole Impedance

The Stoneley wave pressure in a cylindrical borehole is given by

$$P(r,z,t) = C \cdot I_0(nr) e^{i(\omega t - kz)}.$$
(B1)

The average pressure over one half-cycle is found by integrating the time dependence over $T/2$, corresponding to a compressional phase. This pressure is described by

$$P(r) = D \cdot I_0(nr).$$
(B2)

The average of $P(r)$ over the borehole cross section is found by integrating radially:

$$<P> = \frac{1}{\pi R^2} \int_0^R D \cdot I_0(nr) 2\pi r \, dr = \frac{2D}{nR} I_1(nR)$$
(B3)

Axial particle velocity can be obtained from the pressure $P(r,z,t)$ since

$$v(r,t) = \frac{\partial u_k(r,t)}{\partial t} = \frac{\partial}{\partial t} - \frac{ik}{\rho_f \omega^2} P(r,t)$$
(B4)

The average velocity over the borehole cross section is found by integrating radially:

$$<v> = \frac{1}{\pi R^2} \int_0^R \frac{kD}{\rho_f \omega} I_0(nr) 2\pi r \, dr = \frac{2kD}{\rho_f \omega nR} I_1(nR)$$
(B5)

Finally, impedance is simply the ratio of average pressure to velocity. Forming this ratio and simplifying, the borehole impedance of Stoneley wave flow is

$$Z_B = \rho_f c$$
(B6)

Impedance of a Single Fracture

The pressure average at the fracture opening in the borewall is simply P_f. Flow velocity and flow rate are related by

$$q(R) = Sv(R) = 2\pi R L_0 v(R)$$
(B7)

The flow rate $q(r,t)$ is obtained from Darcy's law and is time-averaged over one half-cycle by integrating the time dependence over $T/2$, corresponding to a compressional phase. The result is

$$q(R) = \frac{2\pi R P_f}{\mu} \frac{L_0^3}{12} \left\{ \frac{1}{2R} + \frac{2}{\pi} \left[\frac{12\gamma\mu\omega}{L_0^2} \right]^{1/2} \right\}$$
(B8)

Combining to obtain average velocity, and taking the ratio of pressure to velocity,

$$Z_f = \frac{<P>}{<v>} = \frac{P_f}{q(R)/S} = \frac{L_0^2}{12\mu} \left\{ \frac{1}{2R} + \frac{2}{\pi} \left[\frac{12\gamma\mu\omega}{L_0^2} \right]^{1/2} \right\}$$
(B9)

Fracture Characterization

Notation

α, β, ρ	formation P-velocity, S-velocity, density
α_f, ρ_f	borehole fluid velocity, density
R	borehole radius
μ, γ	borehole fluid dynamic viscosity (Pa-sec) and compressibility (Pa^{-1})
ζ_0	amplitude of P-wave displacement in the formation
$u(t)$	P-wave displacement in the direction of propagation
$\mathbf{n}$	fracture unit normal vector
$\mathbf{p}$	incident P-wave wavenumber unit vector
$\mathbf{b}$	borehole unit direction vector, oriented downward
φ	included angle between P-wavenumber and fracture normal
ϑ	included angle between P-wavenumber and borehole axis
ψ, σ	fracture strike and dip angles
$L(s,t)$	fracture aperture, as a function of 2-D distance s from the "borehole" boundary, and time
L_0	equivalent parallel-plate flow aperture (average over time)
K	fracture permeability ($Length^2$)
K_c	fracture hydraulic conductivity ($Length/Time$)
T	fracture transmissivity ($Length^2/Time$)
$h(s,t)$	hydraulic head for 2-D fracture, as a function of distance s from the "borehole" boundary
$H(s,t)$	2-D fracture pressure
V_{2D}, V_{3D}	volume of fluid ejected into the borehole, for the 2-d and 3-d cases
q_{2D}, q_{3D}	rate of fluid flow into the borehole, for the 2-d and 3-d cases
v_{avg}	average 2-D fracture flow velocity
$F(\omega, \zeta_0/L_0)$	integral proportional to fluid displacement during one half-cycle of fracture wall displacement
$d(L_0)$	effective radius of fracture
$\chi(L_0)$	geometrical conversion factor for converting 2-d to 3-d flow into the borehole
$C(L_0)$	proportionality factor for the dependence of the displacement potential for the generated tube wave on the fracture closure
p_a, p_t	borehole fluid pressure amplitude for the incident P-wave and generated tube wave, respectively.
$c(\omega)$	tube wave phase velocity
k	$= \omega/c$ tube wave axial wavenumber
n	$= k(1-c^2/\alpha_f^2)^{\frac{1}{2}}$ tube wave radial wavenumber from the fluid compressional wave contribution
Φ_f^T	tube wave fluid displacement potential
Δ_f^T	tube wave fluid dilatation
I_0, I_1	Modified Bessel fcns of the first kind
$B(L_0)$	tube:P wave pressure ratio for zero offset, normal incidence geometry
$\mathbf{x}$	aperture, strike, dip fracture parameter solution vector
λ	factor containing orientation dependence of (VSP) displacement model
$\mathbf{A}$	aperture dependence of (VSP) displacement model
$\mathbf{G}$	nonlinear functional representing (VSP) displacement model

$\mathbf{d}$	vector containing spectral ratio observations, for a particular source offset
$\mathbf{W}$	diagonal matrix of weights applied to spectral ratio residuals
$\mathbf{f}$	objective function for nonlinear (VSP) model inversion
J_n	numerical Jacobian of objective function $\mathbf{f}$
D_n, α_n	Levenberg-Marquardt inversion parameters
$\mathbf{s}$	unit vector in direction of solution vector $\mathbf{x}$
P_I, P_R, P_T	tube wave pressure incident on, reflected from, and transmitted through fracture
P_F	transient pressure at fracture opening in borewall
$P(r,z,t)$	tube wave pressure field
v_I, v_R, v_T	tube wave particle velocity incident on, reflected from and transmitted through fracture
v_F	flow velocity at fracture opening in borewall
S_B	borehole cross-sectional area
S_F	cross-sectional area of fracture opening in borewall
Z_B	borehole tube wave impedance
Z_F	fracture flow impedance
P_ζ	constant containing orientation and formation properties dependence of pressure due to incident plane wave
P_f	transient fracture fluid pressure due to incident wave
κ	fracture stiffness ($Stress\,/\,Length$)
$D_1,....,D_4$	coefficients in (VSP) stress model

REFERENCES

Beydoun, W.B., C.H.Cheng and M.N.Toksöz, Detection of open fractures with vertical seismic profiling: JGR, in press, 1985.

Bhashvanija, K., A Finite Difference Model of an Acoustic Logging Tool: The Borehole in a Horizontally Layered Geologic Medium, Ph.D. Thesis (T-2763), Colorado School of Mines, April, 1983.

Biot, M.A., Propagation of elastic waves in a cylindrical bore containing a fluid: Journal of Applied Physics, **23**, 997-1005.

Bower, D.R., Bedrock fracture parameters from the interrpetation of well tides: JGR, **88**, n.B6, p.5025-5035, 1983.

Brown, K.M., Computer Oriented Methods ofr fitting tabular data in the linear and nonlinear least squares sense, Department of Computer, Information, and Control Sciences, TR No. 72-13, Univ. of Minnesota, 1972.

Cheng, C.H. and M.N.Toksöz, Elastic wave propagation in a fluid filled borehole and synthetic acoustic logs: Geophysics, **46**, p.1042-1053, 1981.

Cheng, C.H., M.N.Toksöz and M.E.Willis, Determination of in situ attenuation from full waveform acoustic logs: JGR, **87**, p.5477-5484, 1982.

Cheng, C.H. and M.N.Toksöz, Determination of shear velocities in "slow" formations: Transactions, 24th Annual SPWLA Logging Symposium, Calgary, Alberta, Canada, June 27-30, 1983.

Hamming, R.W., *Digital Filters*, Prentice-Hall Signal Proc. Series, A.V. Oppenheimer, editor, Prentice-Hall, Inc., N.J., 1977.

Hess, A.E., A heat-pulse flowmeter for measuring low velocities in boreholes: U.S. Geological Survey Open-File Report 82-699, 40p.

Huang, C.F. and J.A.Hunter, The correlation of "tube wave" events with open fractures in fluid filled boreholes: Current Research, Part A, Geological Survey of Canada, Paper 81-1A, p.361-376, 1981.

Marquardt, D.W., An Algorithm for Least Squares Estimation of Nonlinear Parameters, SIAM: journal of applied mathematics, **11**, (2), 1963.

Mathieu, F., Application of Full Waveform Acoustic Logging Data to the Estimation of Reservoir Permeability, S.M. Thesis, Mass. Institute of Technology, May, 1984.

Paillet, F.L., Acoustic propagation in the vicinity of fractures which intersect a fluid filled borehole: Transactions, 21st Annual SPWLA Logging Symposium, Lafayette, Louisiana, July 8-11, 1980.

Paillet, F.L., Frequency and scale effects in the optimization of acoustic waveform logs: Transactions, 24th Annual SPWLA Logging Symposium, Calgary, Alberta, Canada, June 27-30, 1983.

Paillet, F., Geophysical Well Log Data for Study of Water Flow in Fractures Near Mirror Lake, New Hampshire, U.S. Geological Survey, Open-File Report 85-340, Open-File Services Section, Denver Federal Center, 1985.

Paternoster, B., Effects of Layer Boundaries on Full Waveform Acoustic Logs, S.M. Thesis, Mass. Institute of Tech., May, 1985.

Schoenberg, M., Elastic wave behavior across linear slip interfaces: Journal Acoustical Soc. Am., **68**, n.5, p.1516, 1980.

Schoenberg, M., T.Marzetta, J.Aron and R.P.Porter, Space-time dependence of acoustic waves in a borehole: Journal Acoustical Soc. Am., **70**, n.5, p.1496, 1981.

Serra, O., *Fundamentals of Well-Log Interpretation:* 1. the acquisition of data, Elsevier, Amsterdam, 423 p., 1984.

Snow, D.T., A Parallel Plate Model of Fractured Permeability Media, Ph.D. dissertation, University of California, Berkeley, California, 1965.

Stephen, R., F. Pardo-Casas and C.H. Cheng, Finite-difference synthetic acoustic logs, Geophysics, **50**, n.10, pp.1588-1609, 1985.

Stewart, R.R., R.M.Turpening and M.N.Tokso*z, Study of a Subsurface Fracture Zone by Vertical Seismic Profiling, Geophys.Res.Letters, **8**, n.11, pp.1132-1135, 1981.

Voegele, M.D., E.L.Hardin, R. Lingle, M. Board, N. Barton, Site Characterization of Joint Permeability Using the Heated Block Test, Proc. of 22nd U.S. Symposium on Rock Mechanics, Mass. Institute of Tech. Center for Adv. Engr. Study, June, 1981.

White, J.E., *Underground Sound*, Elsevier, Amsterdam, 1983.

Willis, M.E., Seismic Velocity and Attenuation from Full Waveform Acoustic Logs, Ph.D. Thesis, Mass. Institute of Tech., April, 1983.

Winters, T., Geohydrologic Setting of Mirror Lake, West Thornton, New Hampshire, U.S. Geological Survey, Water-Resources Investigations Report 84-4266, Open-File Services Section, Denver Federal Center.

Ziegler, T.W., Determination of Rock Mass Permeability, U.S. Army Corps of Engineers, Waterways Experiment Station, Tech.Report S-76-2, January, 1976 (final report), Appendix B.

Table 1. VSP Tube Wave Generation Analysis using Displacement Formulation (Beydoun, et al. 1985) with Linear and Nonlinear Inversion Methods.

Frac Depth (m)	Linear Inversion			Nonlinear Inversion		
	Strike	Dip	$\frac{T}{(cm^2/sec)}$	Strike	Dip	$\frac{T}{(cm^2/sec)}$
Britton Well #2						
290	N7E	35W	4e-6	N5E	31W	4e-6
210	N42W	23W	1e-6	N35W	36W	1e-6
Mirror Lake Well EBR-4						
44	N60E	8S	2e-4	N23W	21W	2e-4
225	N54E	11S	5e-6	N1E	13E	4e-6

Table 2. Summary of fracture Parameters determined from televiewer images, FWAL Stoneley attenuation, VSP model inversion, and independent transmissivity estimates. For the Britton experiment transmissivity was estimated from inflow during drilling. At Mirror Lake a constant-discharge pump test was performed as described in section 3.2.2. Transmissivity was also calculated from FWAL attenuation, for the Mirror Lake experiment. The tabulated results were obtained by studying Stoneley attenuation in data acquired using a sparker source tool operating at approximately 5kHz (Figure 12). The analysis method is explained in section 2.2, and a portion of the complete calculated transmissivity log is presented as Figure 34.

Parameter	Televiewer	FWAL Attenuation (5 kHz.)	VSP Inversion (Nonlinear)	Independent Estimate
210 m in Britton well #2				
T(cm**2/sec)			1e-6	~0.5
Strike	N40W		N35W	
Dip	40W		30W	
290 m in Britton well #2				
T(cm**2/sec)			4e-6	~0.5
Strike	N10E		N5E	
Dip	30W		20W	
44m in Mirror Lake well EBR-4				
T(cm**2/sec)		1.2	2e-4	~1.0
Strike	N110E		N25W	
Dip	10S		20W	
225m in Mirror Lake well EBR-4				
T(cm**/sec)		0.1	4e-6	
Strike	N60E		NS	
Dip	15S		15E	

Table 3. Pump Test Analysis, Mirror Lake Well EBR-4 (after Paillet and Hess, 1986). Briefly, the test consists of pumping from EBR-4 at the indicated flow rate, and observing water levels in adjacent wells EBR-1,2 and 3. A sensitive flowmeter was used in all the wells to establish horizons of inflow and outflow. In the table, the largest and smallest observed flow rates are reported.

Infinite Flat Fracture of Uniform Aperture, Borehole Couplet					
Obs. Well	Separation (m)	Head Diff. (m)	Flow Rate Range (l/min)	T (cm^2/sec)	Equiv. Aperture (mm)
EBR-1	13	1.2	2.3	2.3	0.8
			1.1	1.1	0.7
EBR-2	10	3.9	2.3	0.65	0.5
			1.1	0.3	0.4
EBR-3	10	1.1	0.8	0.7	0.5
			0.4	0.35	0.4

Equivalent Cylindrical Conduit (Tube) of Tortuosity = 2.				
Observation Well	Well Separation (m)	Head Difference (m)	Flow Rate (l/min)	Tube Radius (mm)
EBR-1	13	1.2	2.3	5.2
			1.1	4.3
EBR-2	10	3.9	2.3	3.6
			1.1	3.0
EBR-3	10	1.1	0.8	3.7
			0.4	3.1

Table 4. Annotated driller's log from Britton well #2, with calculated inflow.

Start Time/Depth(m) (breakover)	Finish Time/Depth(m) (each stand)	Elapsed Time to Breakover (min)	Breakover Pressure (MPa)	Inflow Rate (lpm)	Change at Frac. (lpm)
Beginning of day 1/21/82		900	?		
10:02/120	10:43/126	?	0.9		
10:52/126	11:19/132	9	0.9	22.6	
11:40/132	12:18/138	21	0.9	10.0	
12:29/138	13:15/144	17	0.97	12.9	
13:26/144	14:17/493	17	0.97	12.9	
14:35/150	15:07/156	18	0.97	15.5	2.6
15:22/156	16:11/163	16	1.1	15.7	
16:26/163	17:00/169	15	1.1	16.5	
Beginning of day 1/22/82		900	1.31		
9:49/164	10:32/170	9	1.07	26.0	
10:42/170	11:42/176	10	1.07	24.1	
11:58/176	13:01/182	13	1.07	18.6	
Beginning of day 1/26/82		900	1.55		
9:47/188	11:07/194	?	1.24		
11:18/194	12:31/200	15	1.24	19.2	
12:43/200	13:48/206	17	1.24	17.8	
14:05/206	15:03/212	15	1.45	21.8	3.9
15:18/212	16:17/218	12	1.48	27.8	6.0
16:29/218	17:30/224	13	1.48	26.5	
Beginning of day 1/27/82		900	1.93		
9:55/224	11:12/230	13	1.66	28.6	
11:26/230	12:30/236	14	1.66	26.8	
12:46/236	13:51/242	16	1.69	23.9	
14:07/242	15:12/248	16	1.69	23.9	
15:26/248	16:35/255	14	1.72	27.8	
16:48/255	17:53/261	13	1.72	30.4	2.6
Beginning of day 1/28/82		900	2.24		
9:50/261	11:18/267	15	2.00	29.9	
11:30/267	12:43/273	14	2.00	32.3	
12:56/273	14:09/279	17	2.03	27.0	
14:22/279	15:42/285	15	2.07	30.7	
15:56/285	17:01/291	14	2.07	29.9	
Beginning of day 1/29/82		900	2.24		
11:05/291	12:19/297	13	2.17	33.9	3.9
12:33/297	13:55/303	14	2.17	34.4	
14:15/303	15:27/309	13	2.21	38.3	

Table A1. Parameter Study of Model Coefficients			
$\rho = 2700\ kg/m^3 \qquad \alpha = 5.8\ km/s \qquad \beta = 3.3\ km/s$ zero offset geometry $\lvert \varepsilon \rvert = 10^{-6}\ cm/cm$ $\gamma = 5\times10^{-10}\ Pa^{-1}$			
κL_0 (Pa)	$\lvert (D_1/D_4)(\partial P/\partial t) \rvert$	$\lvert (D_2/D_4)(\partial P/\partial t) \rvert$	$\lvert (D_3/D_4)P(\partial P/\partial t) \rvert$
Frequency = 100 Hz., $\lvert u(t) \rvert = 10\ \mu m,\ P_t = 156\ nt \cdot m \cdot \sec$			
2×10^9	2.0		
5×10^9	3.5		
10^{10}	11.0	4.9×10^{-5}	4.9×10^{-5}
2×10^{10}	12.3		
5×10^{10}	26.0		
Frequency = 200 Hz., $\lvert u(t) \rvert = 5\ \mu m,\ P_t = 78\ nt \cdot m \cdot \sec$			
2×10^9	2.0		
5×10^9	3.5		
10^{10}	11.0	4.9×10^{-5}	4.9×10^{-5}
2×10^{10}	12.3		
5×10^{10}	26.0		
Frequency = 400 Hz., $\lvert u(t) \rvert = 2\ \mu m,\ P_t = 31\ nt \cdot m \cdot \sec$			
2×10^9	2.0		
5×10^9	3.5		
10^{10}	11.0	3.9×10^{-5}	3.9×10^{-5}
2×10^{10}	12.3		
5×10^{10}	26.0		

Figure 1. Schematic hydrophone VSP survey geometry for Britton Well #2. Hamilton Massachusetts. Multichannel hydrophone streamer is deployed on a wireline cable in the central well #2. Fractional charges are detonated in the peripheral shot holes, which typically penetrate 50 meters into the crystalline bedrock.

TIME (msec)

0   **250**
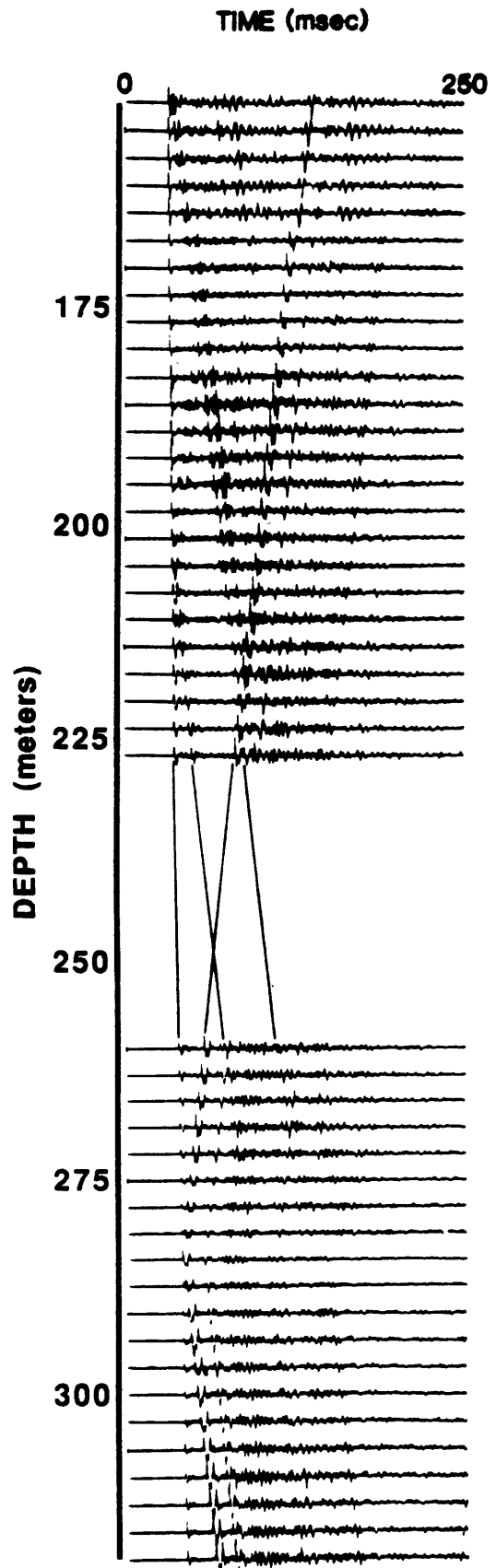
Figure 2. Hydrophone VSP field data from Britton Well #2, Hamilton, Mass. This section corresponds to shot point B7, located 180 meters east of the observation well at a depth of 123 meters.
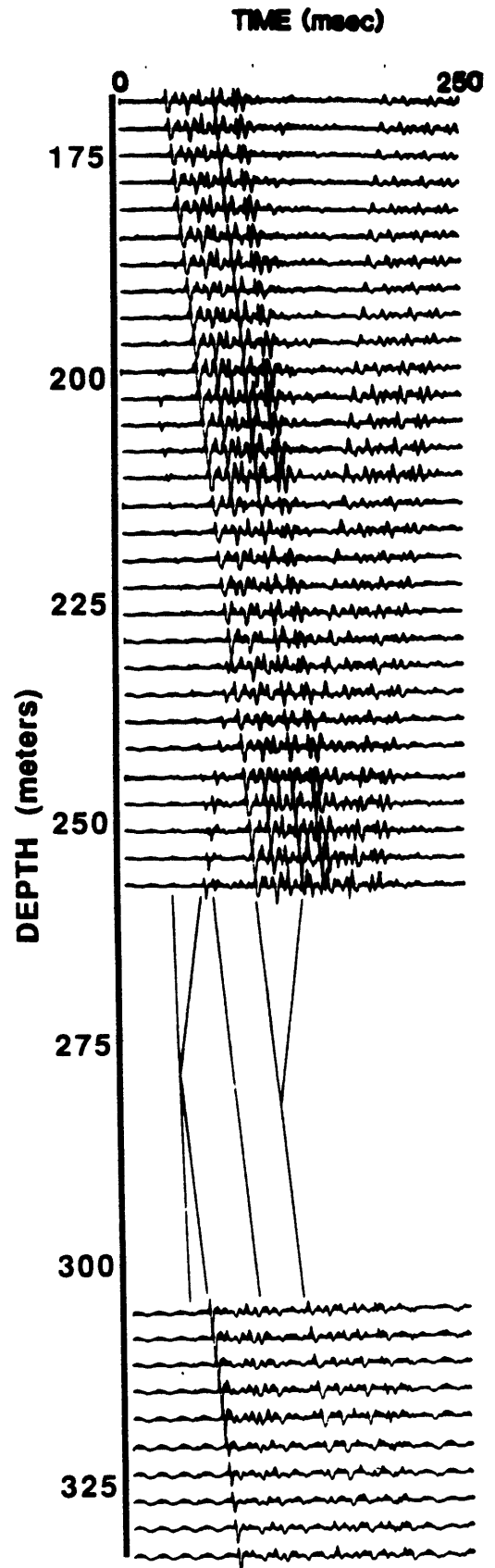
Figure 3. Hydrophone VSP field data from Britton Well #2, Hamilton, Mass. This section corresponds to shot point B9, located 12 meters north of the observation well at a depth of 62 meters.
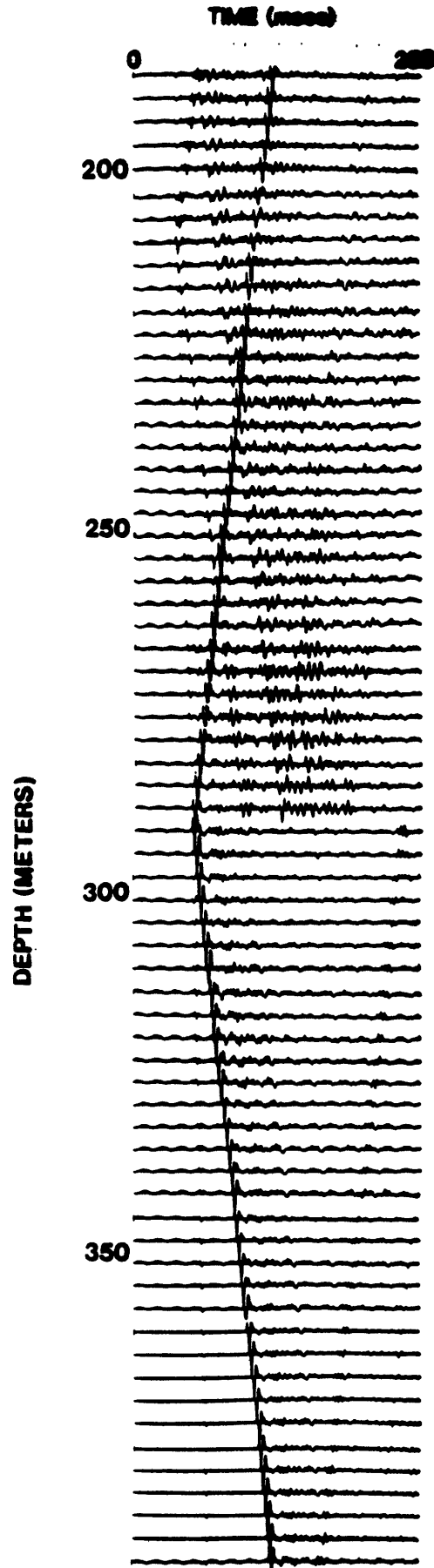
Figure 4. Hydrophone VSP field data from Britton Well #2, Hamilton, Mass. This section corresponds to shot point B10, located 146 meters south of the observation well at a depth of 58 meters.
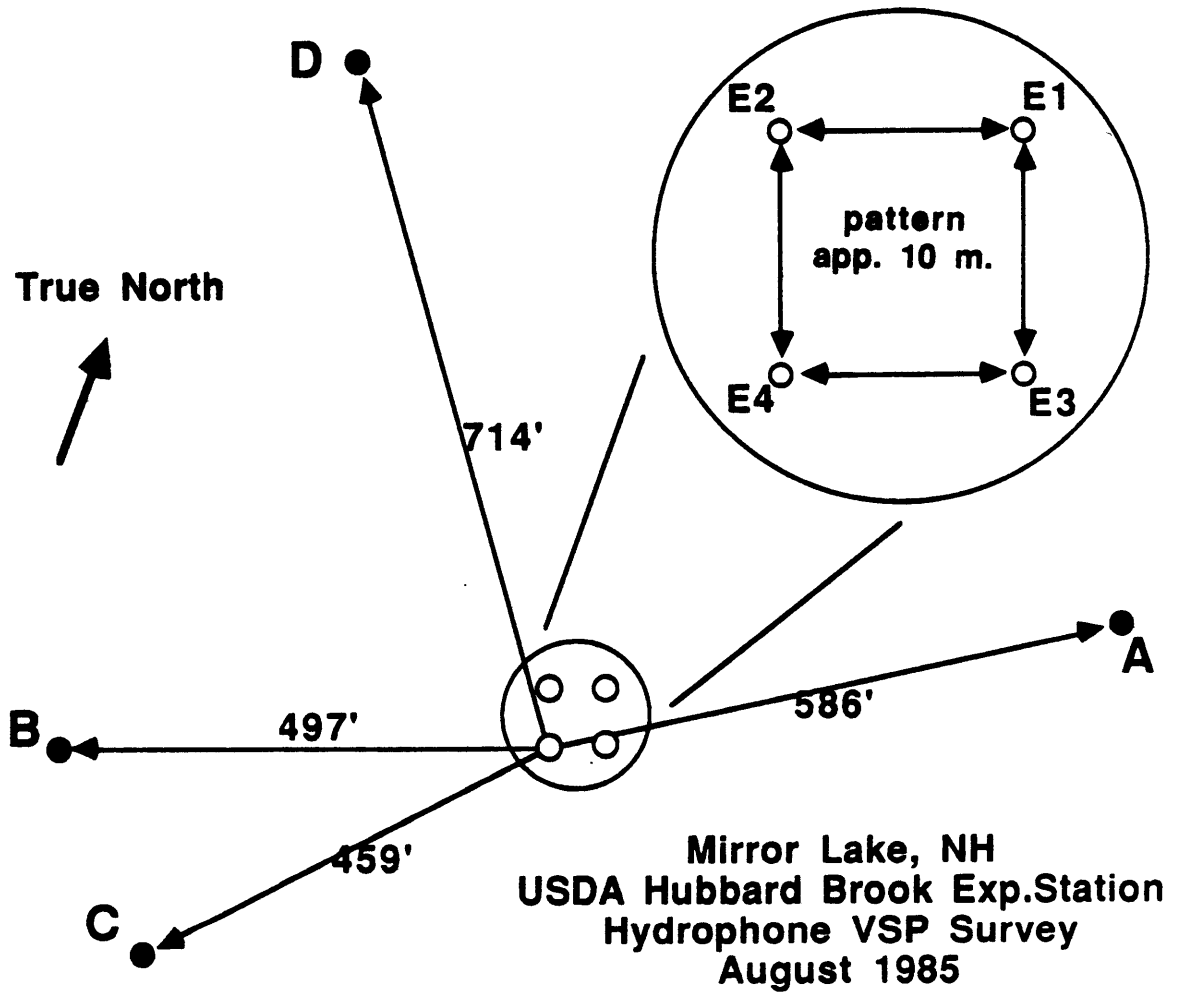
Figure 5. Schematic of VSP geometry at Mirror Lake site. Generated tube
waves were observed in well EBR-4, by a string of hydrophones
which could be moved up- and downhole. Timing and monitor
phone signals were conveyed from distant shot holes A thru D, to
recording equipment at EBR-4, by means of a multi-conductor
surface cable.
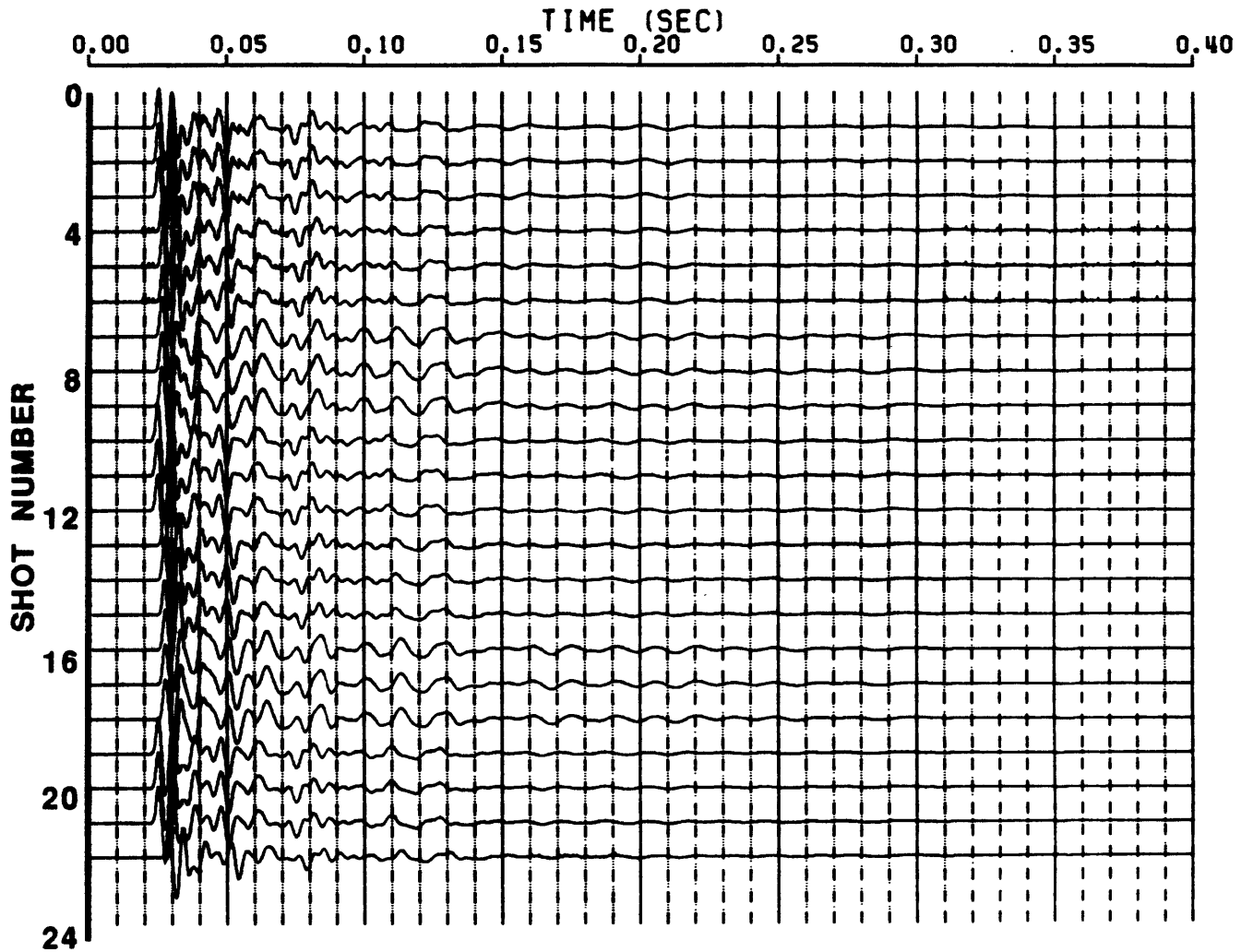
Figure 6. Monitor phone records from shot hole C, Mirror Lake site. Source timing and signature were monitored by a 14 Hz. geophone buried several meters from the shot hole. Of the four shot points, consistently higher frequency source energy was obtained with C.
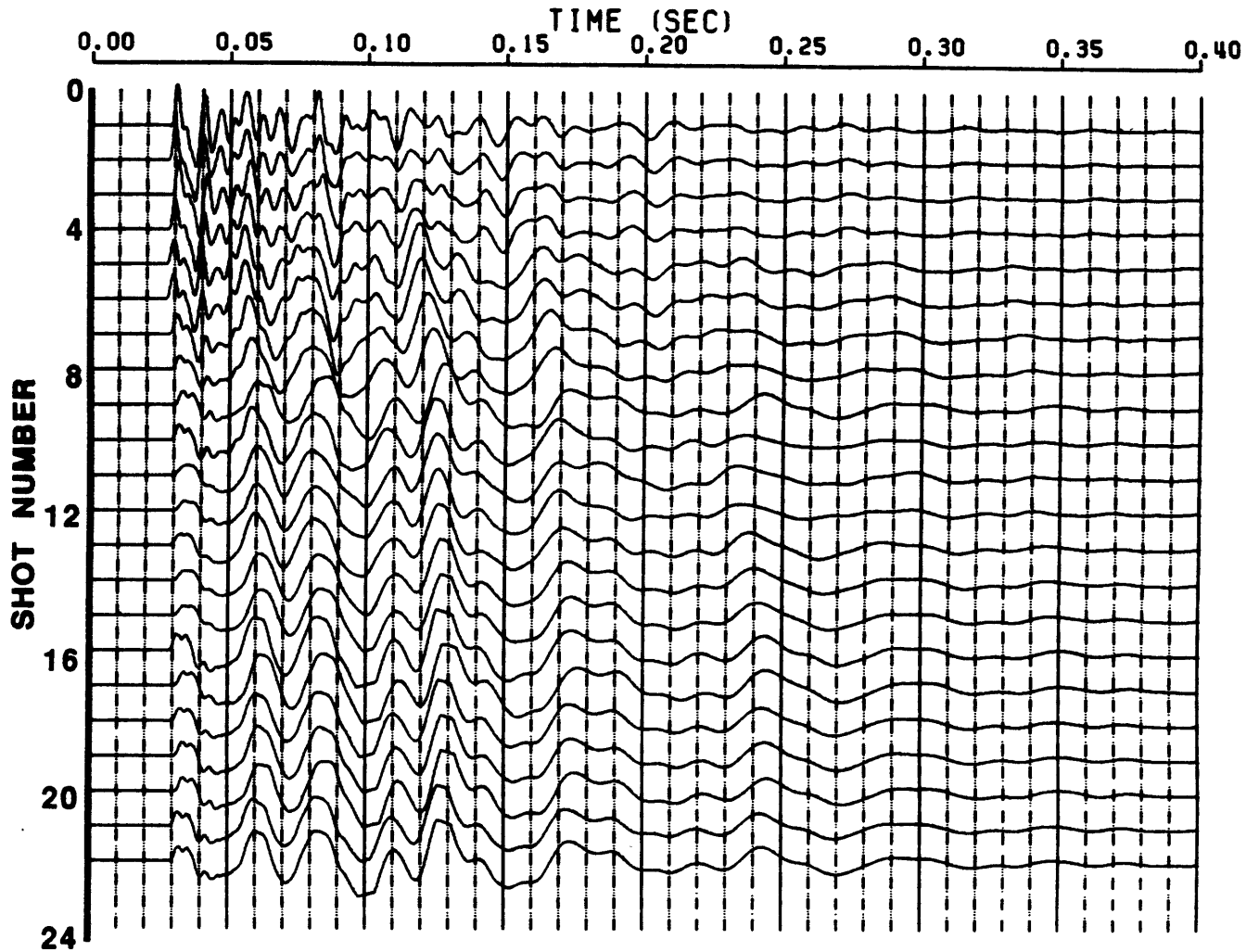
Figure 7. Monitor phone records from shot hole D. Mirror Lake site. Source timing and signature were monitored by a 14 Hz. geophone buried several meters from the shot hole. Gradual degradation of the shot hole casing lowered the source band center frequency.
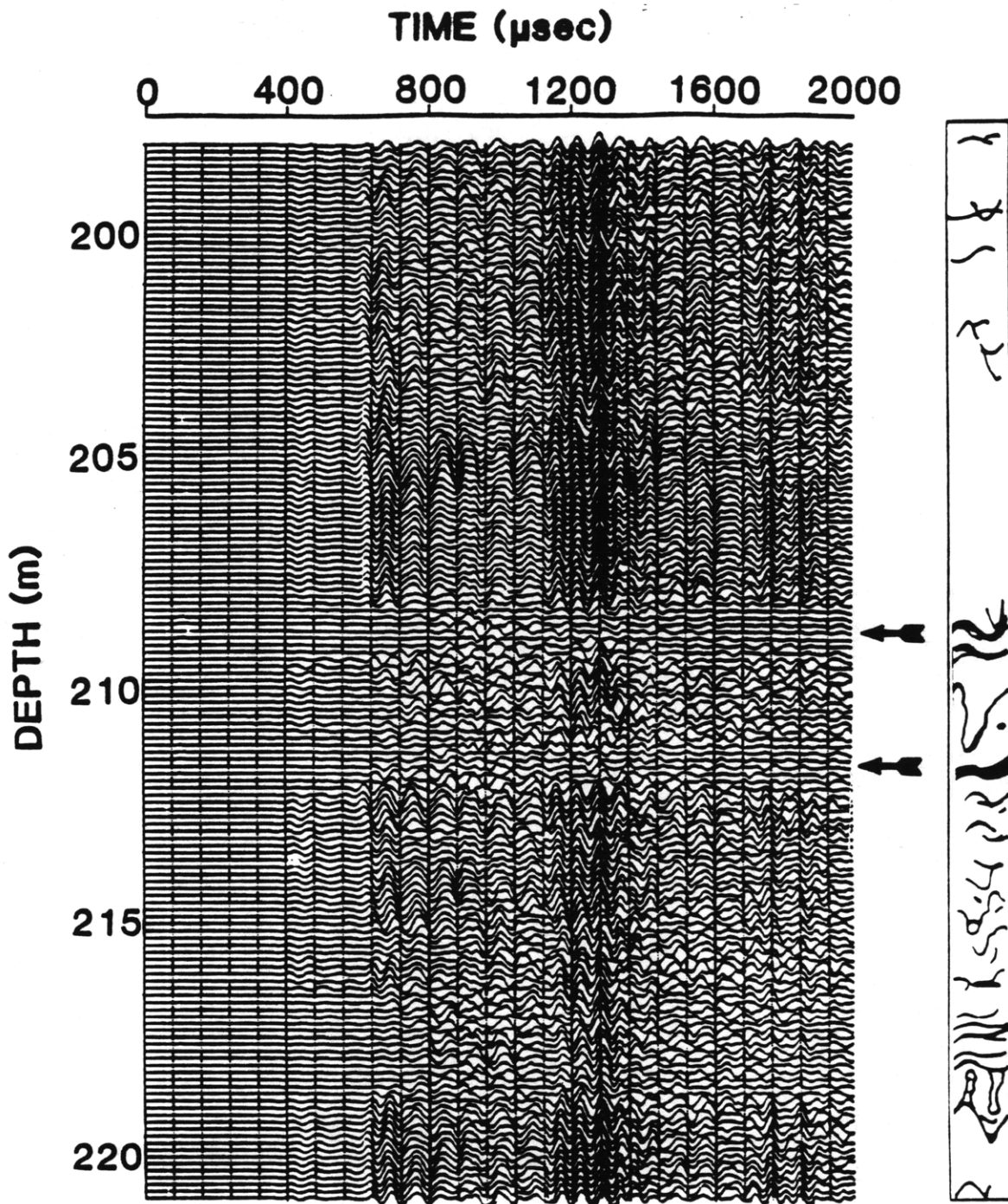
Figure 8. Full waveform acoustic log from Britton well #2, interval around the (VSP) tube wave generating horizon at 210 meters. Substantially all phases of the waveform are completely attenuated at the fracture. The Stoneley wave is not excited efficiently, relative to the pseudo-Rayleigh modes, in this borehole. Transmitter-receiver separation: 2.1 meters, approx. center source band frequency: 15 kHz.
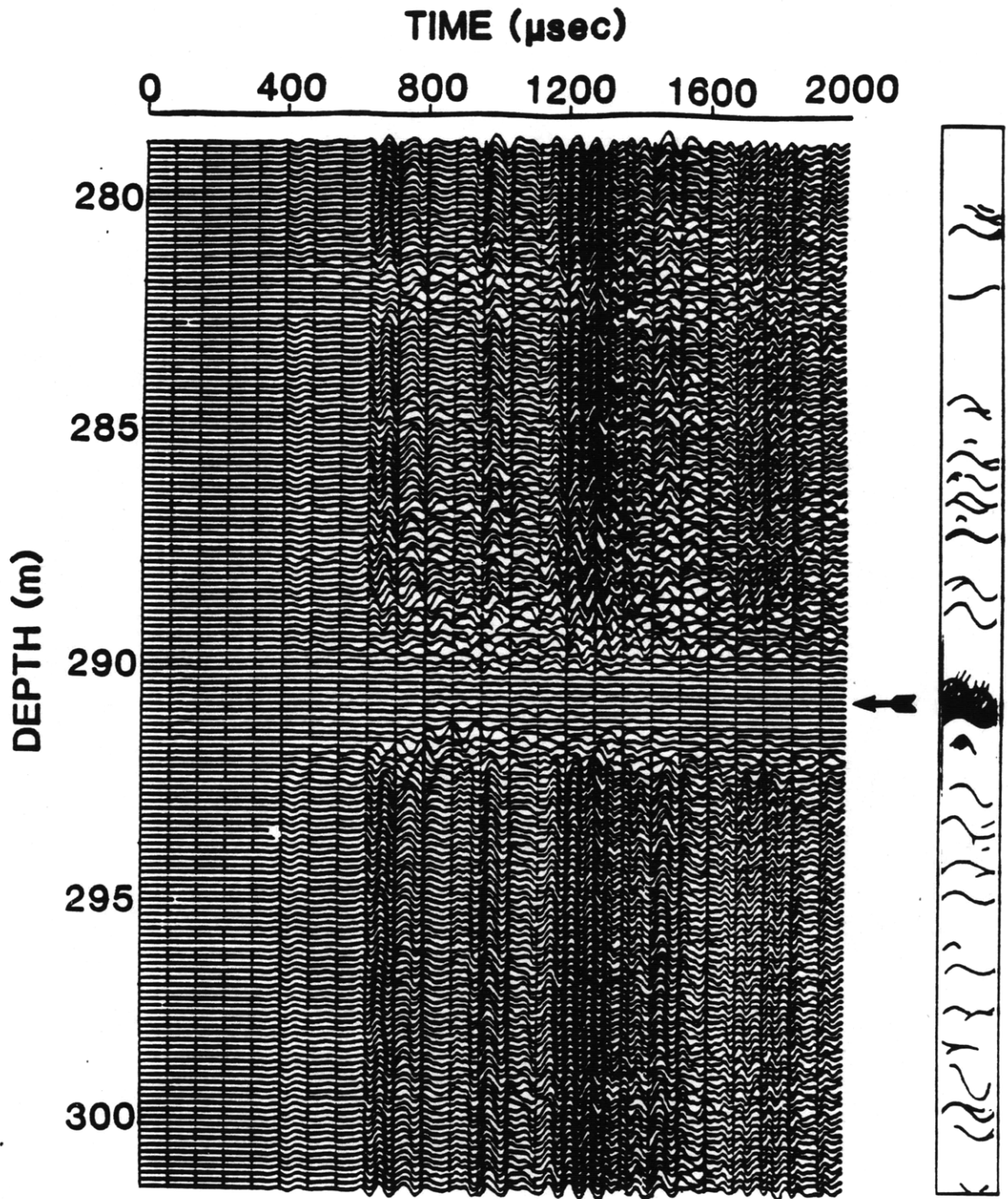
Figure 9. Full waveform acoustic log from Britton well #2, interval around
the outstanding (VSP) tube wave generating horizon at 290
meters. All phases of the waveform are completely attenuated at
the fracture. The Stoneley wave is not excited efficiently, relative
to the pseudo-Rayleigh modes, in this borehole. Transmitter-
receiver separation: 2.1 meters, approx. center source frequency:
15 kHz.
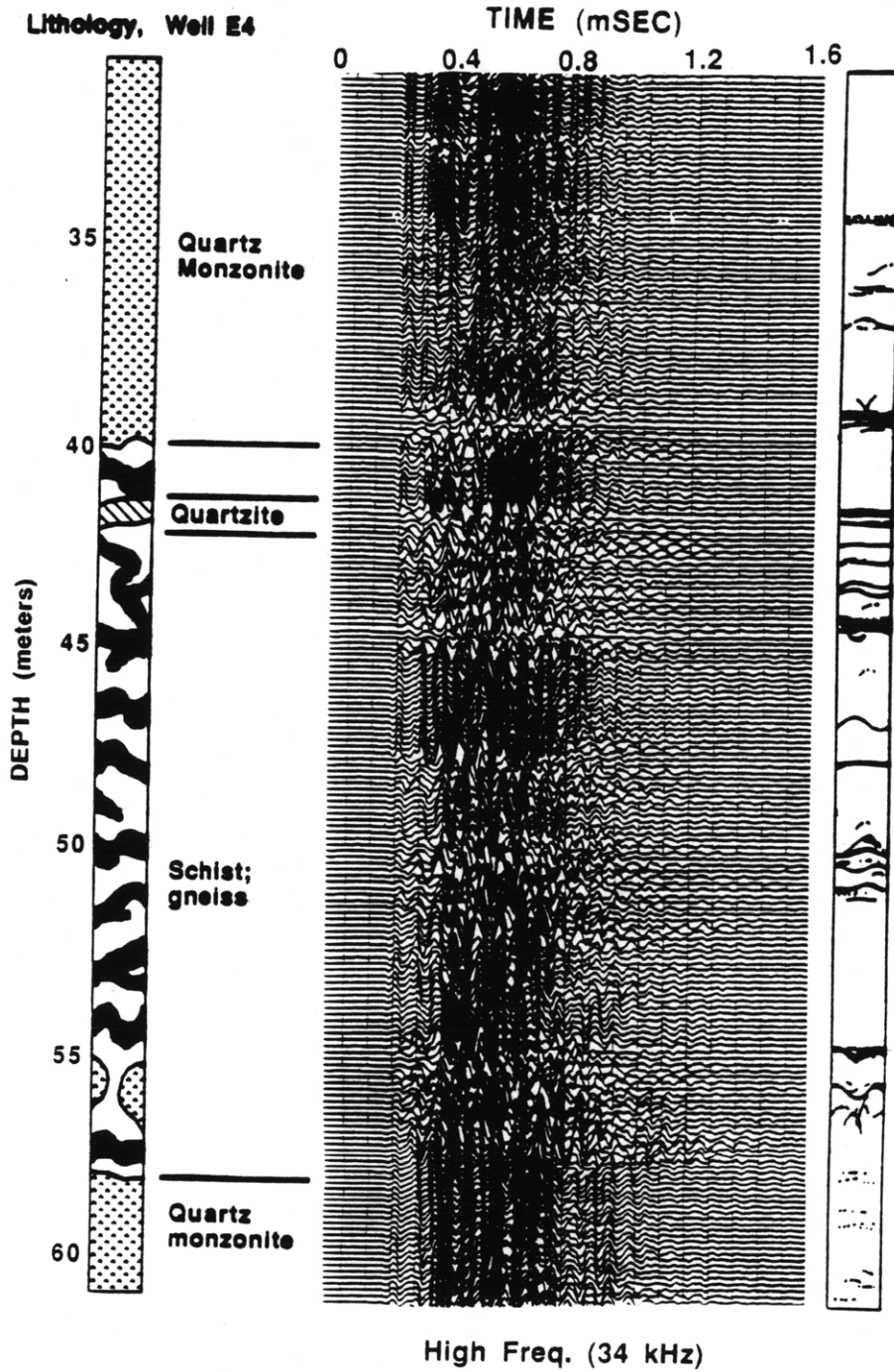
Figure 10. Full waveform acoustic log from EBR-4 Mirror Lake well, interval from 30 to 60 meters containing tube wave generating horizon at 44 meters. Separation: 0.91 meters, approx. source band center frequency: 34 kHz. Stoneley wave is nearly indistinguishable from the pseudo-Rayleigh modes.

Full Waveform Acoustic Log
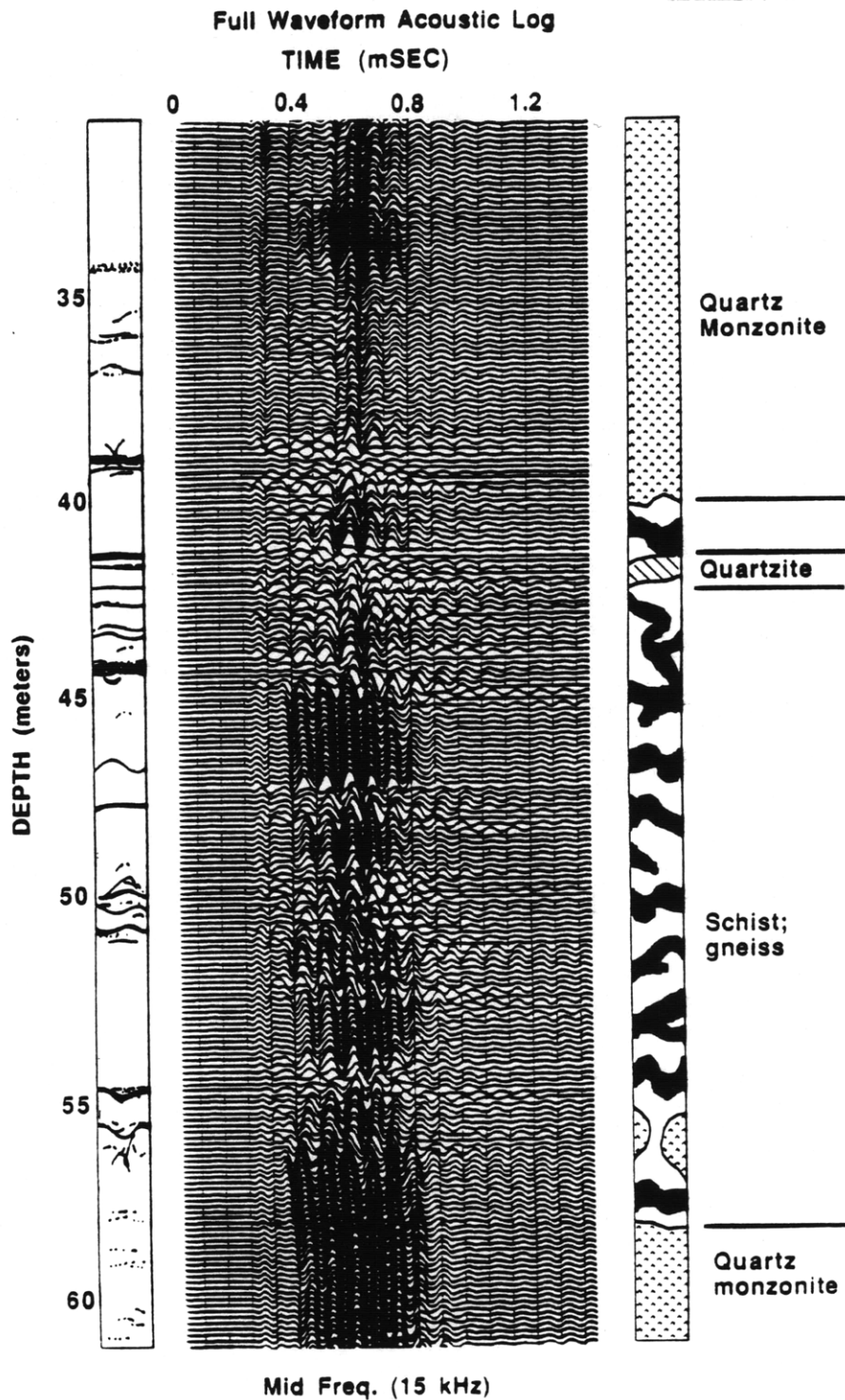
Figure 11. Full waveform acoustic log from EBR-4 Mirror Lake well, interval from 30 to 60 meters containing tube wave generating horizon at 44 meters. Separation: 0.91 meters, approx. source band center frequency: 15 kHz. Stoneley packet can be distinguished from pseudo-Rayleigh, although not at every depth.

Full Waveform Acoustic Log

TIME (mSEC)

Low Freq. (Sparker)
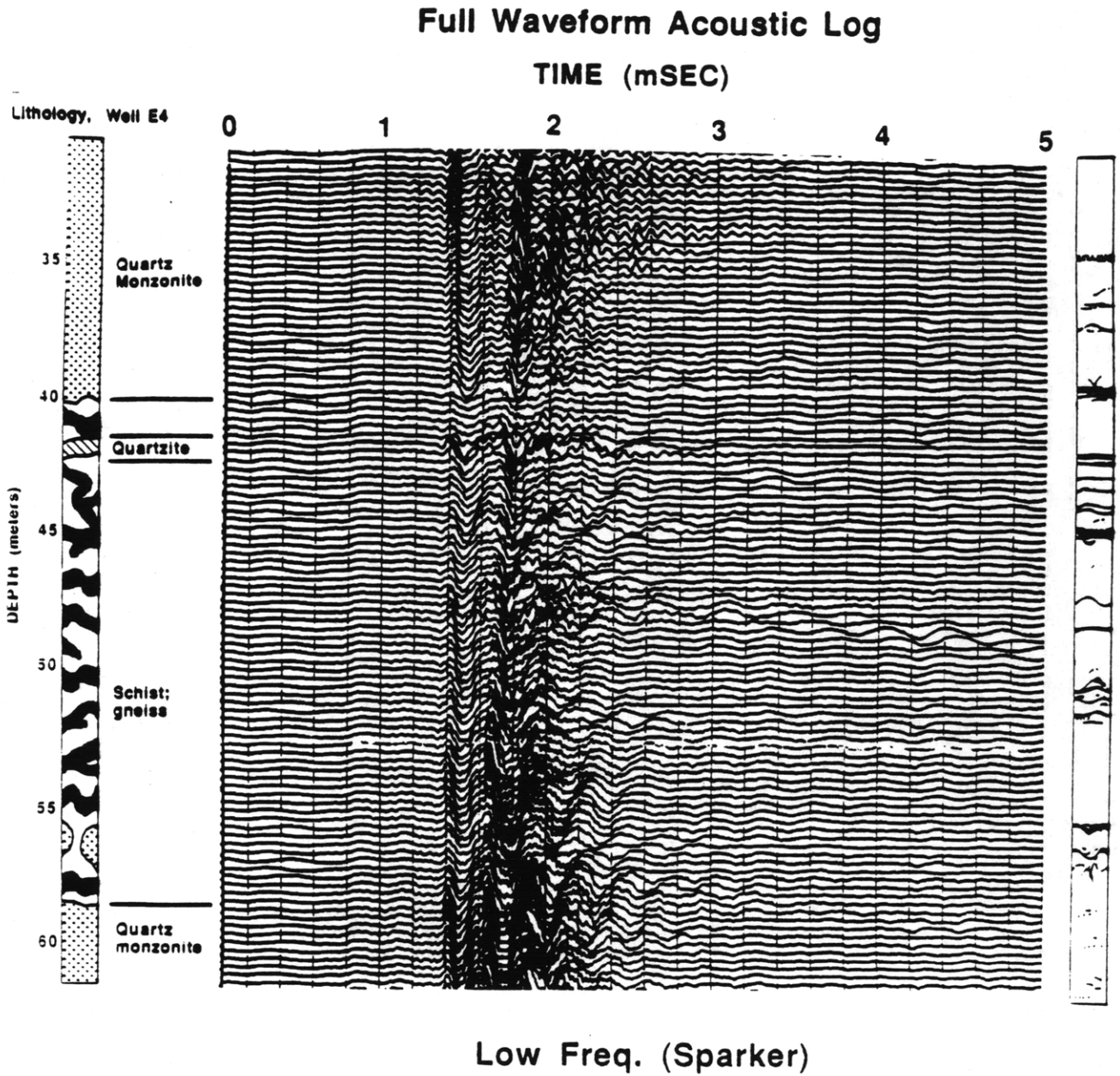
Figure 12. Full waveform acoustic log from EBR-4 Mirror Lake well, interval from 30 to 60 meters containing tube wave generating horizon at 44 meters. Separation 3.0 meters, approx. source band center frequency: 5 kHz. Pseudo-Rayleigh waves are not present since the source band is mostly below the cutoff frequency of the first mode.
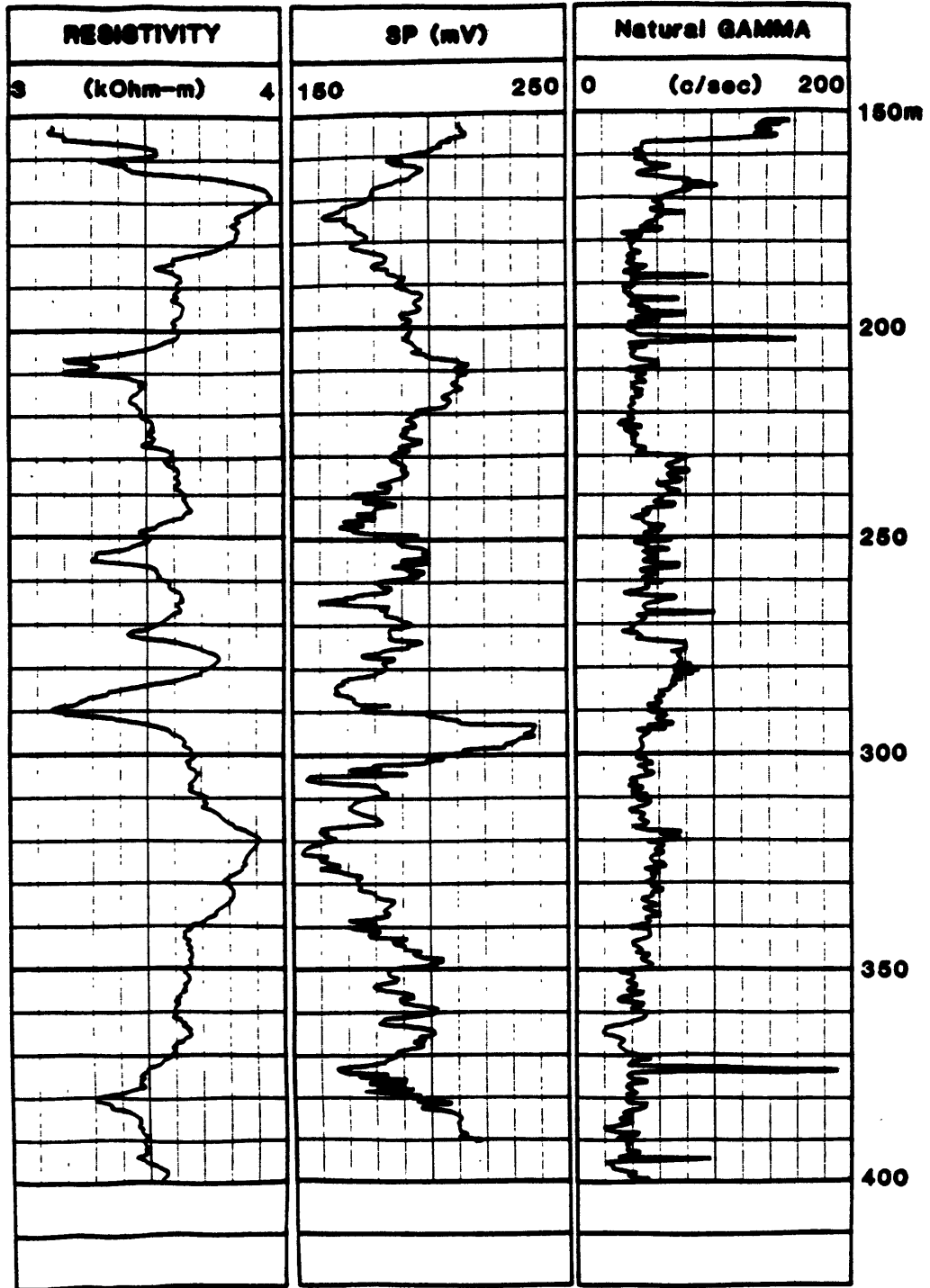
Figure 13. Wireline logs: resistivity (single point), self potential (SP). and natural gamma (displayed in uncalibrated counts per second). Depth interval 150 to 400 meters in Britton well #2. Hamilton, Massachusetts.
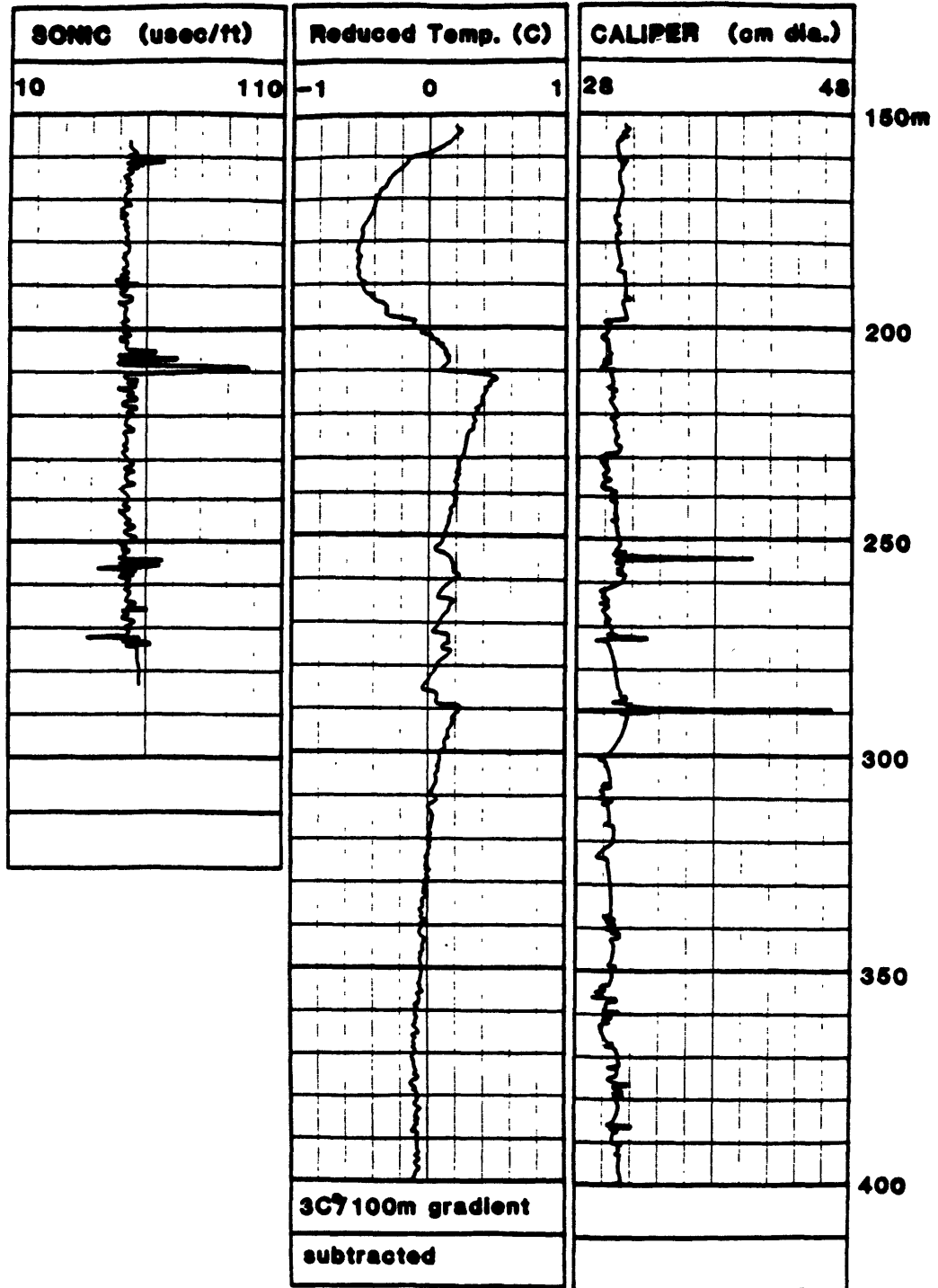
Figure 14. Wireline logs: sonic (uncompensated, noncentralized), first-run reduced temperature (first entry into borehole, reduced by subtracting 3C°/100m. geothermal gradient), and caliper. Depth interval 150 to 400 meters (except sonic) in Britton well #2, Hamilton, Massachusetts.
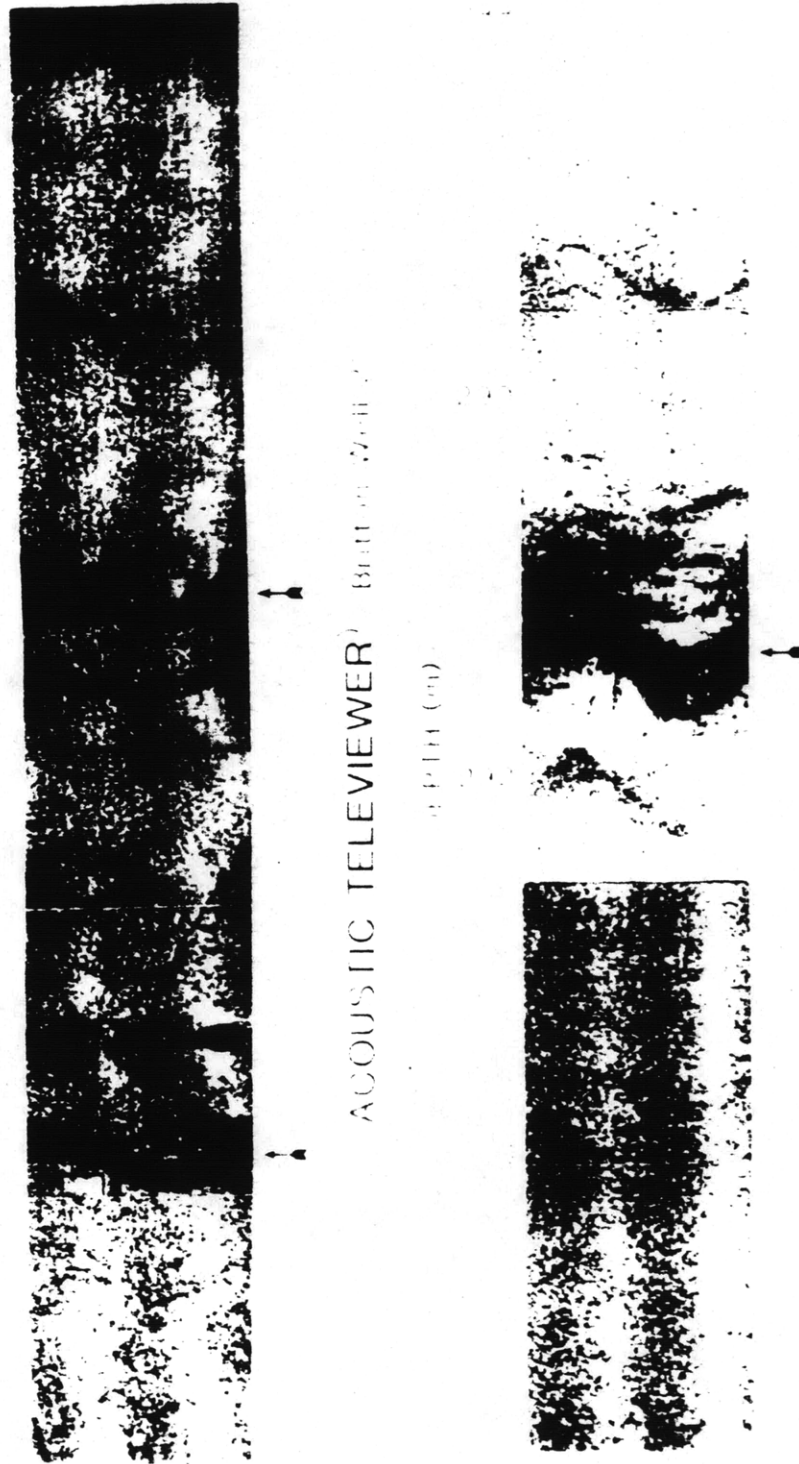
Figure 15. Borehole televiewer images from (VSP) tube wave generating horizons at 210 and 290 meters, Britton well #2. Fractures are tabular features with distinct orientation, and apparent aperture of 10-20 cm. at the borewall.
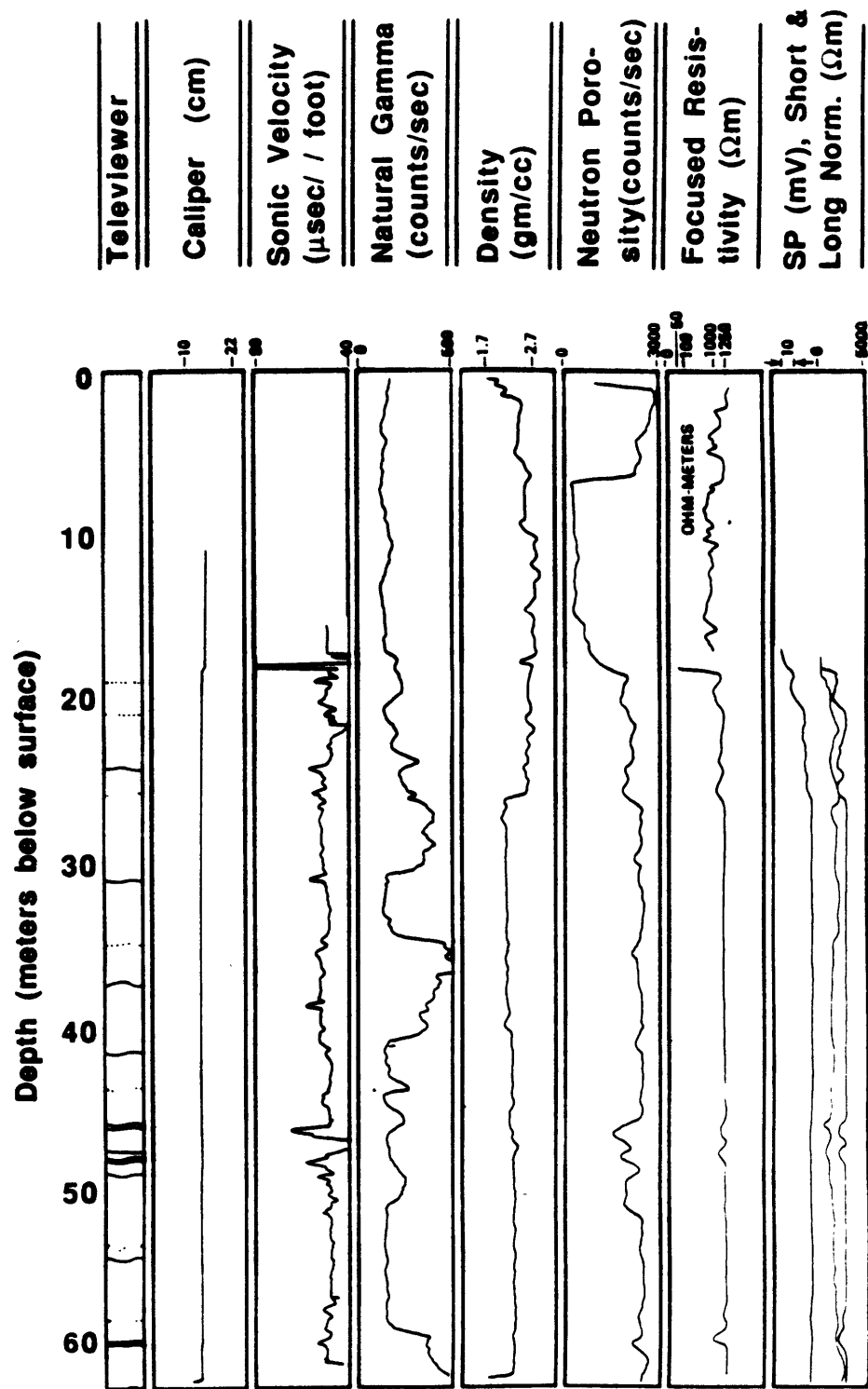
Figure 16. Wireline logs from Mirror Lake EBR-3, adjacent to observation well EBR-4. Artist's synopsis of televiewer images plotted for comparison (after Winters, 1984).
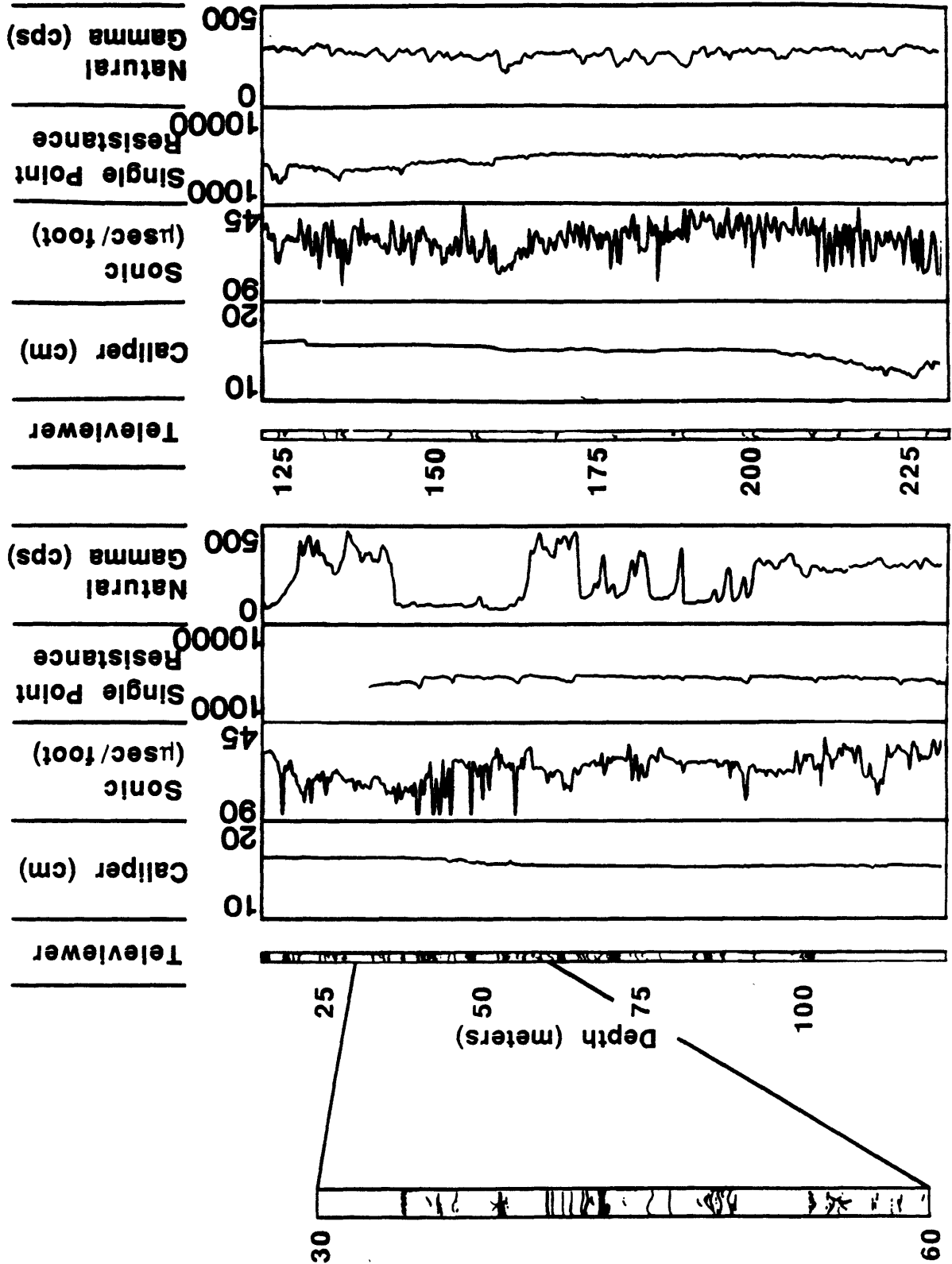
Figure 17. Wireline logs from Mirror Lake EBR-4. Artist's synopsis of televiewer images plotted for comparison (after Paillet, 1985).
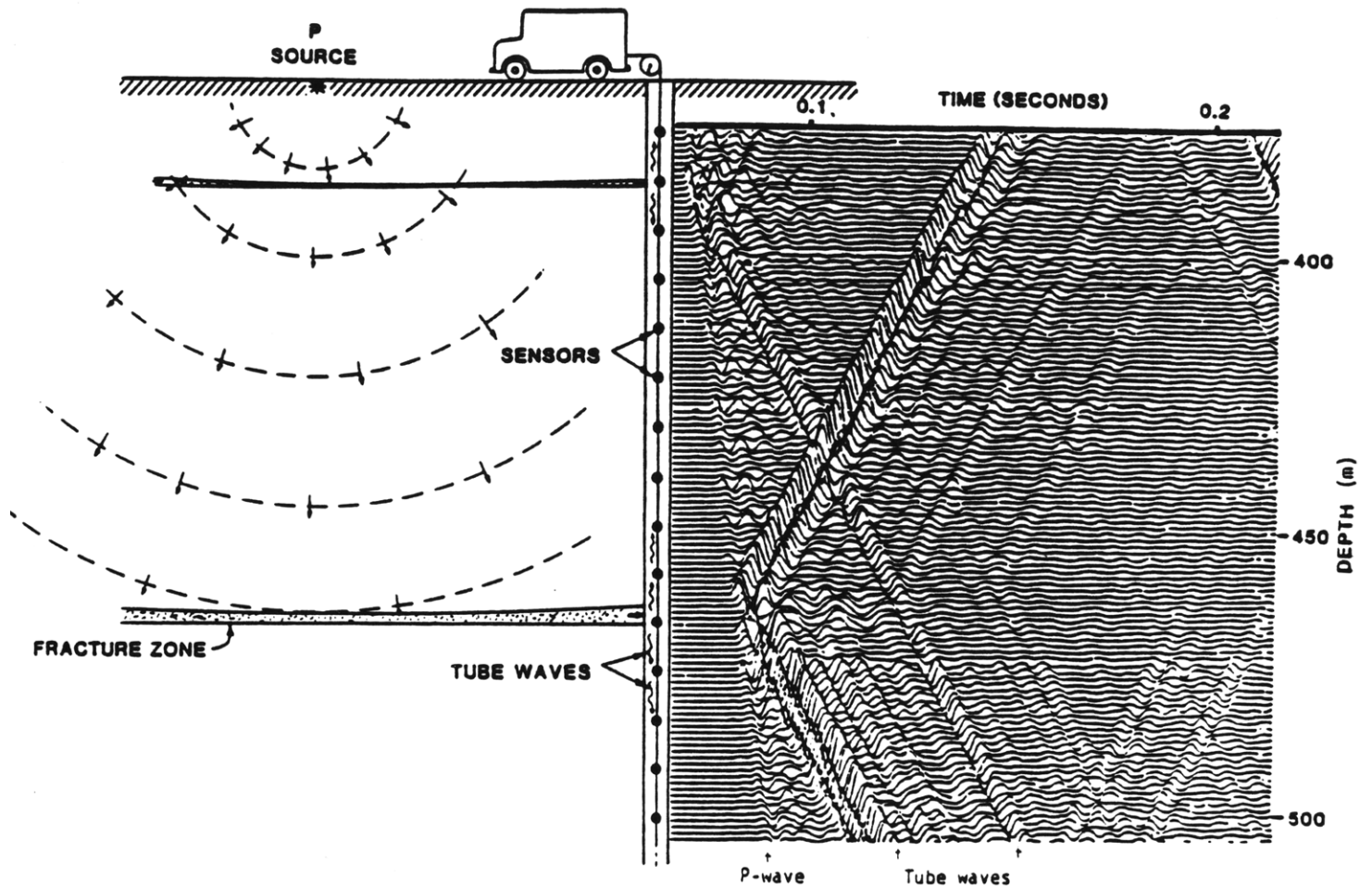
Figure 18. VSP generation mechanism schematic. A direct compressional wave interacts with the fracture, resulting in mass transfer to the borehole and a generated tube wave.
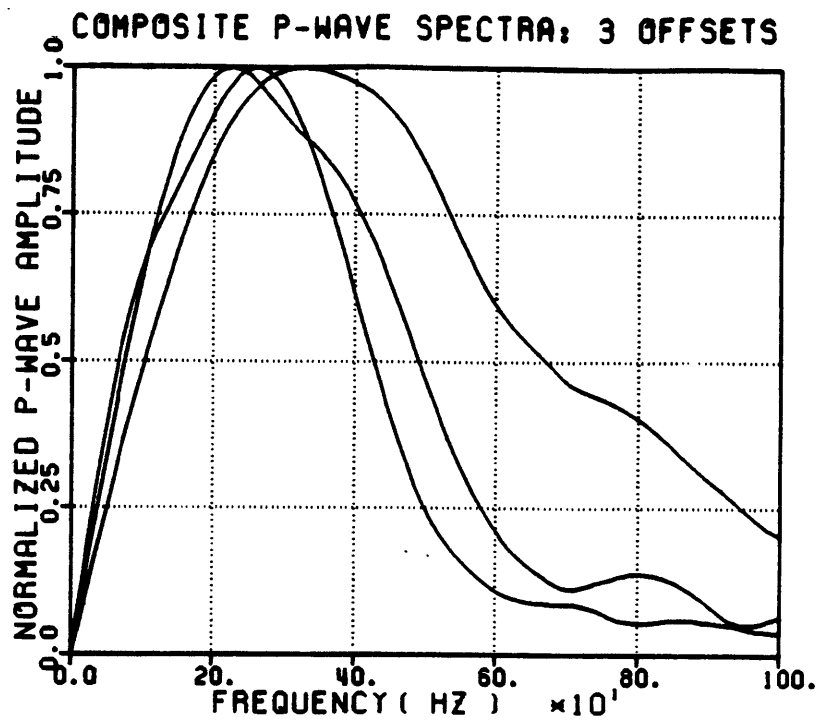
Figure 19. Composite source spectra (averaged over several traces) for the three different VSP offsets used for Britton well #2.

TIME (msec)
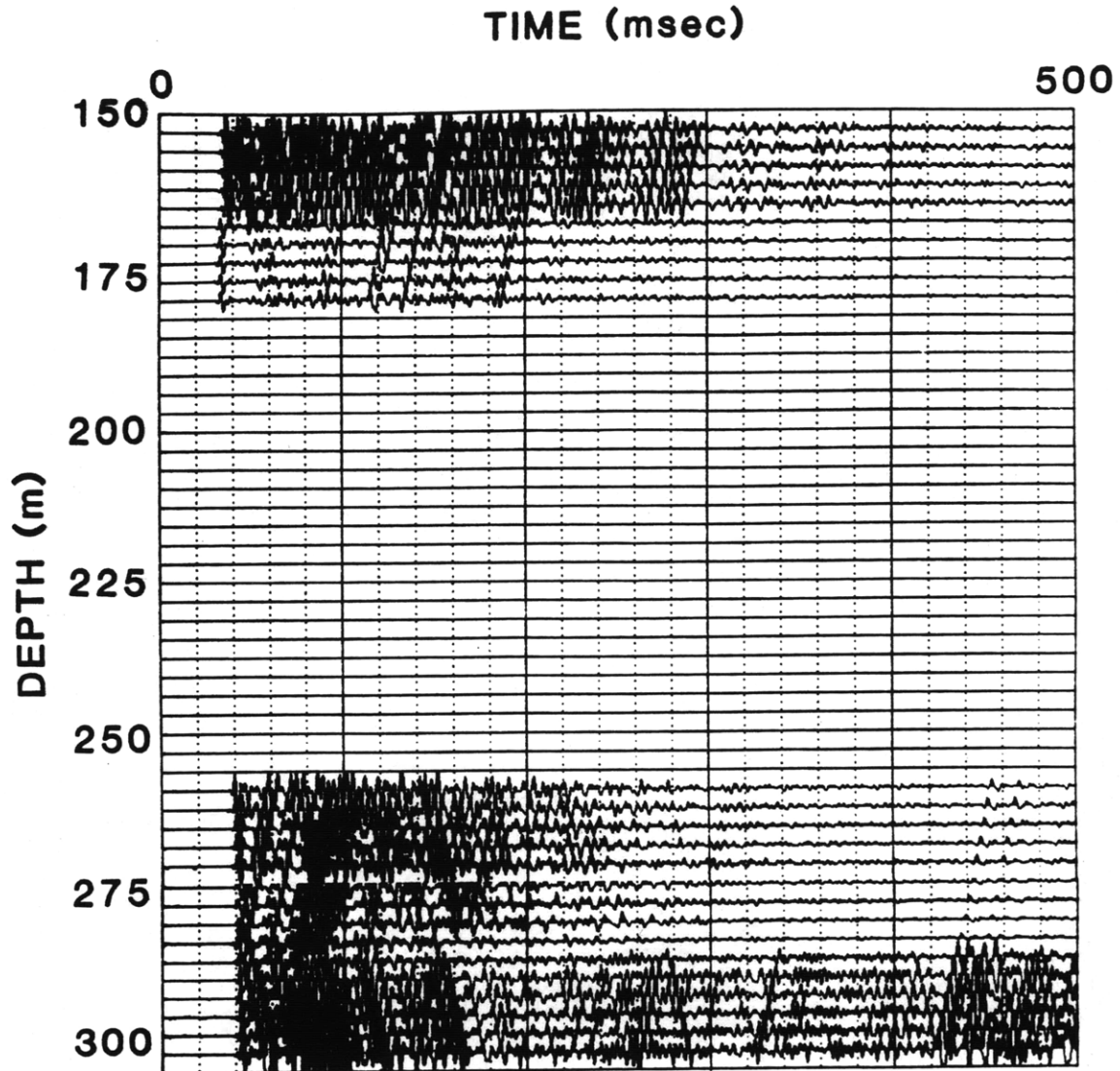
Figure 20. Hydrophone VSP section for source offset B7, Britton well #2. Traces are bandpass filtered (150-400 Hz.) and (predictive) filtered to remove line noise and harmonics.
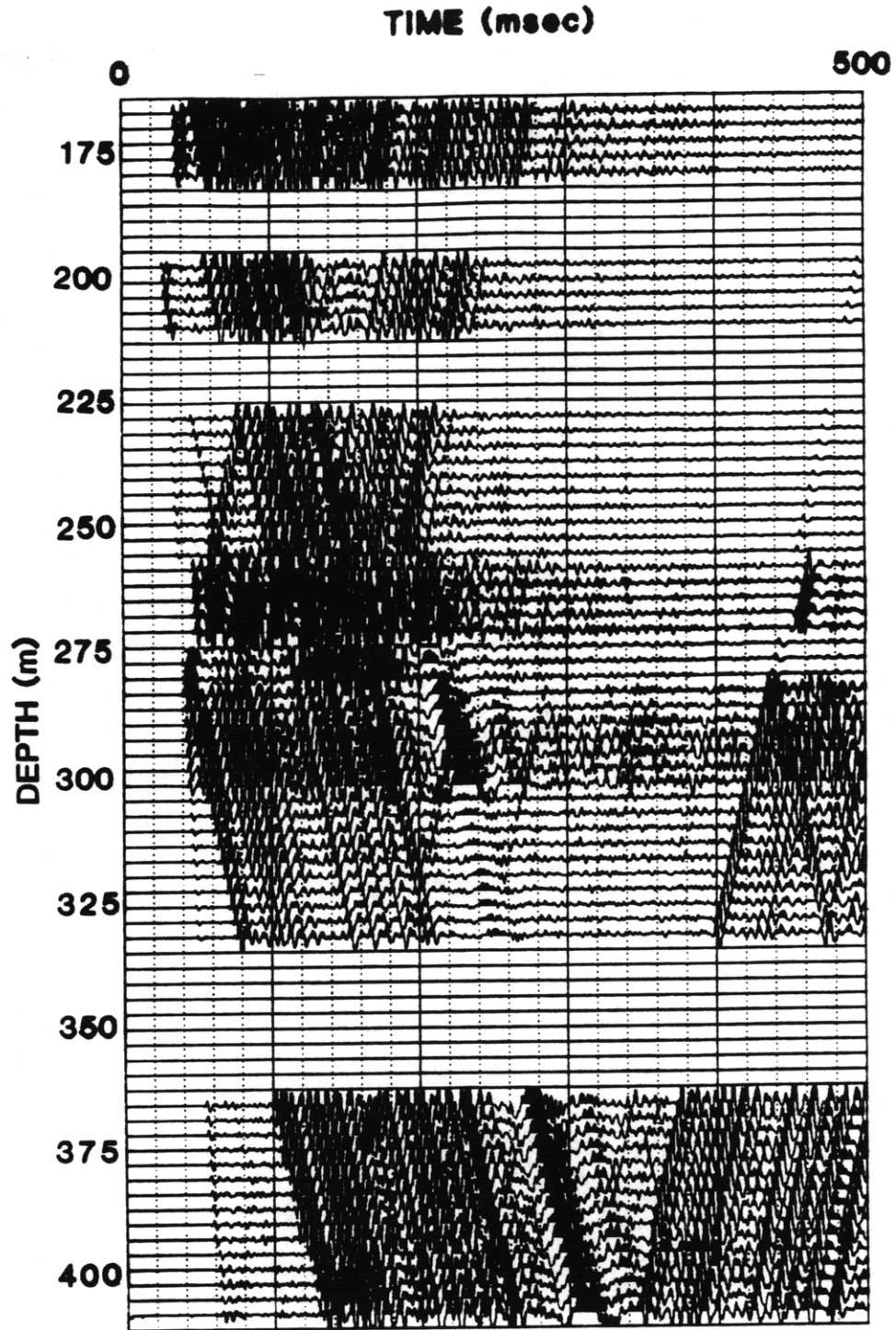
Figure 21. Hydrophone VSP section for source offset B9 (zero offset). Britton well #2. Traces are bandpass filtered (150-400 Hz.) and (predictive) filtered to remove line noise and harmonics.
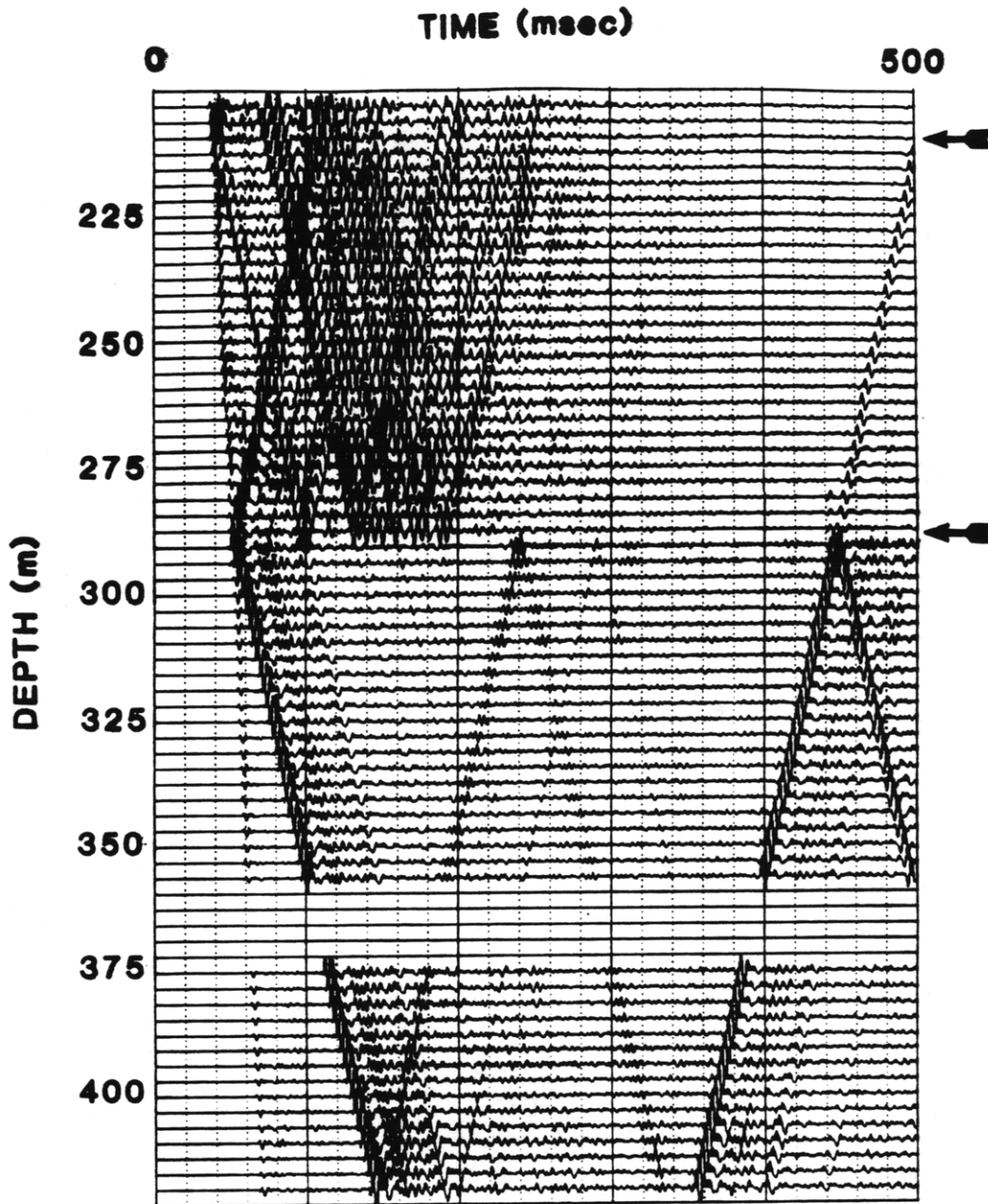
Figure 22. Hydrophone VSP section for source offset B10, Britton well #2. Traces are bandpass filtered (150-400 Hz.) and (predictive) filtered to remove line noise and harmonics.
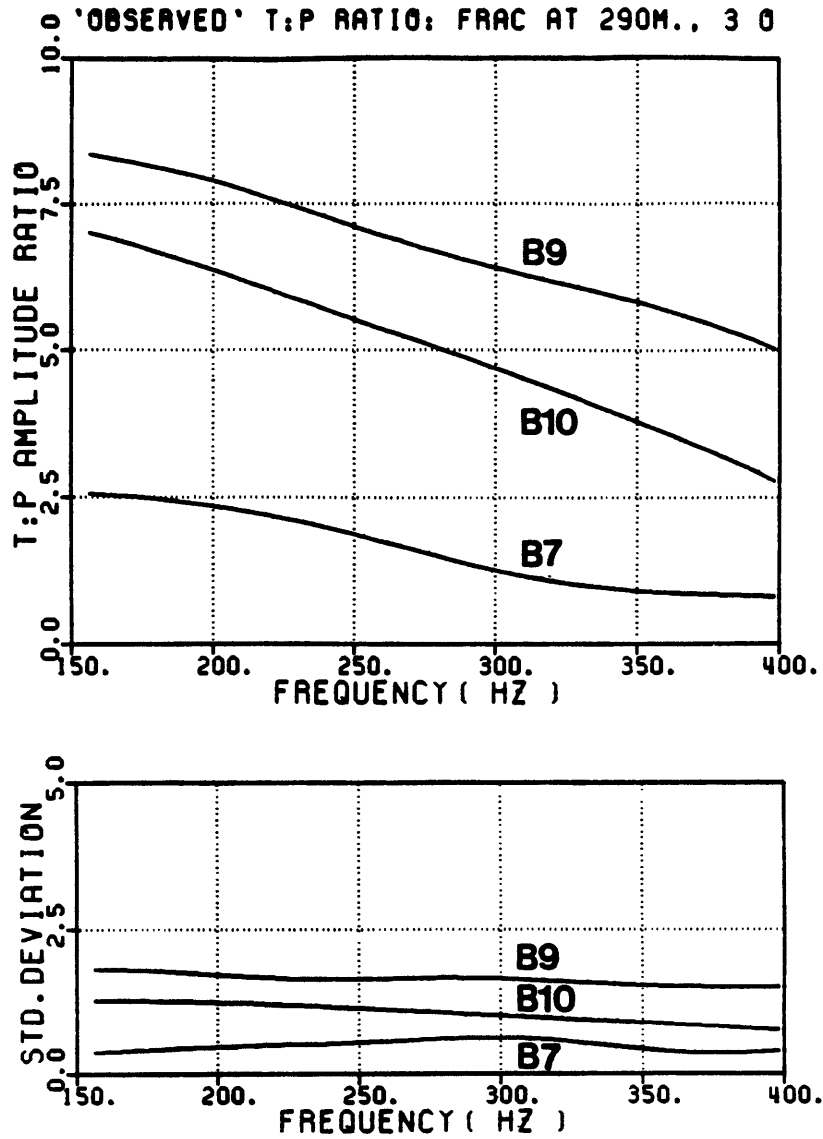
Figure 23. Tube:P wave amplitude ratio spectra for offset B7, B9 and B10, Britton well #2. Spectra are composites averaged from several traces. Standard deviations of the averages are plotted below.
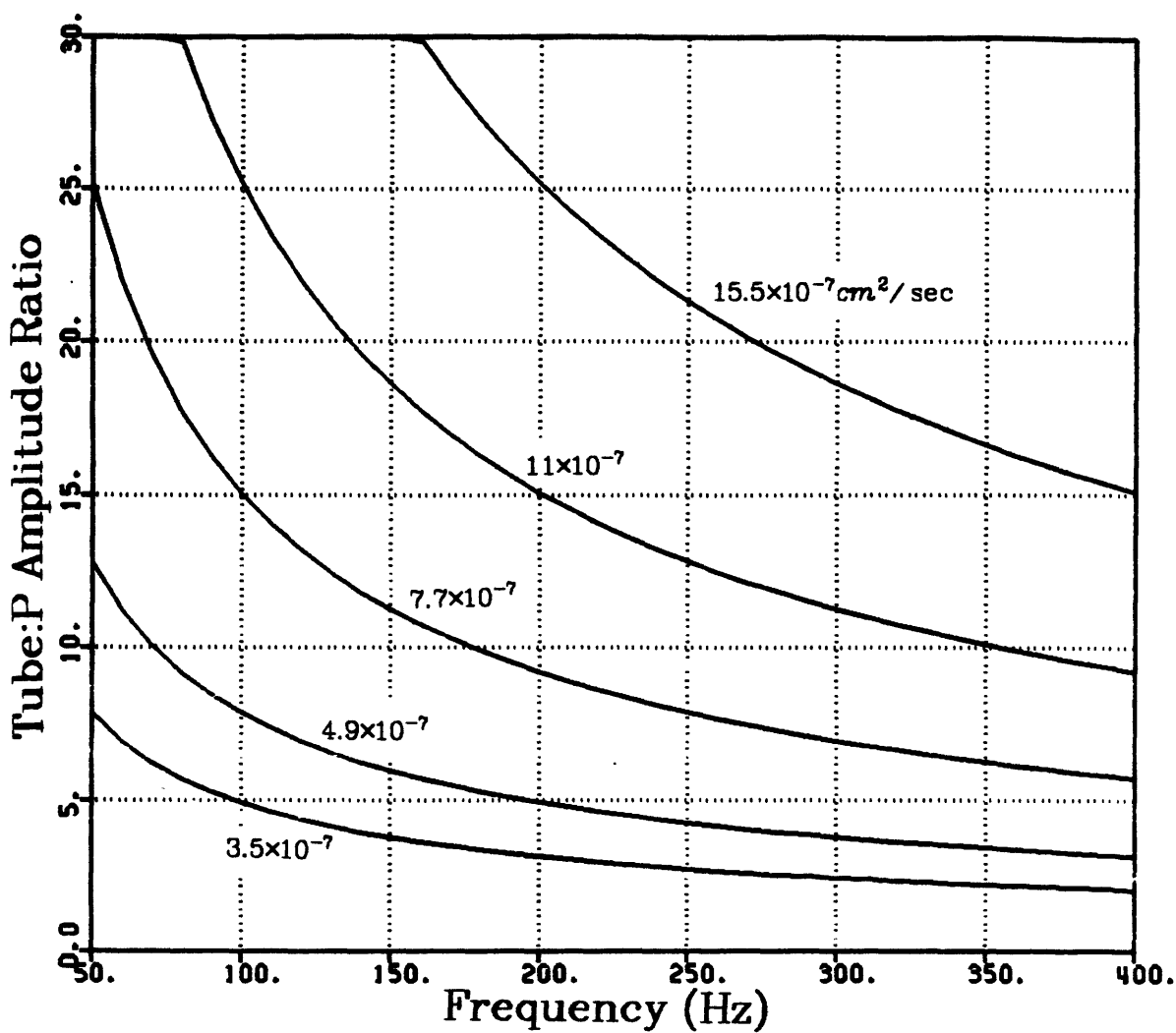
Figure 24. Theoretical tube:P wave amplitude ratio spectra for Britton well #2, fracture at 290 meters, using displacement formulated model of Beydoun, et al. (1985). Different curves correspond to different values of hydraulic transmissivity as indicated.
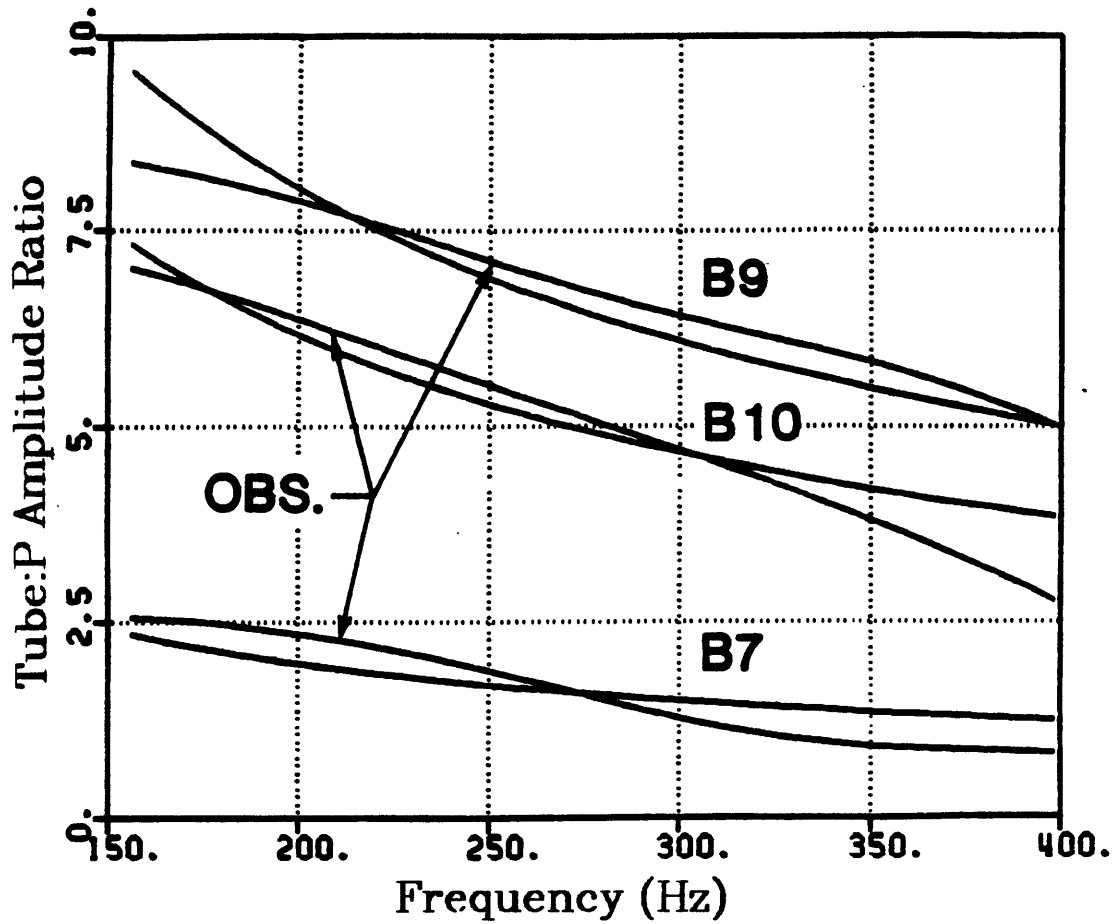
Figure 25. Tube:P wave amplitude spectra for fracture at 290 meters in Britton well #2. Different source offsets B7, B9 and B10 are indicated. Best-fit (nonlinear inversion scheme) theoretical spectra using the Beydoun model are also plotted.

(a)

SSQ VS.STRIKE VARIATION FROM SOLN

(c)

SSQ VS.APERTURE VARIATION FROM SOLN

(b)

SSQ VS.DIP VARIATION FROM SOLN
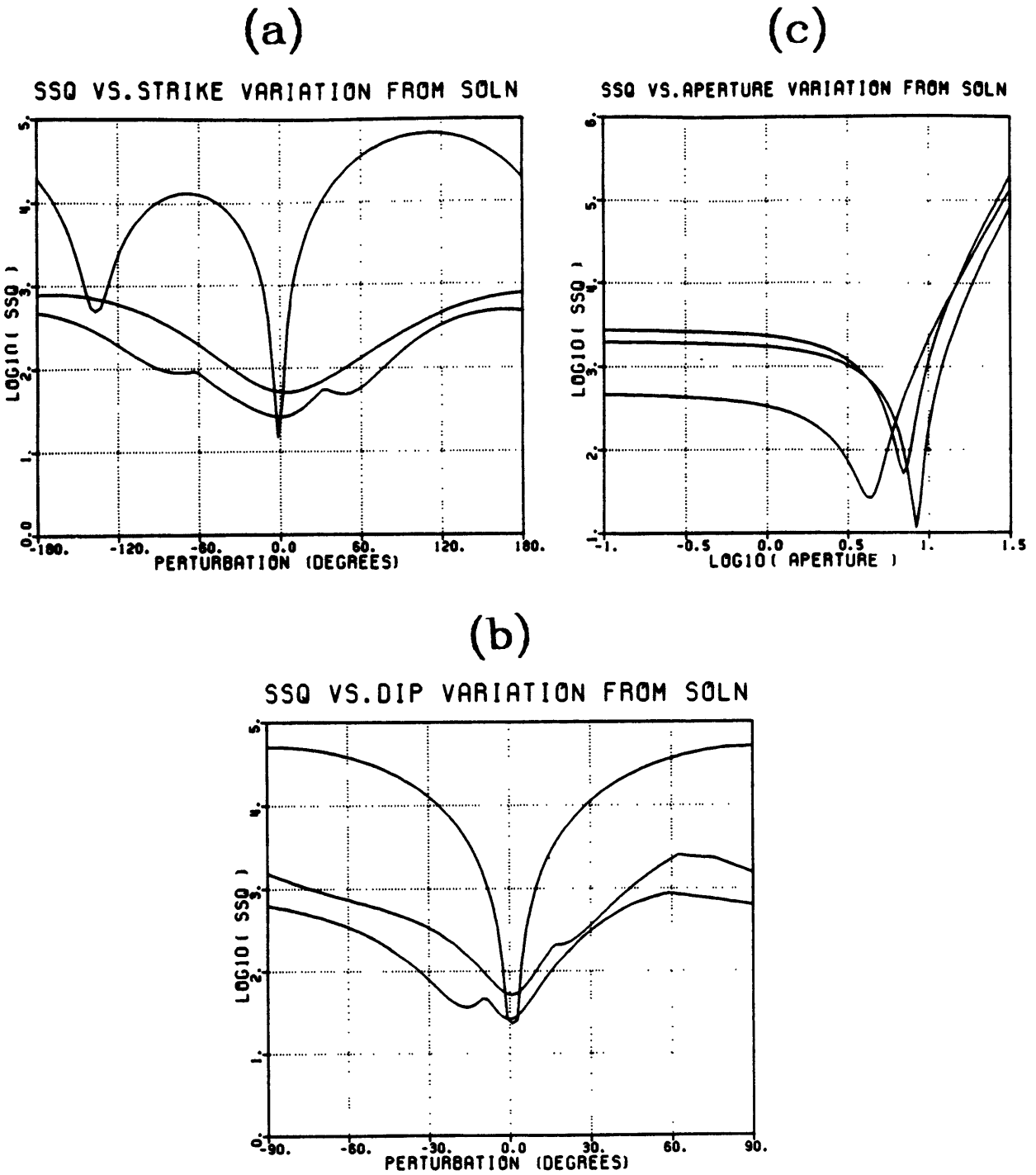
Figure 26. Variation of the sum of squared residuals (SSQ) in the nonlinear inversion, with respect to perturbation of components of the solution vector about the best-fit (fracture at 290 m., Britton well #2). Independent perturbation of (a) strike angle, (b) dip angle, and (c) $\log_{10}$ aperture.
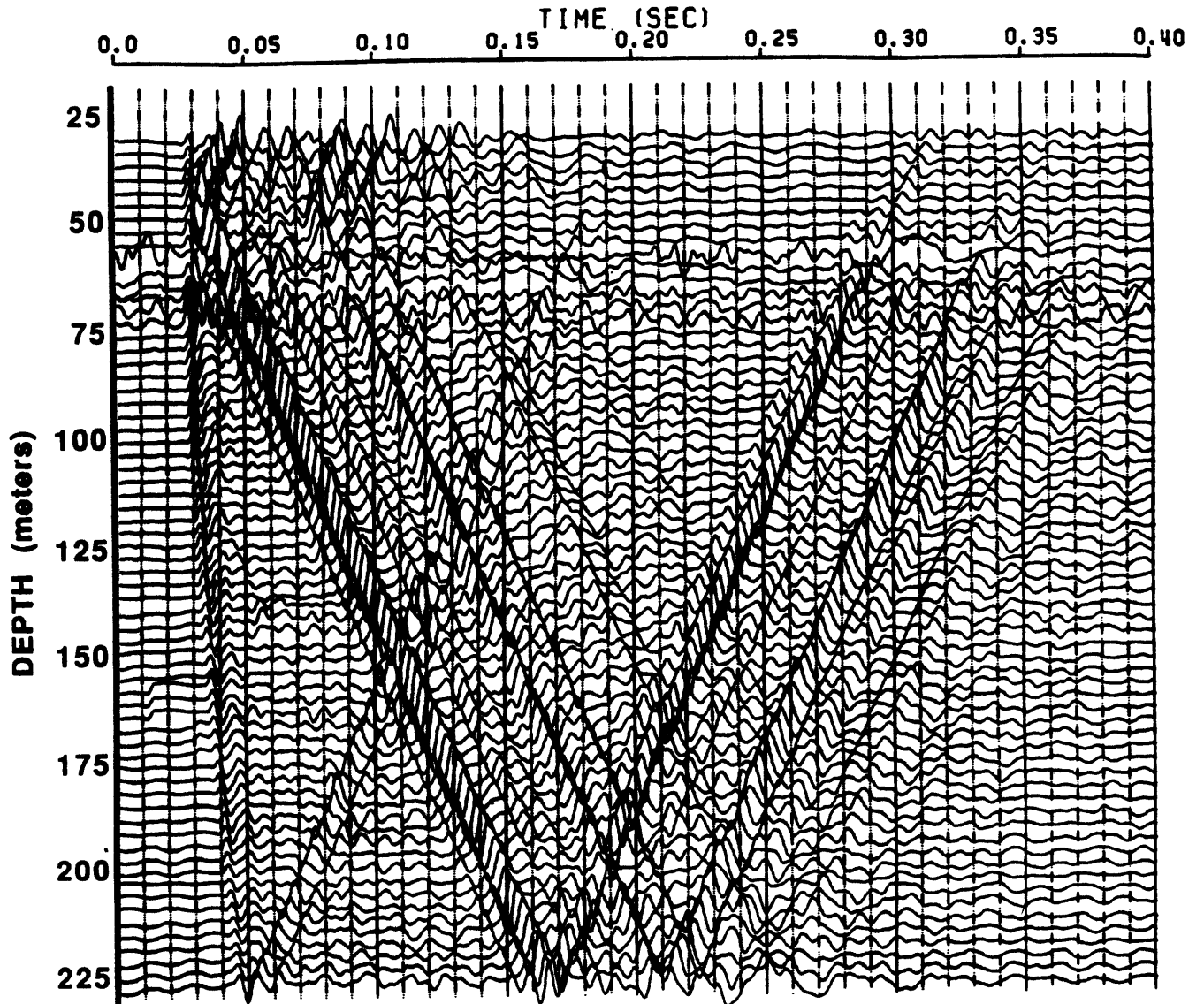
Figure 27. Hydrophone VSP section from Mirror Lake experiment, observation well EBR-4, shot hole A. Traces are bandpass filtered (100-300 Hz.) and shifted to zero-time defined by the monitor phone break.
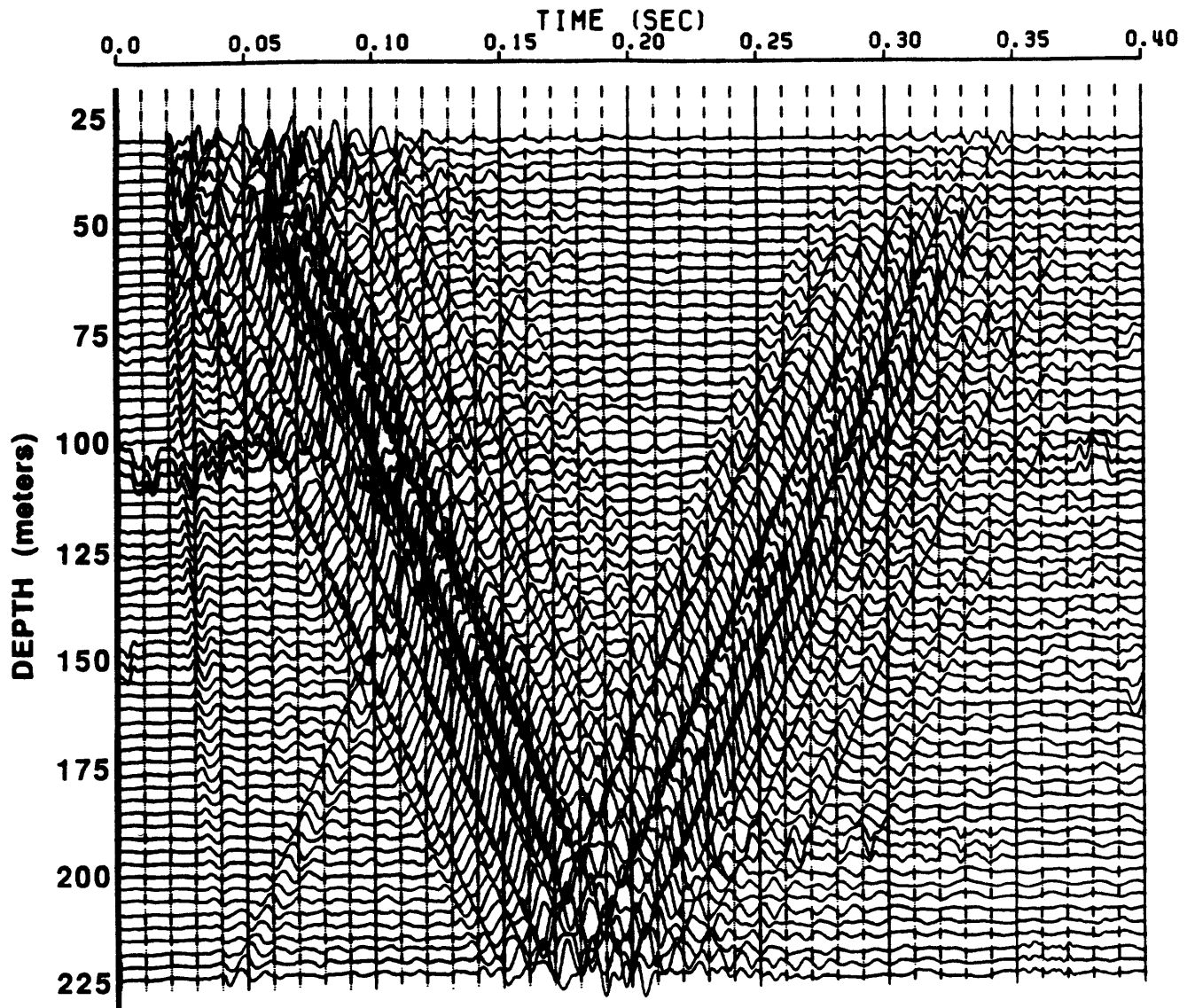
Figure 28. Hydrophone VSP section from Mirror Lake experimen' observation well EBR-4, shot hole B. Traces are bandpass filtered (100-300 Hz.) and shifted to zero-time defined by the monitor phone break.
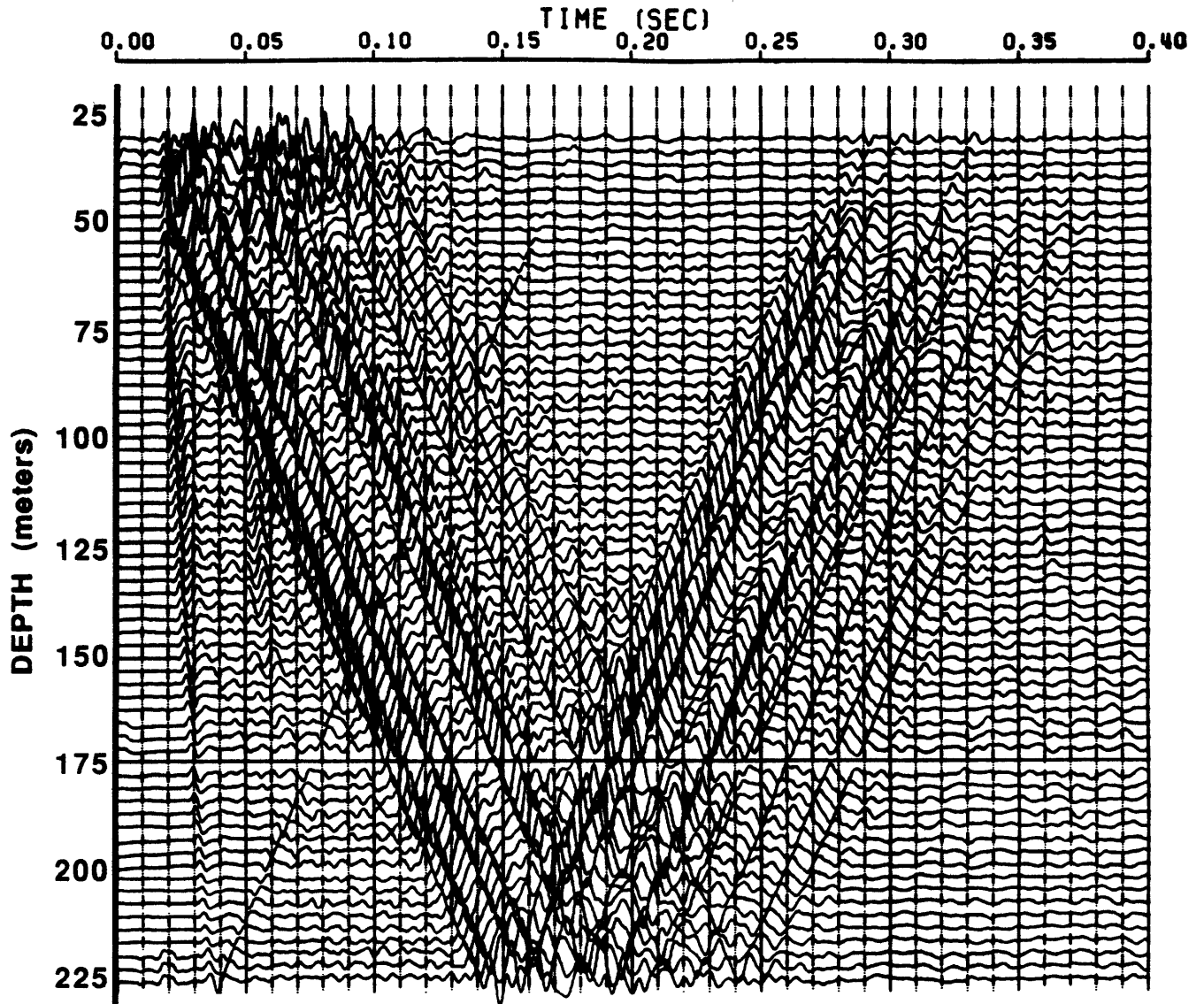
Figure 29. Hydrophone VSP section from Mirror Lake experiment, observation well EBR-4, shot hole C. Traces are bandpass filtered (100-300 Hz.) and shifted to zero-time defined by the monitor phone break.
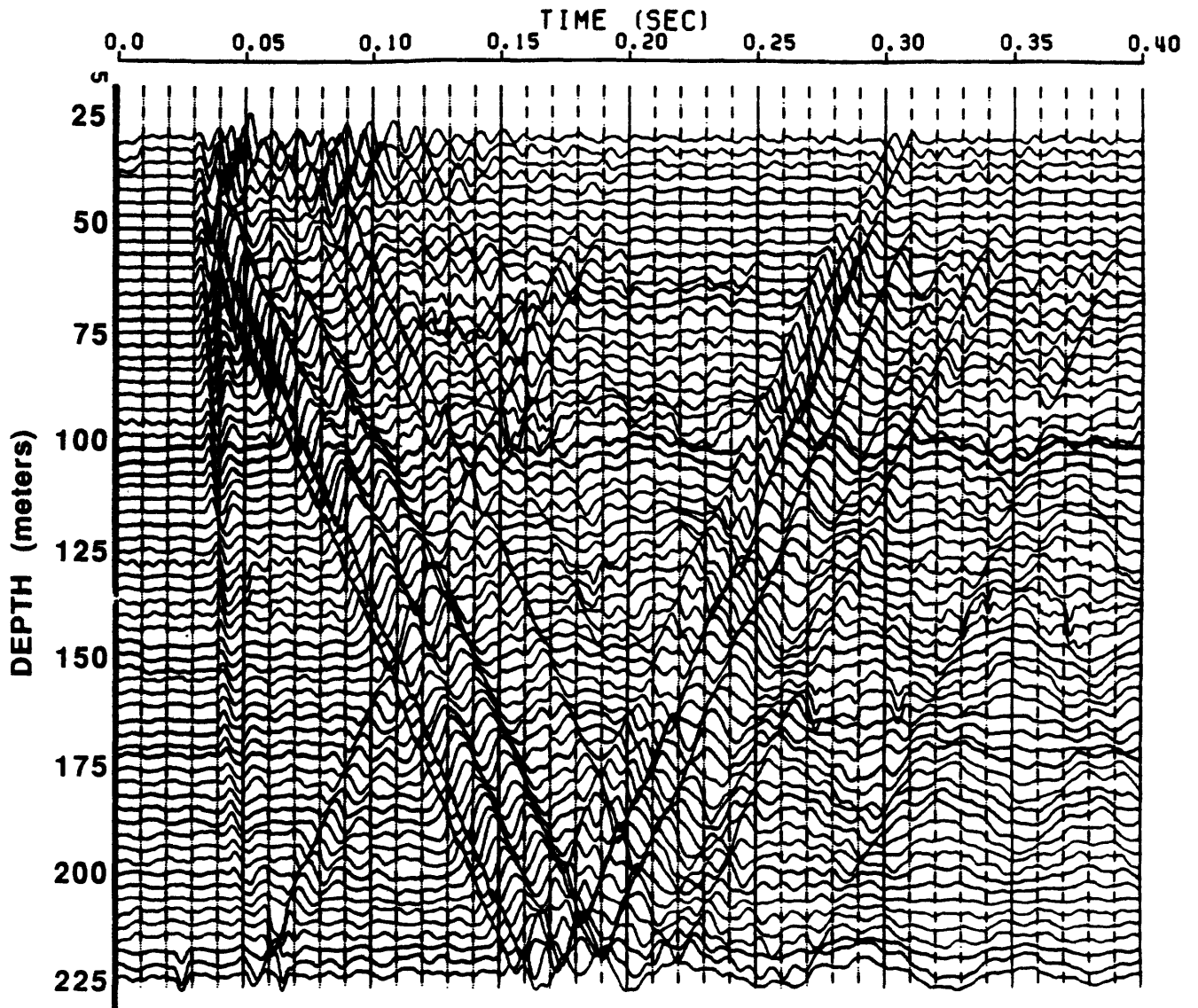
Figure 30. Hydrophone VSP section from Mirror Lake experiment, observation well EBR-4, shot hole D. Traces are bandpass filtered (100-300 Hz.) and shifted to zero-time defined by the monitor phone break.
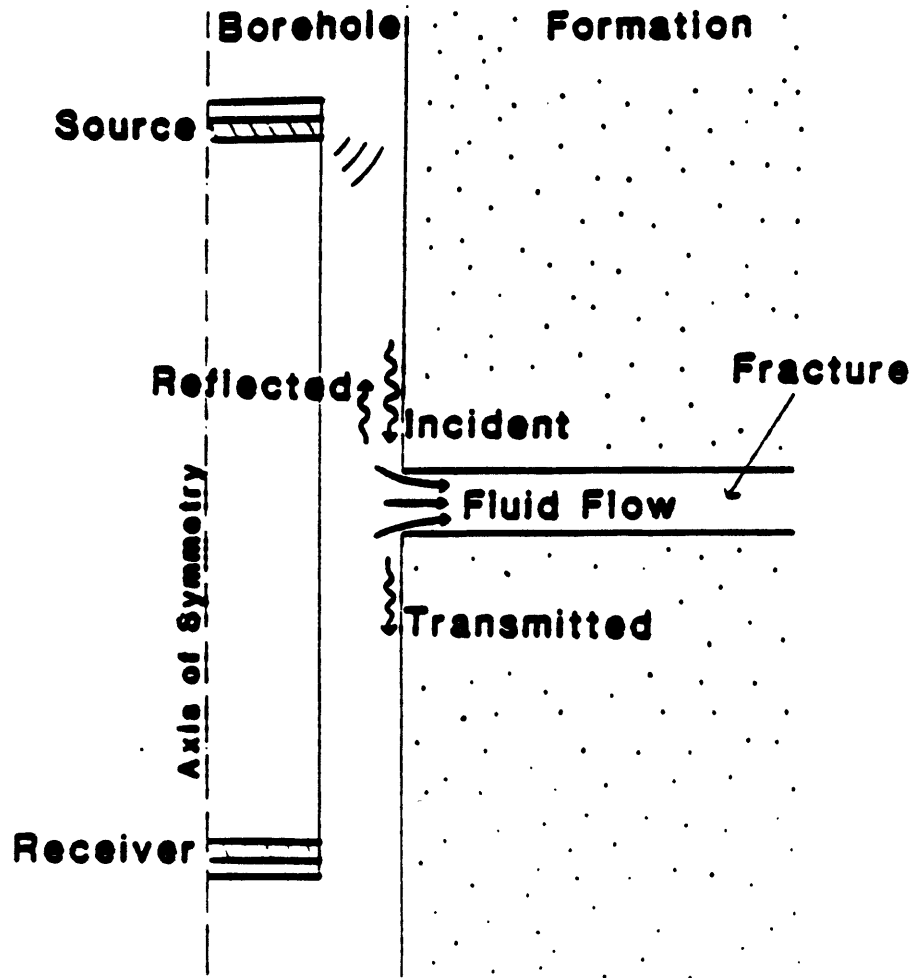
Figure 31. Schematic of FWAL Stoneley phase attenuation m...ar ...
Dynamic pressure at the opening of the fracture into the
borehole is the sum of pressure signals due to fracture flo... a...
incident/reflected/transmitted Stoneley waves.
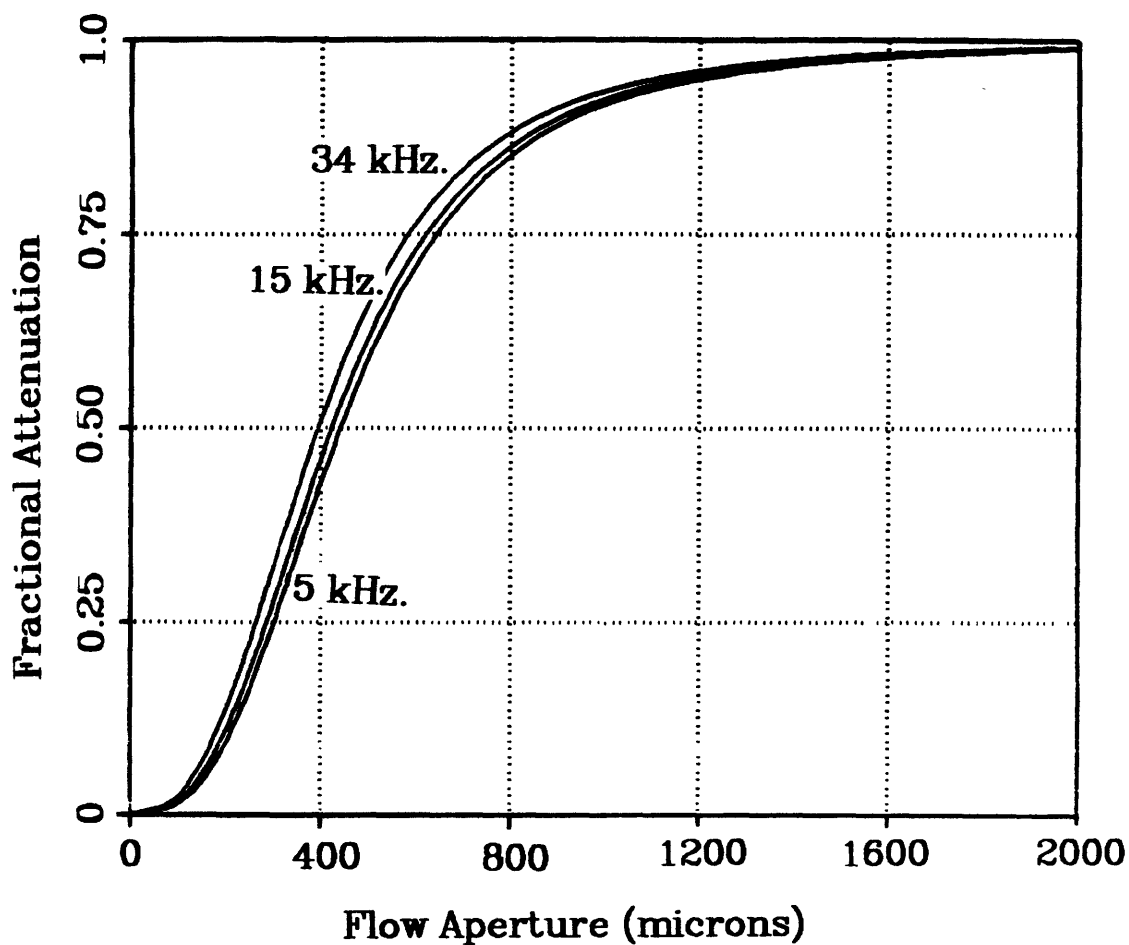
Figure 32. Fractional Stoneley attenuation (ratio of far/near receivers) vs fracture flow-aperture. Different curves correspond to different frequencies as indicated.
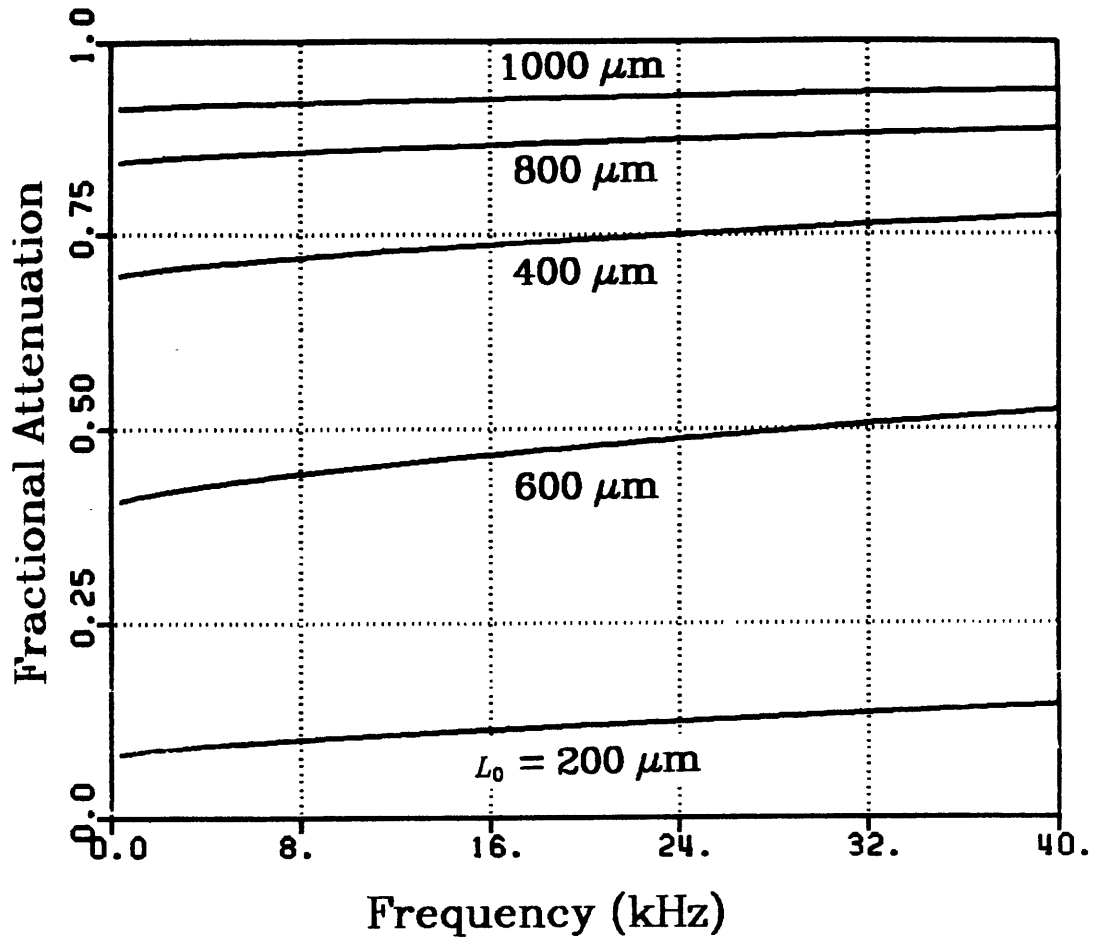
Figure 33. Fractional Stoneley attenuation (ratio of far-near receivers) vs frequency. Different curves correspond to different values of fracture flow-aperture
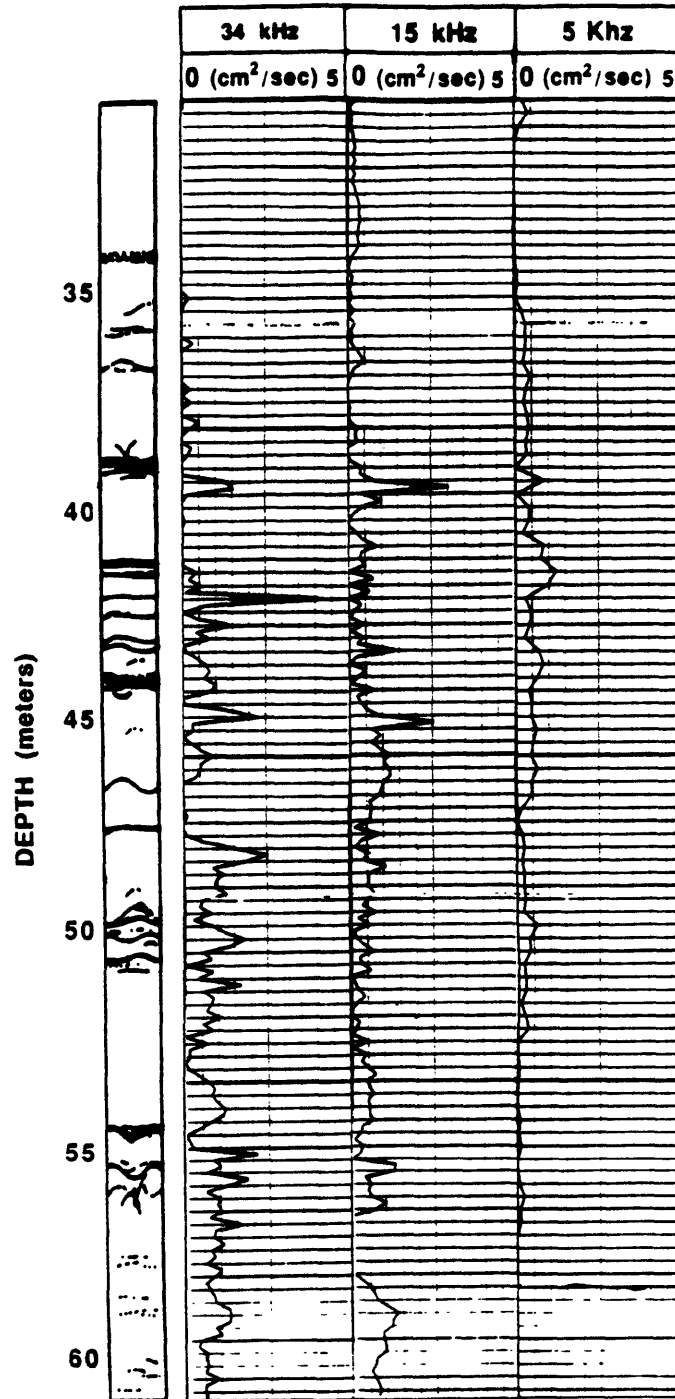
Figure 34. Calculated transmissivity vs. depth, from FWAL Stoneley attenuation. (a) Tx/Rx separations: 0.6 and 0.91 meters., 34 kHz. magnetostrictive source (b) Tx/Rx separations: 0.6 and 0.91 meters., 15 kHz. magnetostrictive source (c) Tx/Rx separations: 2.1 and 3.0 meters., 5 kHz., sparker source.
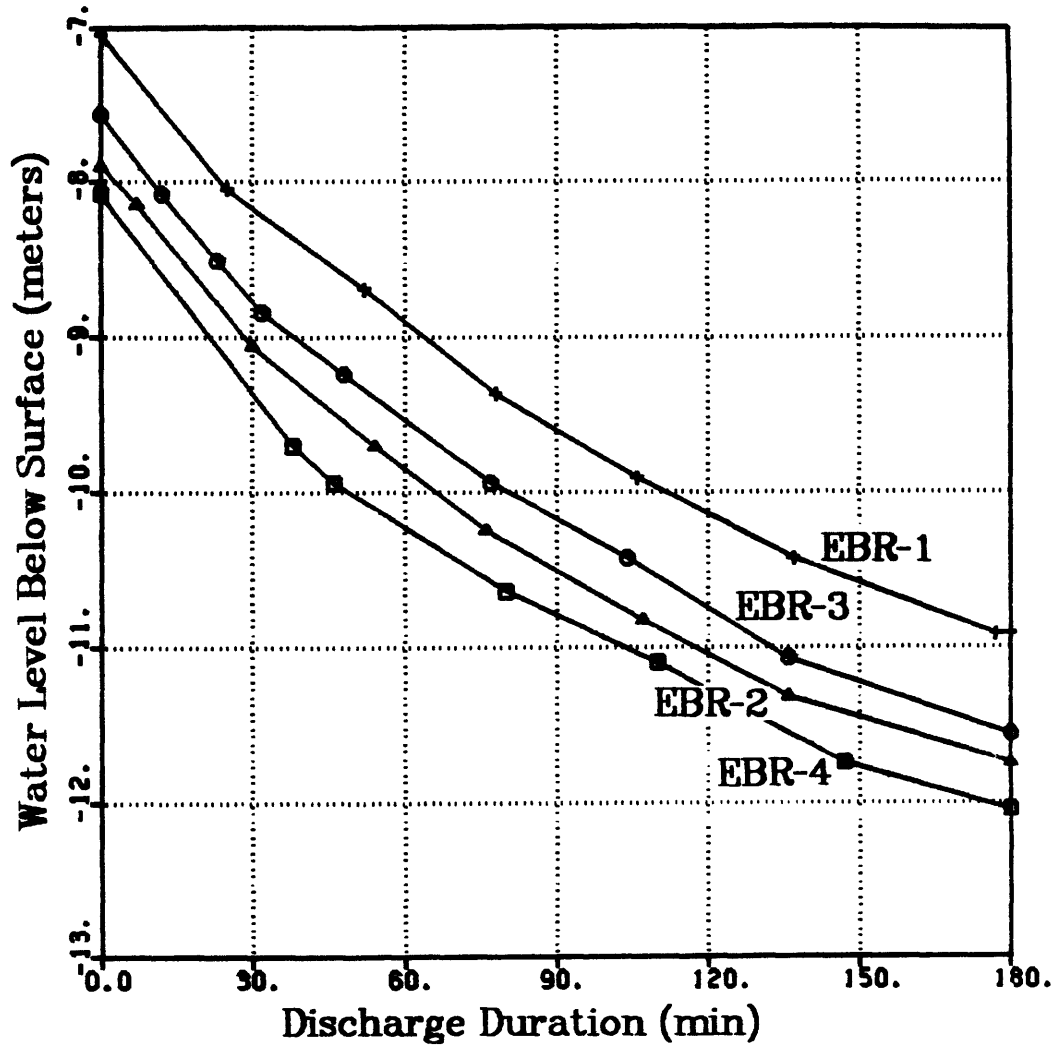
Figure 35. Head fall in wells EBR-1,2 and 3 vs. time, during EBR-4 constant discharge pump test (after Paillet). EBR-4 is the pumped well.
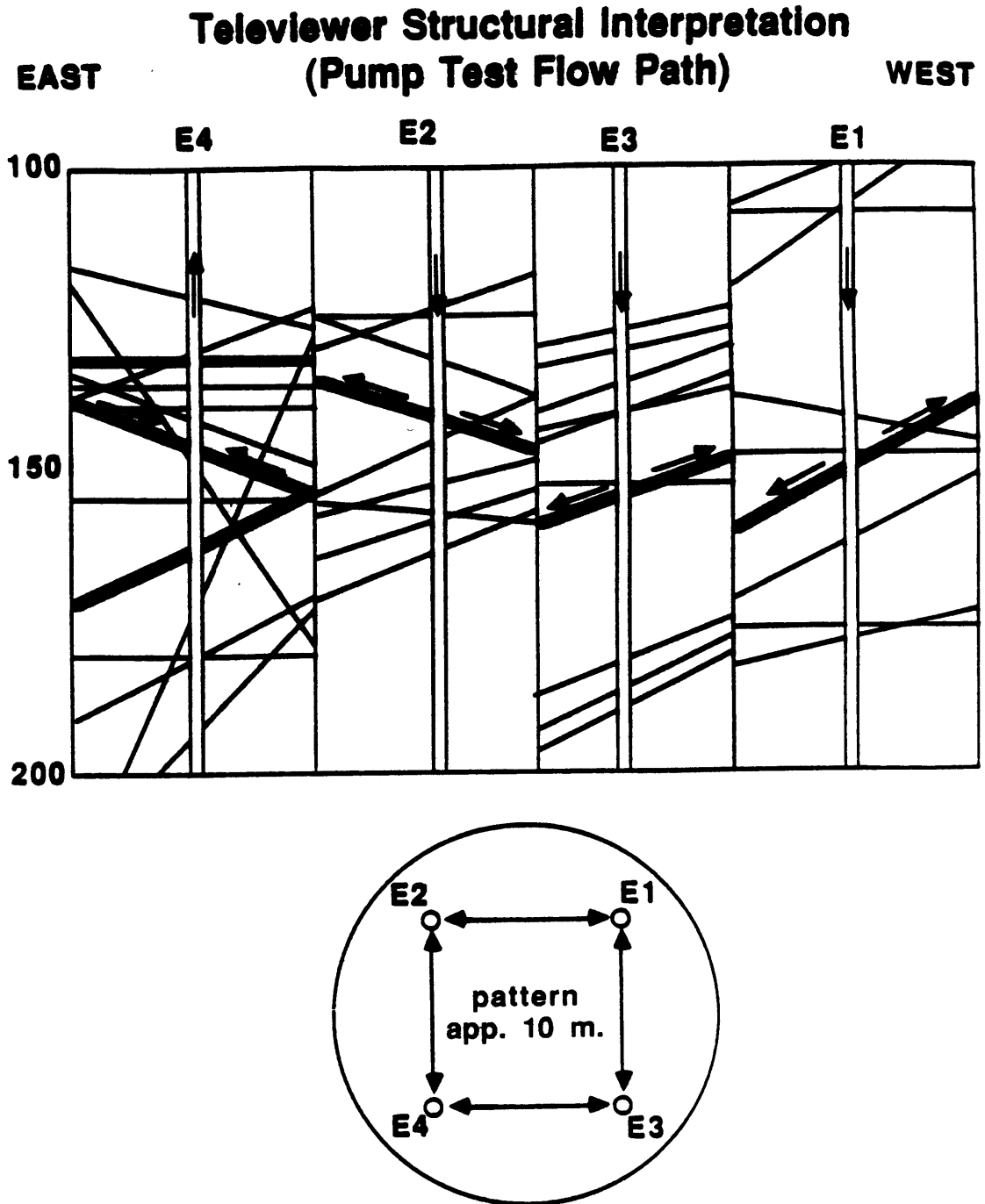
Figure 36. East-west cross-sections through wells EBR-1 thru -4, superposed to show possible flow paths. During discharge from EBR-4, all communicative flow in the other wells was observed near the depth of inflow into EBR-4.
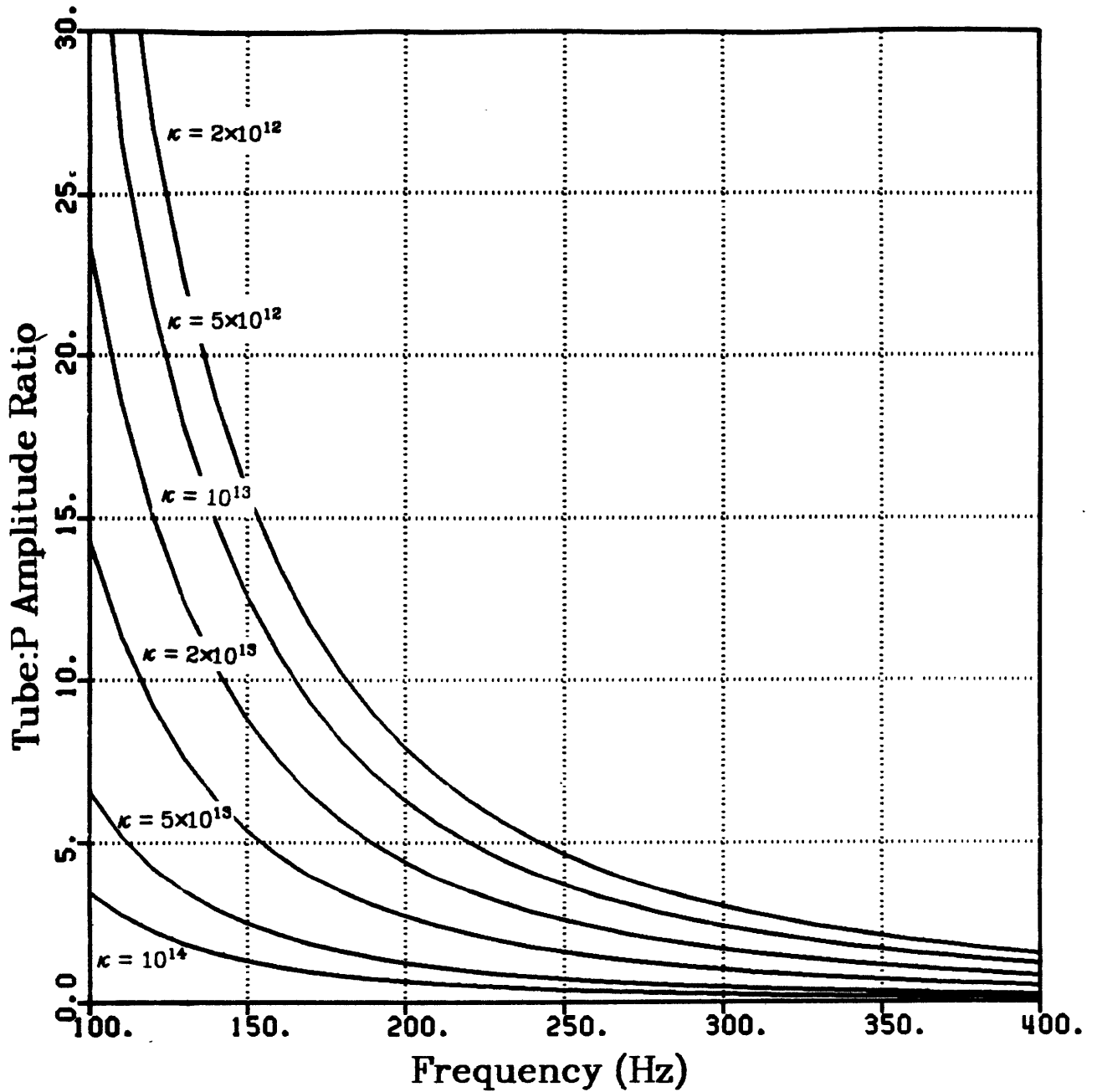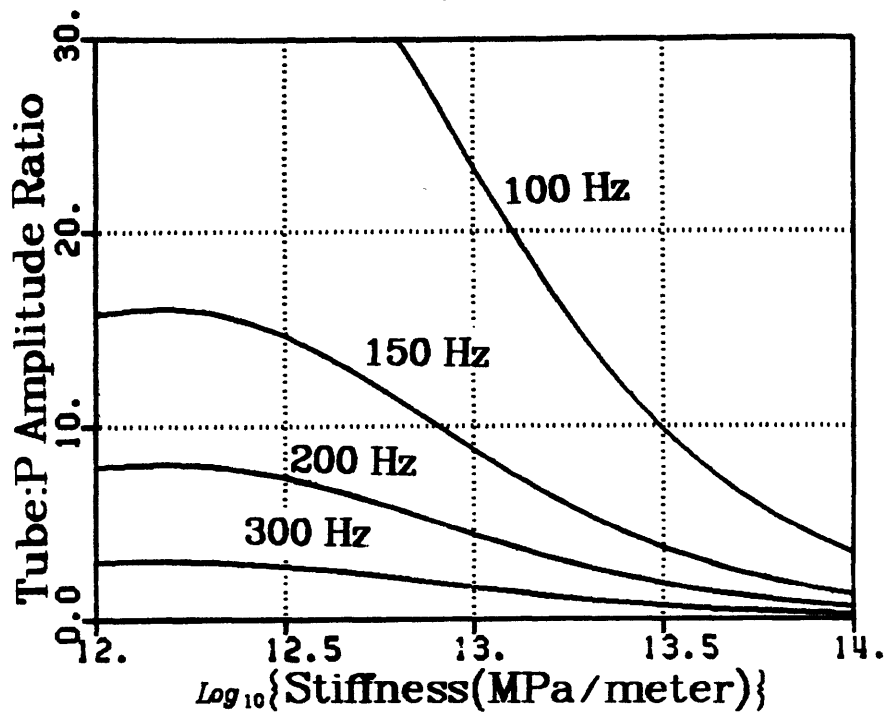
Figure 37. Tube:P amplitude ratio vs. frequency, from stress formulation, using zero offset, normal incidence geometery, and parameters appropriate to well EBR-4 (fracture at 44m). Different curves correspond to different values of fracture stiffness, as indicated.

Stiffness = 2×10^{13} **(MPa/m)**
Flow Aperture = 1 mm

Figure 38. Tube:P amplitude ratio vs. stiffness, from stress formulation using parameters appropriate to Mirror Lake well EBR-4 (fracture at 44m.). Different curves correspond to different geometries for source offsets A,B,C and D.
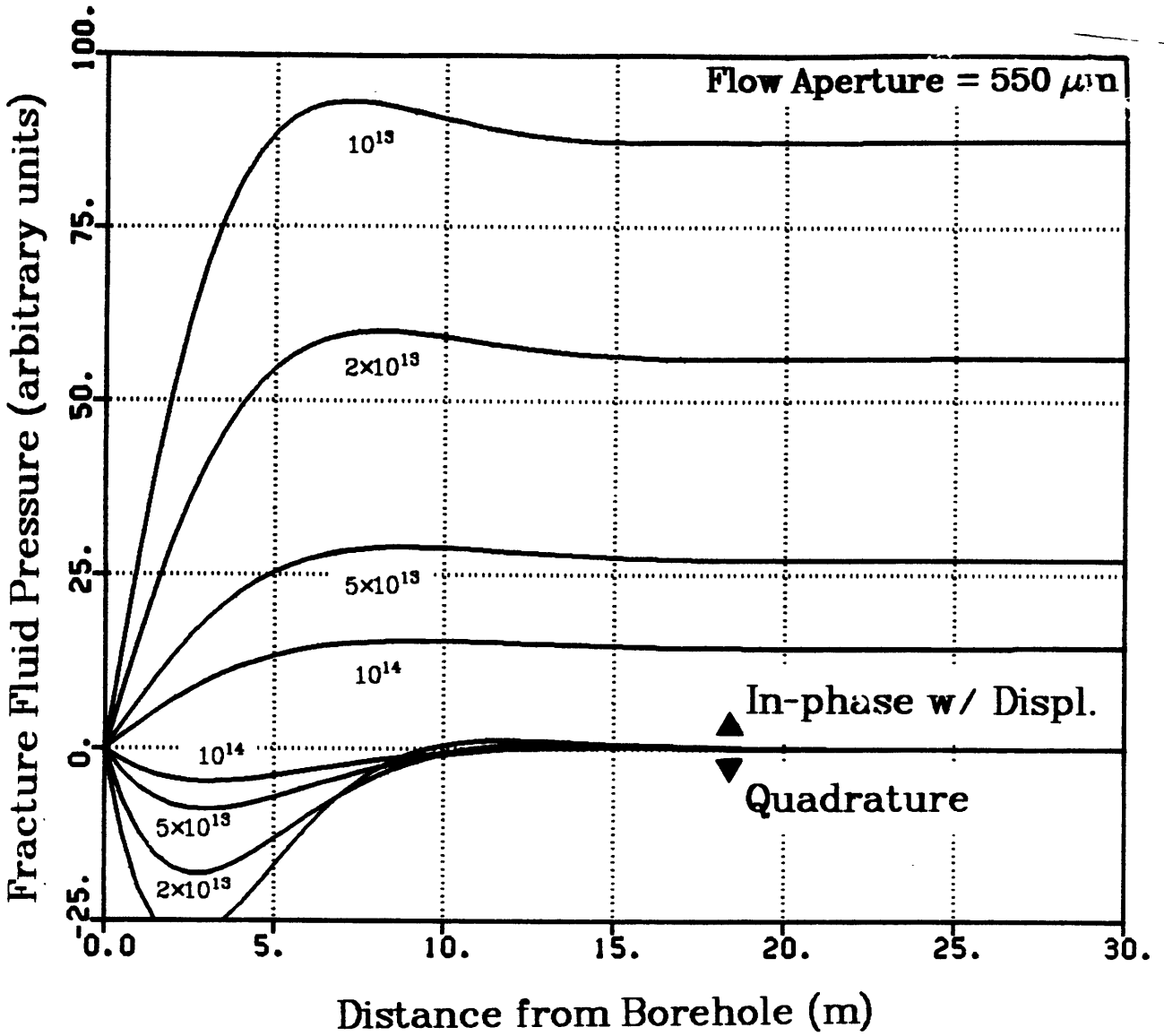
Figure 39. Dynamic 2-D pressure transfer function for stress formulation. Real and imaginary components are plotted for several values of fracture stiffness.
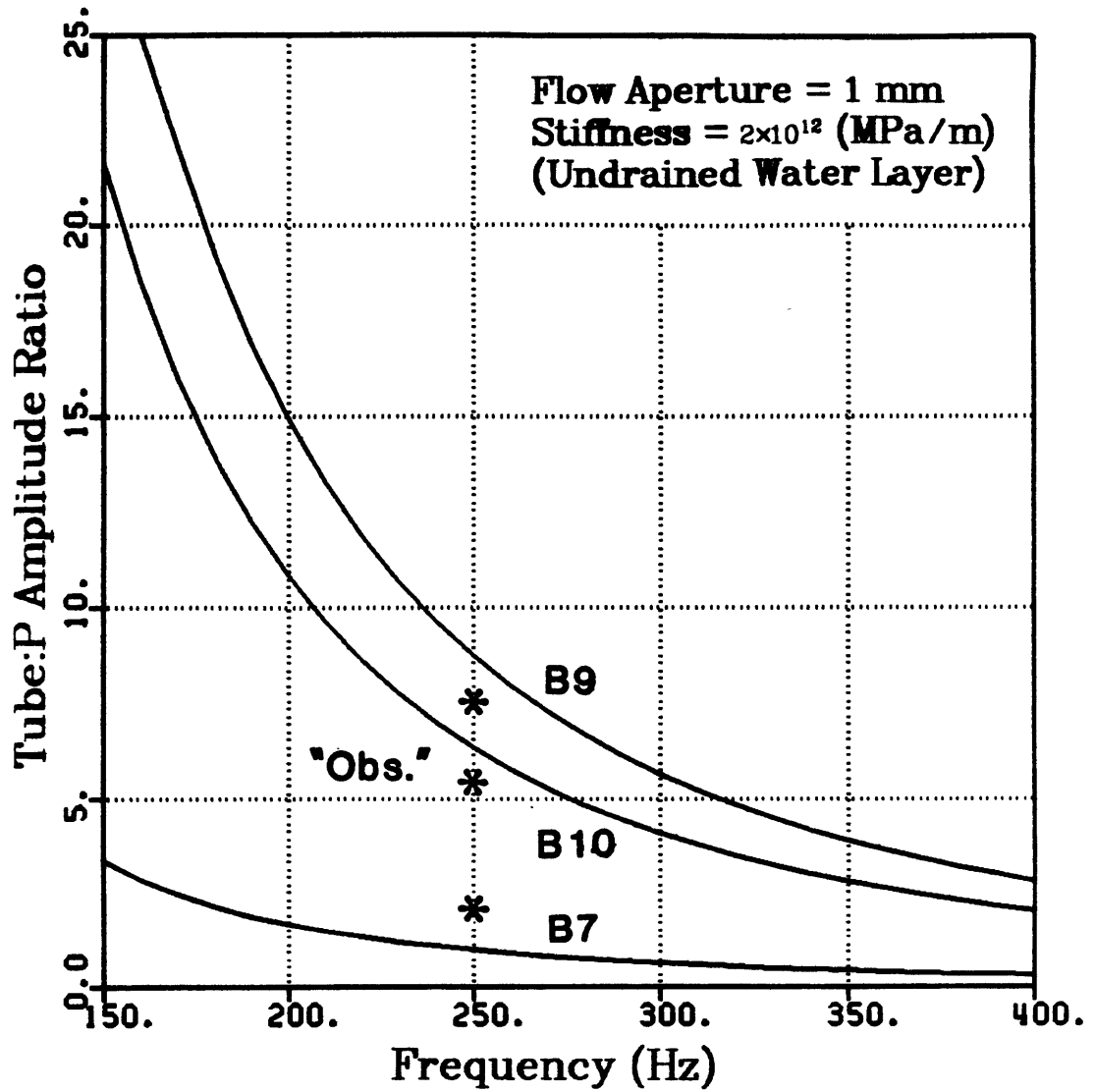
Figure 40. Tube:P amplitude ratio vs. frequency, from stress formulation, using geometry specific to Mirror Lake survey. Intrinsic stiffness is estimated from the stiffness of an undrained water layer with thickness equal to the experimentally-determined equivalent flow aperture. Different curves correspond to source offsets A, B, C and D as indicated. "Observed" ratio at 150 Hz. peak frequency is plotted for each offset.